

Density Model for Striped Dolphin (*Stenella coeruleoalba*) for the U.S. East Coast: Supplementary Report

Model Version 5.1

Duke University Marine Geospatial Ecology Laboratory*

2023-05-27


Citation

When citing our methodology or results generally, please cite Roberts et al. (2016, 2023). The complete references appear at the end of this document. We are preparing a new article for a peer-reviewed journal that will eventually replace those. Until that is published, those are the best general citations.

When citing this model specifically, please use this reference:

Roberts JJ, Yack TM, Cañadas A, Fujioka E, Halpin PN, Barco SG, Boisseau O, Chavez-Rosales S, Cole TVN, Cotter MP, Cummings EW, Davis GE, DiGiovanni Jr. RA, Garrison LP, Gowan TA, Jackson KA, Kenney RD, Khan CB, Lockhart GG, Lomac-MacNair KS, McAlarney RJ, McLellan WA, Mullin KD, Nowacek DP, O'Brien O, Pabst DA, Palka DL, Quintana-Rizzo E, Redfern JV, Rickard ME, White M, Whitt AD, Zoidis AM (2022) Density Model for Striped Dolphin (*Stenella coeruleoalba*) for the U.S. East Coast, Version 5.1, 2023-05-27, and Supplementary Report. Marine Geospatial Ecology Laboratory, Duke University, Durham, North Carolina.

Copyright and License

 This document and the accompanying results are © 2023 by the Duke University Marine Geospatial Ecology Laboratory and are licensed under a [Creative Commons Attribution 4.0 International License](https://creativecommons.org/licenses/by/4.0/).

Model Version History

Version	Date	Description
1	2014-10-22	Initial version.
2	2014-11-20	Reconfigured detection hierarchy and adjusted NARWSS detection functions based on additional information from Tim Cole. Removed CumVGPM180 predictor. Updated documentation.
3	2014-12-04	Fixed bug that applied the wrong detection function to segments NE_narwss_1999_widgeon_hapo dataset. Refitted model. Updated documentation.
3.1	2015-03-06	Updated the documentation. No changes to the model.
3.2	2015-05-14	Updated calculation of CVs. Switched density rasters to logarithmic breaks. No changes to the model.
3.3	2015-10-05	Updated the documentation. No changes to the model. Model files released as supplementary information to Roberts et al. (2016).

*For questions or to offer feedback please contact Jason Roberts (jason.roberts@duke.edu) and Tina Yack (tina.yack@duke.edu)

(continued)

Version	Date	Description
4	2018-04-14	Began update to Roberts et al. (2015) model. Introduced new surveys from AMAPPS, NARWSS, UNCW, VAMSC, and the SEUS NARW teams. Updated modeling methodology. Refitted detection functions and spatial models from scratch using new and reprocessed covariates. Model released as part of a scheduled update to the U.S. Navy Marine Species Density Database (NMSDD).
5	2022-06-20	This model is a major update over the prior version, with substantial additional data, improved statistical methods, and an increased spatial resolution. It was released as part of the final delivery of the U.S. Navy Marine Species Density Database (NMSDD) for the Atlantic Fleet Testing and Training (AFTT) Phase IV Environmental Impact Statement. Several new collaborators joined and contributed survey data: New York State Department of Environmental Conservation, TetraTech, HDR, and Marine Conservation Research. We incorporated additional surveys from all continuing and new collaborators through the end of 2020. (Because some environmental covariates were only available through 2019, certain models only extend through 2019.) We increased the spatial resolution to 5 km and, at NOAA's request, we extended the model further inshore from New York through Maine. We reformulated and refitted all detection functions and spatial models. We updated all environmental covariates to newer products, when available, and added several covariates to the set of candidates. For models that incorporated dynamic covariates, we estimated model uncertainty using a new method that accounts for both model parameter error and temporal variability.
5.1	2023-05-27	Completed the supplementary report documenting the details of this model. The model itself was not changed.

1 Survey Data

We built this model from data collected between 1998-2019 (Table 1, Figure 1). We excluded surveys that did not target small cetaceans or were otherwise problematic for modeling them. In keeping with our primary strategy for the 2022 modeling cycle, we excluded data prior to 1998 in order to utilize biological covariates derived from satellite ocean color observations, which were only available for a few months before 1998. We excluded data after 2019 in order to utilize zooplankton and micronekton biomass estimates from SEAPODYM (Lehodey et al. 2008), which preliminary modeling indicated were effective spatial covariates but were only available through 2019. We restricted the model to aerial survey transects with sea states of Beaufort 4 or less (for a few surveys we used Beaufort 3 or less) and shipboard transects with Beaufort 5 or less (for a few we used Beaufort 4 or less). We also excluded transects with poor weather or visibility for surveys that reported those conditions.

Table 1: Survey effort and observations considered for this model. Effort is tallied as the cumulative length of on-effort transects. Observations are the number of groups and individuals encountered while on effort. Off effort observations and those lacking an estimate of group size or distance to the group were excluded.

Institution	Program	Period	Effort	Observations		
			1000s km	Groups	Individuals	Mean Group Size
Aerial Surveys						
HDR	Navy Norfolk Canyon	2018-2019	10	14	990	70.7
NEFSC	AMAPPS	2010-2019	83	13	461	35.5
NEFSC	NARWSS	2003-2016	380	0	0	
NEFSC	Pre-AMAPPS	1999-2008	45	1	130	130.0
SEFSC	AMAPPS	2010-2019	110	1	110	110.0
SEFSC	MATS	2002-2005	27	0	0	
UNCW	MidA Bottlenose	2002-2002	15	0	0	
UNCW	Navy Cape Hatteras	2011-2017	34	7	1,021	145.9
UNCW	Navy Jacksonville	2009-2017	92	0	0	
UNCW	Navy Norfolk Canyon	2015-2017	14	12	1,614	134.5
UNCW	Navy Onslow Bay	2007-2011	49	0	0	
UNCW	SEUS NARW EWS	2005-2008	106	0	0	
VAMSC	MD DNR WEA	2013-2015	15	0	0	
VAMSC	Navy VACAPES	2016-2017	18	0	0	
VAMSC	VA CZM WEA	2012-2015	19	0	0	
		Total	1,017	48	4,326	90.1
Shipboard Surveys						
MCR	SOTW Visual	2012-2019	9	3	48	16.0
NEFSC	AMAPPS	2011-2016	15	174	6,881	39.5
NEFSC	Pre-AMAPPS	1998-2007	13	96	4,926	51.3
NJDEP	NJEBS	2008-2009	14	0	0	
SEFSC	AMAPPS	2011-2016	16	11	1,554	141.3
SEFSC	Pre-AMAPPS	1998-2006	30	74	7,018	94.8
		Total	96	358	20,427	57.1
		Grand Total	1,113	406	24,753	61.0

Table 2: Institutions that contributed surveys used in this model.

Institution	Full Name
HDR	HDR, Inc.
MCR	Marine Conservation Research
NEFSC	NOAA Northeast Fisheries Science Center
NJDEP	New Jersey Department of Environmental Protection
SEFSC	NOAA Southeast Fisheries Science Center
UNCW	University of North Carolina Wilmington
VAMSC	Virginia Aquarium & Marine Science Center

Table 3: Descriptions and references for survey programs used in this model.

Program	Description	References
AMAPPS	Atlantic Marine Assessment Program for Protected Species	Palka et al. (2017), Palka et al. (2021)
MATS	Mid-Atlantic Tursiops Surveys	
MD DNR WEA	Aerial Surveys of the Maryland Wind Energy Area	Barco et al. (2015)
MidA Bottlenose	Mid-Atlantic Onshore/Offshore Bottlenose Dolphin Surveys	Torres et al. (2005)
NARWSS	North Atlantic Right Whale Sighting Surveys	Cole et al. (2007)
Navy Cape Hatteras	Aerial Surveys of the Navy’s Cape Hatteras Study Area	McLellan et al. (2018)
Navy Jacksonville	Aerial Surveys of the Navy’s Jacksonville Study Area	Foley et al. (2019)
Navy Norfolk Canyon	Aerial Surveys of the Navy’s Norfolk Canyon Study Area	Cotter (2019), McAlarney et al. (2018)
Navy Onslow Bay	Aerial Surveys of the Navy’s Onslow Bay Study Area	Read et al. (2014)
Navy VACAPES	Aerial Survey Baseline Monitoring in the Continental Shelf Region of the VACAPES OPAREA	Malette et al. (2017)
NJEBS	New Jersey Ecological Baseline Study	Geo-Marine, Inc. (2010), Whitt et al. (2015)
Pre-AMAPPS	Pre-AMAPPS Marine Mammal Abundance Surveys	Mullin and Fulling (2003), Garrison et al. (2010), Palka (2006)
SEUS NARW EWS	Southeast U.S. Right Whale Early Warning System Surveys	
SOTW Visual	R/V Song of the Whale Visual Surveys	Ryan et al. (2013)
VA CZM WEA	Virginia CZM Wind Energy Area Surveys	Malette et al. (2014), Malette et al. (2015)

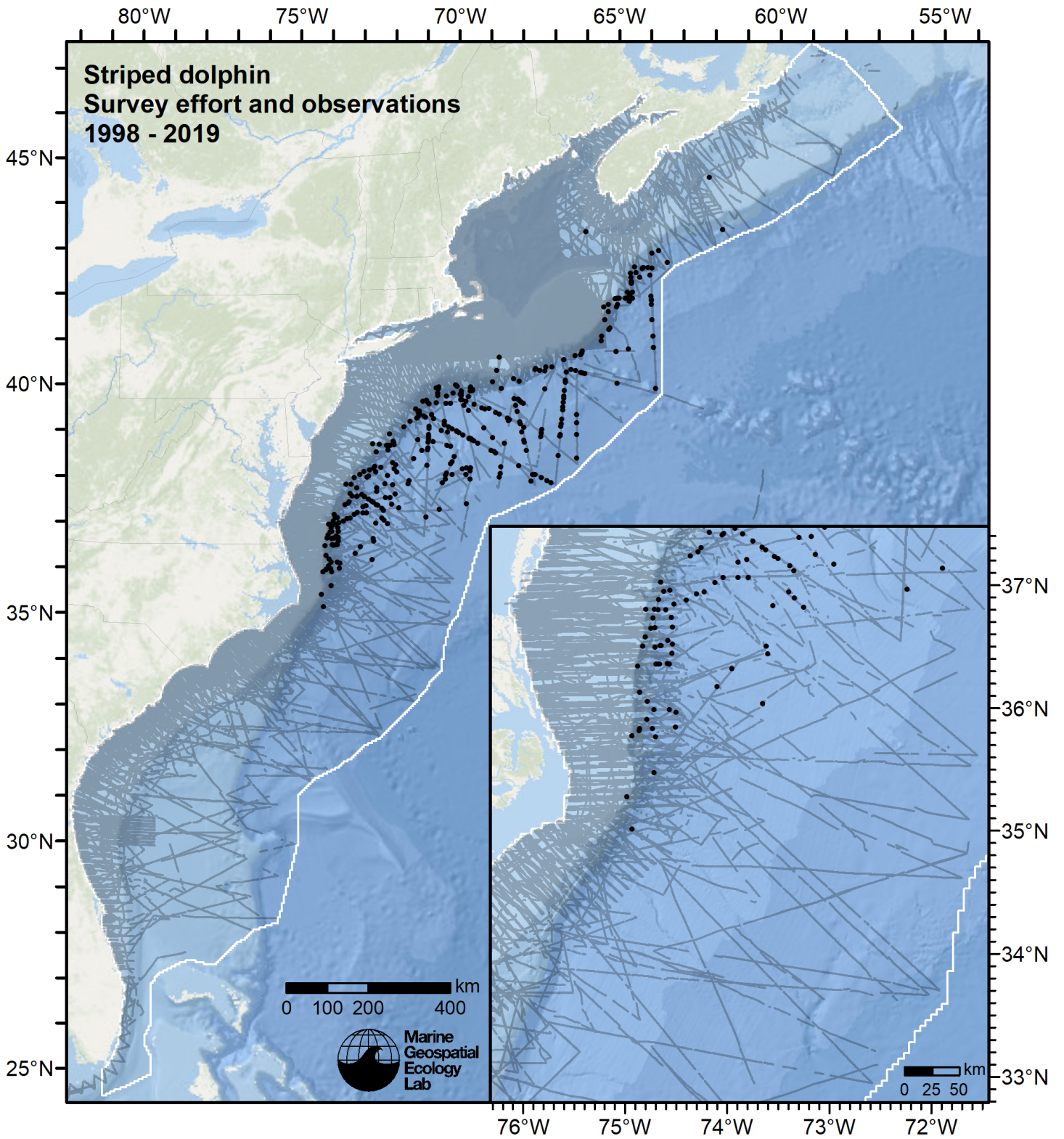


Figure 1: Survey effort and striped dolphin observations available for density modeling, after detection functions were applied, and excluded segments and truncated observations were removed.

2 Detection Functions

2.1 With a Taxonomic Covariate

We fitted the detection functions in this section to pools of species with similar detectability characteristics and used the taxonomic identification as a covariate (`ScientificName`) to account for differences between them. We consulted the literature and observer teams to determine appropriate poolings. We usually employed this approach to boost the counts of observations in the detection functions, which increased the chance that other covariates such as Beaufort sea state could be used to account for differences in observing conditions. When defining the taxonomic covariate, we sometimes had too few observations of species to allocate each of them their own level of the covariate and had to group them together, again consulting the literature and observers for advice on species similarity. Also, when species were observed frequently enough to be allocated their own levels but statistical tests indicated no significant difference between the levels, we usually grouped them together into a single level.

2.1.1 Aerial Surveys

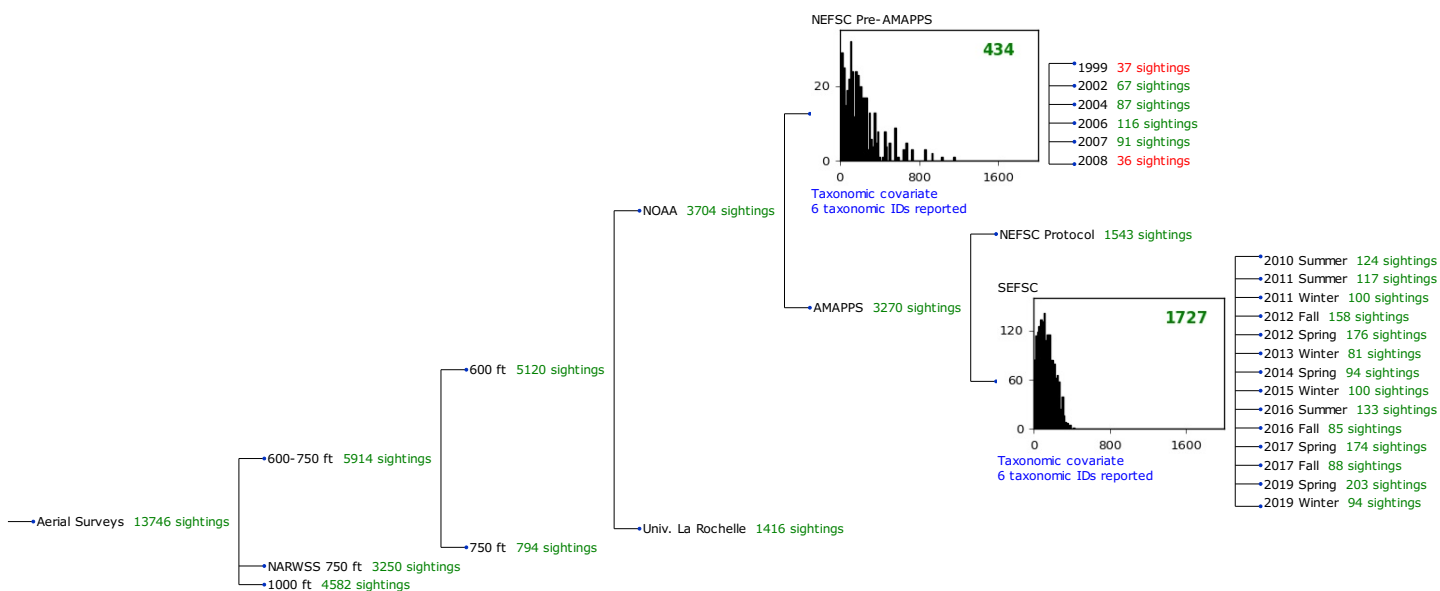


Figure 2: Detection hierarchy for aerial surveys, showing how they were pooled during detectability modeling, for detection functions that pooled multiple taxa and used a taxonomic covariate to account for differences between them. Each histogram represents a detection function and summarizes the perpendicular distances of observations that were pooled to fit it, prior to truncation. Observation counts, also prior to truncation, are shown in green when they met the recommendation of Buckland et al. (2001) that detection functions utilize at least 60 sightings, and red otherwise. For rare taxa, it was not always possible to meet this recommendation, yielding higher statistical uncertainty. During the spatial modeling stage of the analysis, effective strip widths were computed for each survey using the closest detection function above it in the hierarchy (i.e. moving from right to left in the figure). Surveys that do not have a detection function above them in this figure were either addressed by a detection function presented in a different section of this report, or were omitted from the analysis.

2.1.1.1 NEFSC Pre-AMAPPS

After right-truncating observations greater than 600 m, we fitted the detection function to the 413 observations that remained (Table 4). The selected detection function (Figure 3) used a hazard rate key function with Beaufort (Figure 4) and `ScientificName` (Figure 5) as covariates.

Table 4: Observations used to fit the NEFSC Pre-AMAPPS detection function.

ScientificName	n
Delphinus, Lagenodelphis, Stenella	239
Lagenorhynchus	128
Tursiops, Steno	46
Total	413

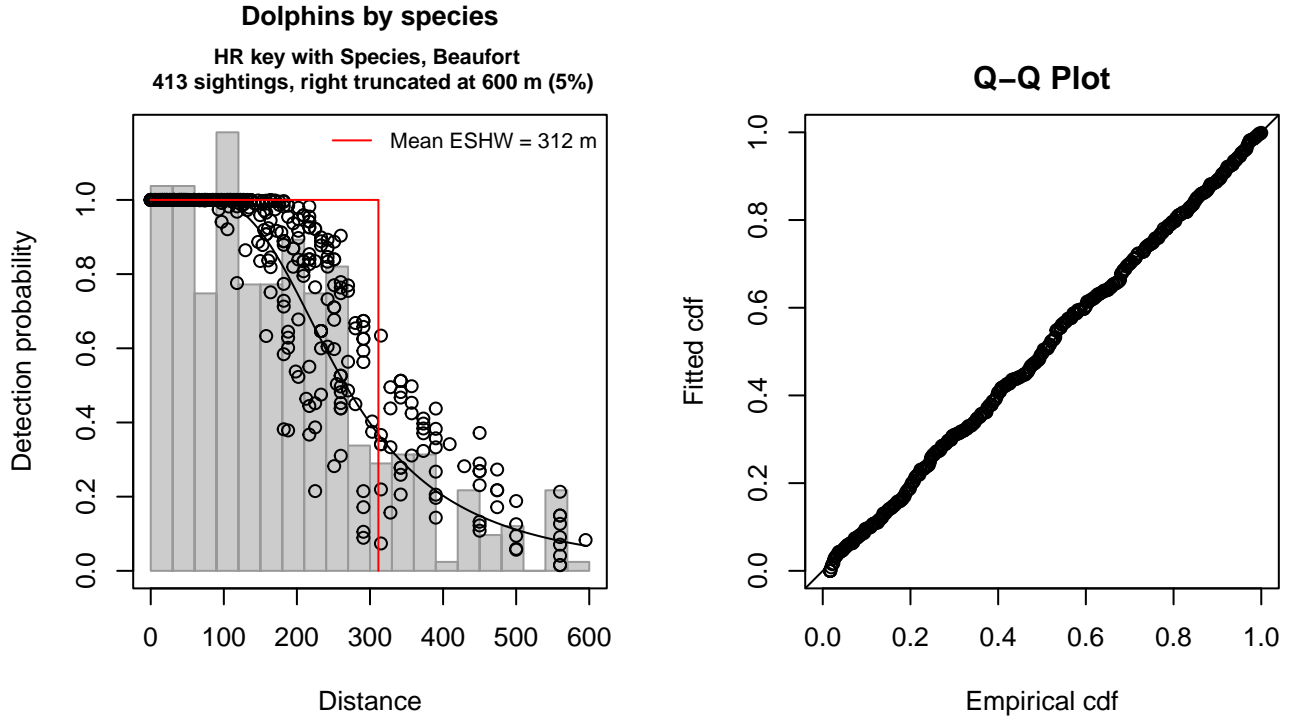


Figure 3: NEFSC Pre-AMAPPS detection function and Q-Q plot showing its goodness of fit.

Statistical output for this detection function:

Summary for ds object

Number of observations : 413
 Distance range : 0 - 600
 AIC : 5043.994

Detection function:
 Hazard-rate key function

Detection function parameters

Scale coefficient(s):

	estimate	se
(Intercept)	5.3188665	0.15126469
ScientificNameLagenorhynchus	-0.1872175	0.11165678
ScientificNameTursiops, Steno	-0.5457529	0.14785313
Beaufort	0.1451869	0.05844944

Shape coefficient(s):

	estimate	se
(Intercept)	1.107015	0.1176733

Estimate	SE	CV
----------	----	----

Average p 0.4982478 0.02373666 0.04764026
 N in covered region 828.9047438 49.28440455 0.05945726

Distance sampling Cramer-von Mises test (unweighted)
 Test statistic = 0.023324 p = 0.992716

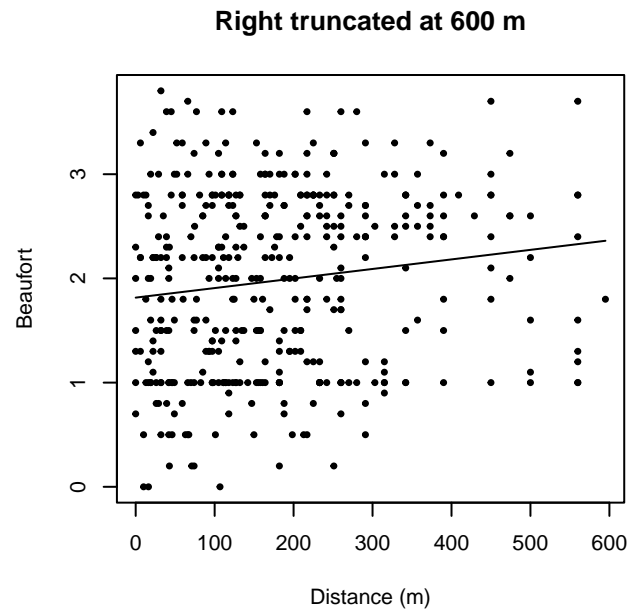
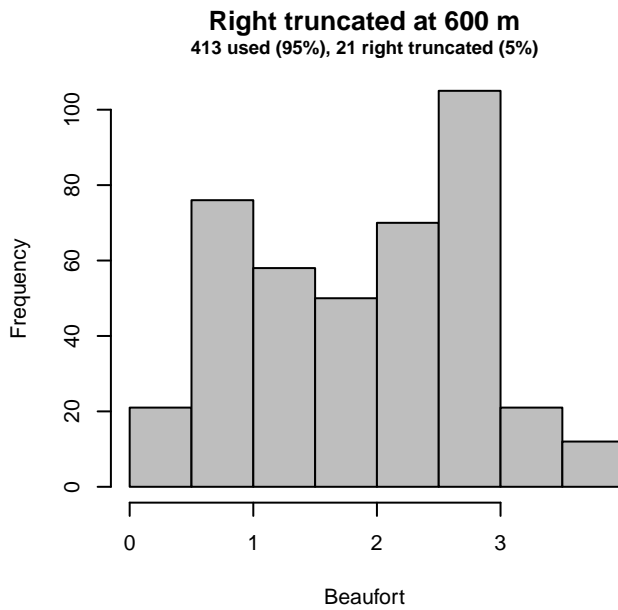
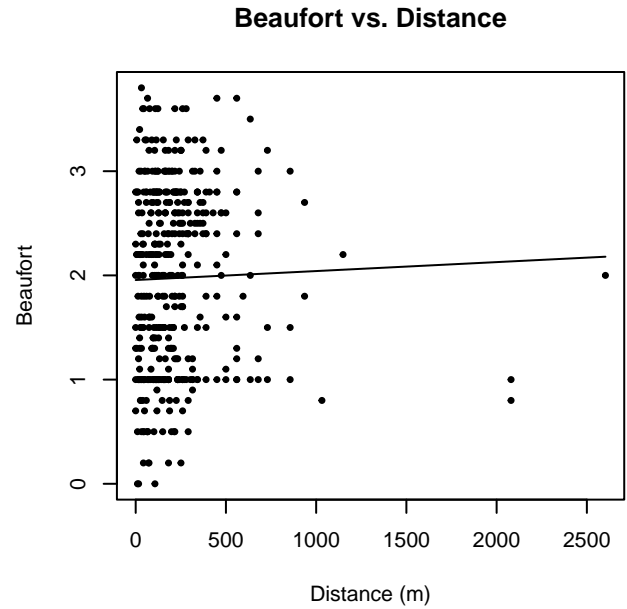
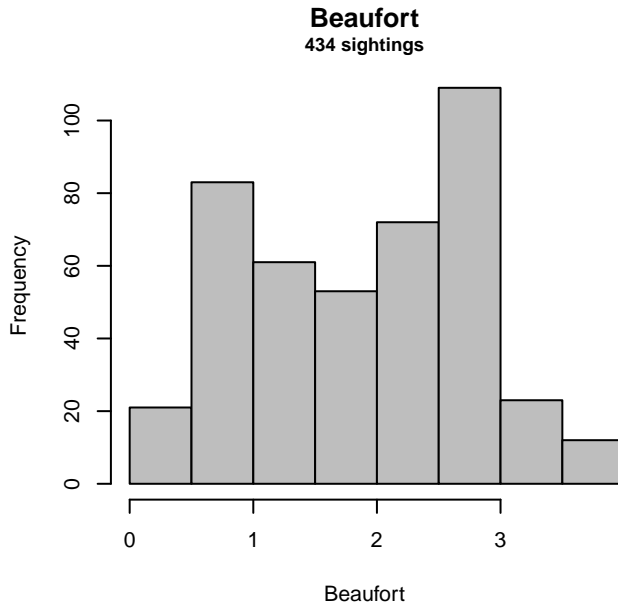


Figure 4: Distribution of the Beaufort covariate before (top row) and after (bottom row) observations were truncated to fit the NEFSC Pre-AMAPPS detection function.

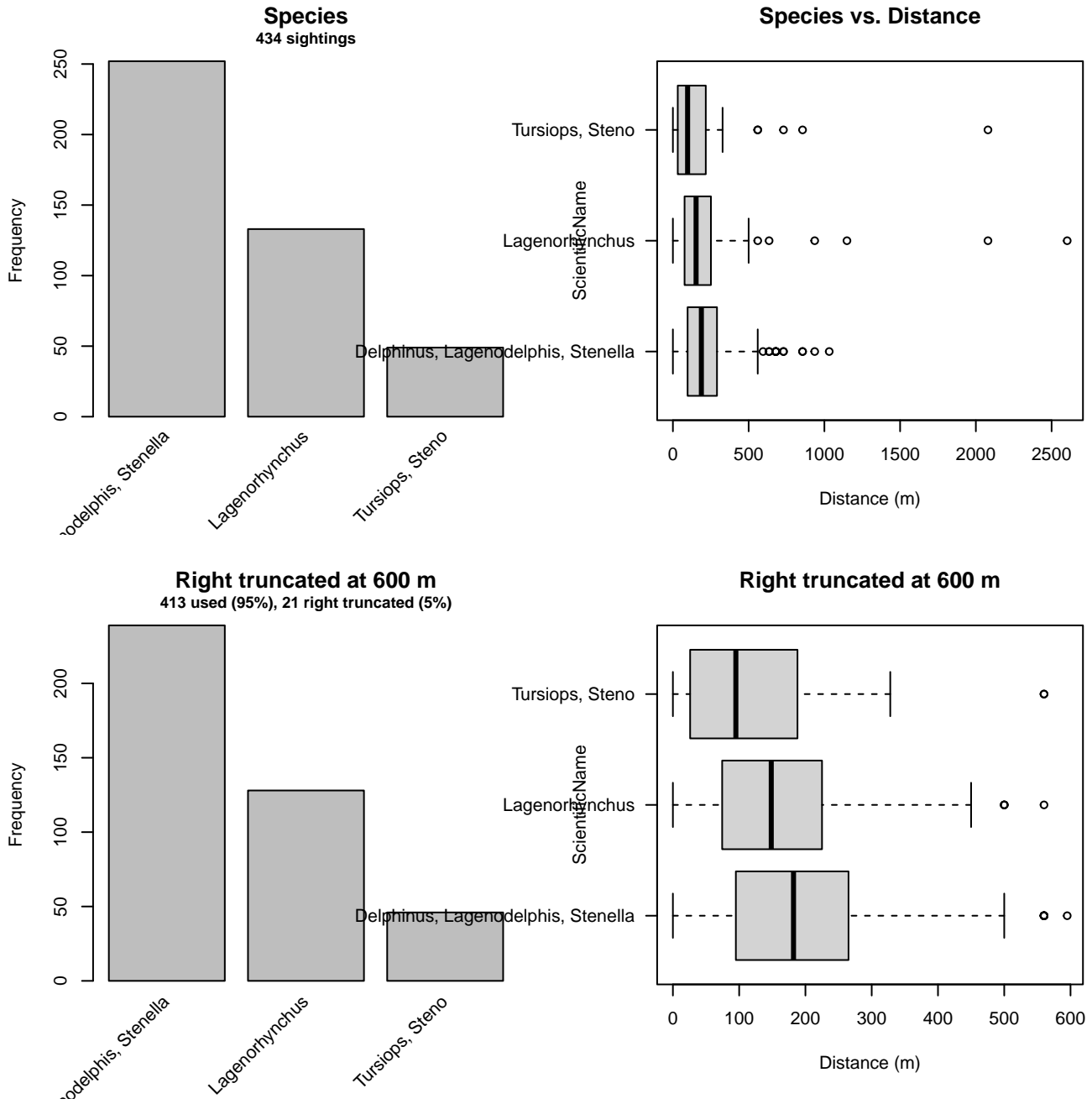


Figure 5: Distribution of the ScientificName covariate before (top row) and after (bottom row) observations were truncated to fit the NEFSC Pre-AMAPPS detection function.

2.1.1.2 SEFSC AMAPPS

After right-truncating observations greater than 325 m and left-truncating observations less than 15 m (Figure 7), we fitted the detection function to the 1628 observations that remained (Table 5). The selected detection function (Figure 6) used a hazard rate key function with Beaufort (Figure 8), ScientificName (Figure 9) and Season (Figure 10) as covariates.

Table 5: Observations used to fit the SEFSC AMAPPS detection function.

ScientificName	n
Delphinus, Tursiops, Lagenorhynchus, Steno	1422
Stenella, Lagenodelphis	206
Total	1628

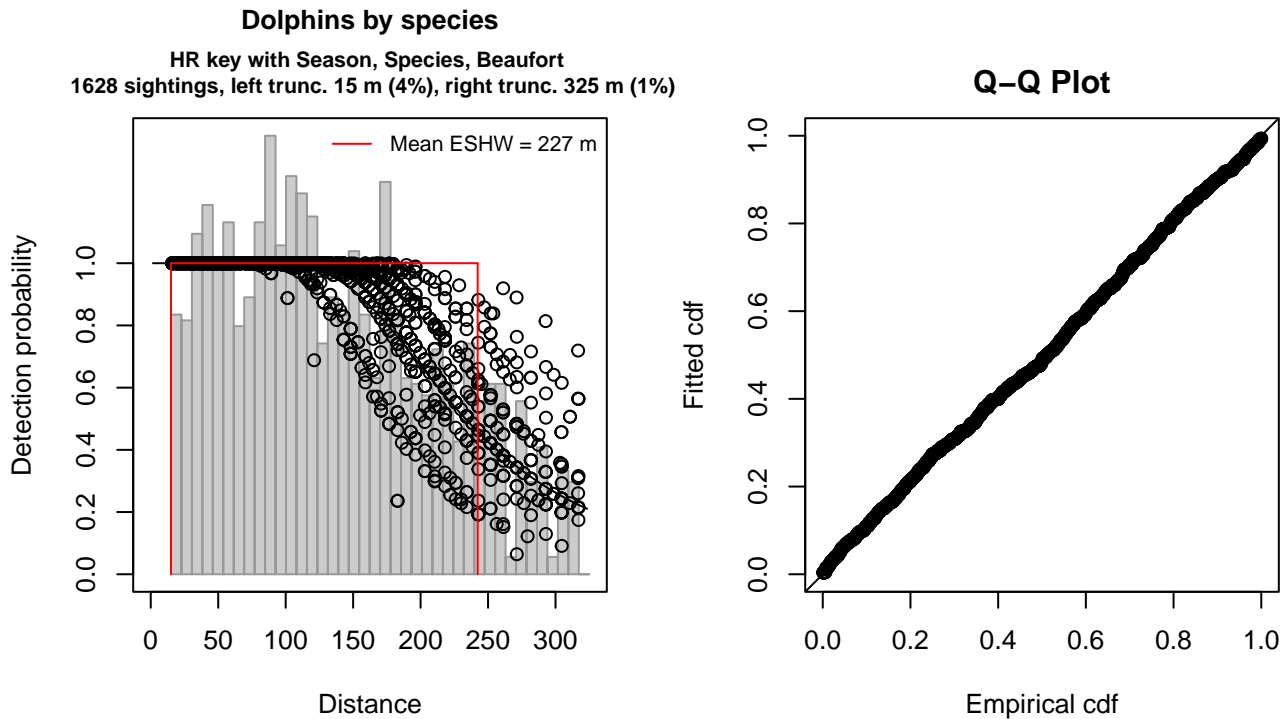


Figure 6: SEFSC AMAPPS detection function and Q-Q plot showing its goodness of fit.

Statistical output for this detection function:

Summary for ds object

Number of observations : 1628
Distance range : 15 - 325
AIC : 18351.39

Detection function:

Hazard-rate key function

Detection function parameters

Scale coefficient(s):

	estimate	se
(Intercept)	5.4780735	0.08251975
SeasonSummer	0.1269645	0.06172358
SeasonWinter	-0.2356803	0.06102237
ScientificNameStenella, Lagenodelphis	0.2204074	0.08699872
Beaufort2	-0.1192230	0.08713320
Beaufort3	-0.1846083	0.08971655
Beaufort4	-0.4027356	0.12330363

Shape coefficient(s):

	estimate	se
(Intercept)	1.266688	0.1150367

	Estimate	SE	CV
Average p	0.720161	0.01522909	0.02114679
N in covered region	2260.605761	56.60731047	0.02504077

Distance sampling Cramer-von Mises test (unweighted)

Test statistic = 0.138923 p = 0.425167

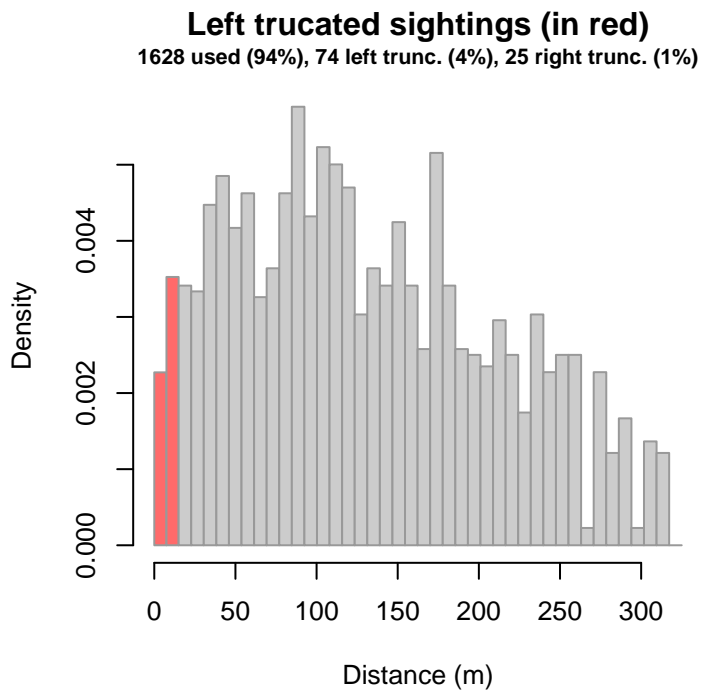


Figure 7: Density histogram of observations used to fit the SEFSC AMAPPS detection function, with the left-most bar showing observations at distances less than 15 m, which were left-truncated and excluded from the analysis [Buckland et al. (2001)]. (This bar may be very short if there were very few left-truncated sightings, or very narrow if the left truncation distance was very small; in either case it may not appear red.)

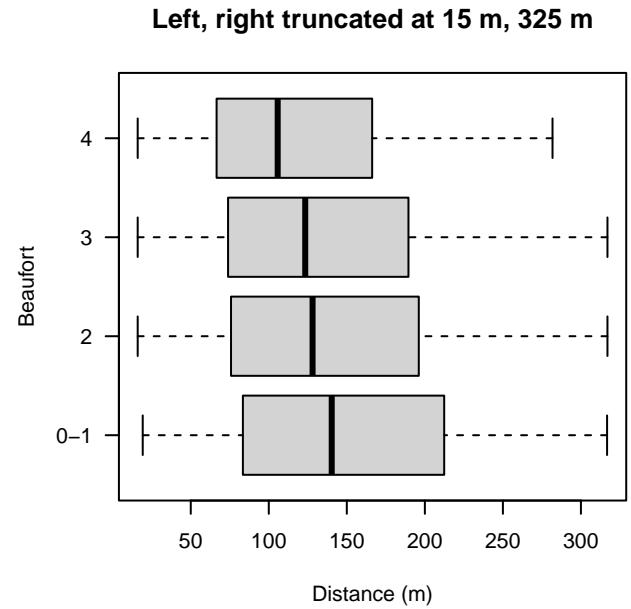
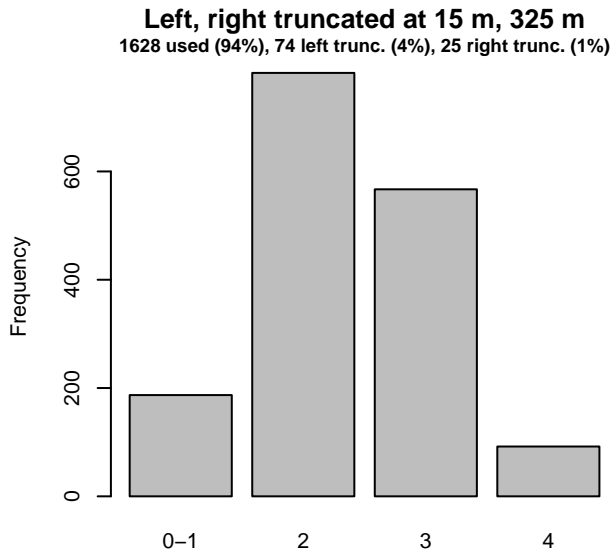
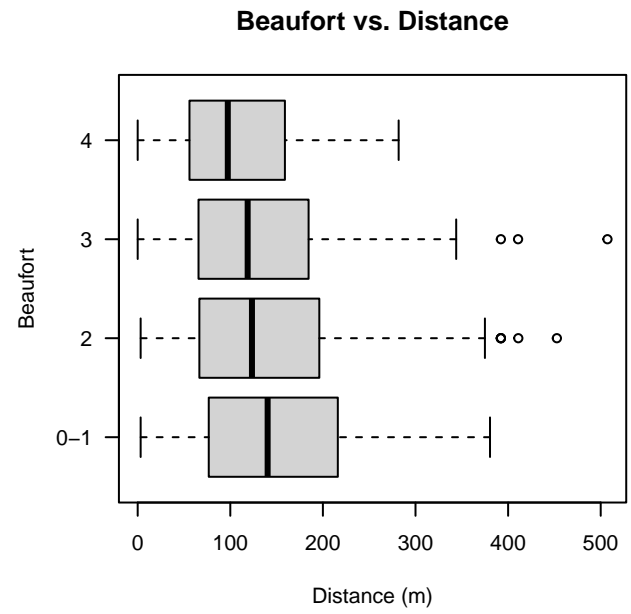
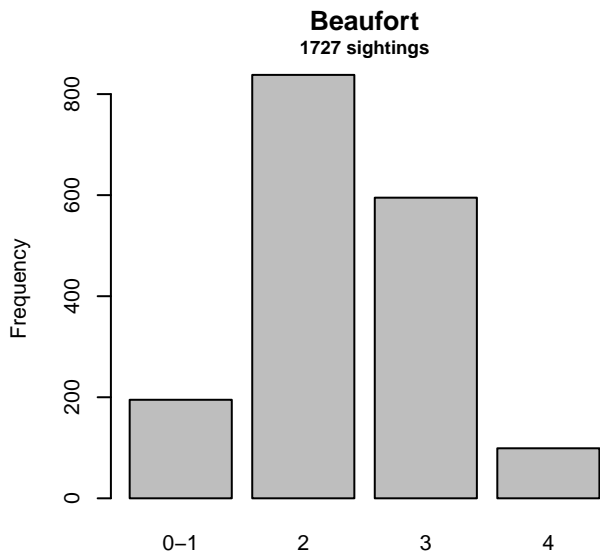


Figure 8: Distribution of the Beaufort covariate before (top row) and after (bottom row) observations were truncated to fit the SEFSC AMAPPS detection function.

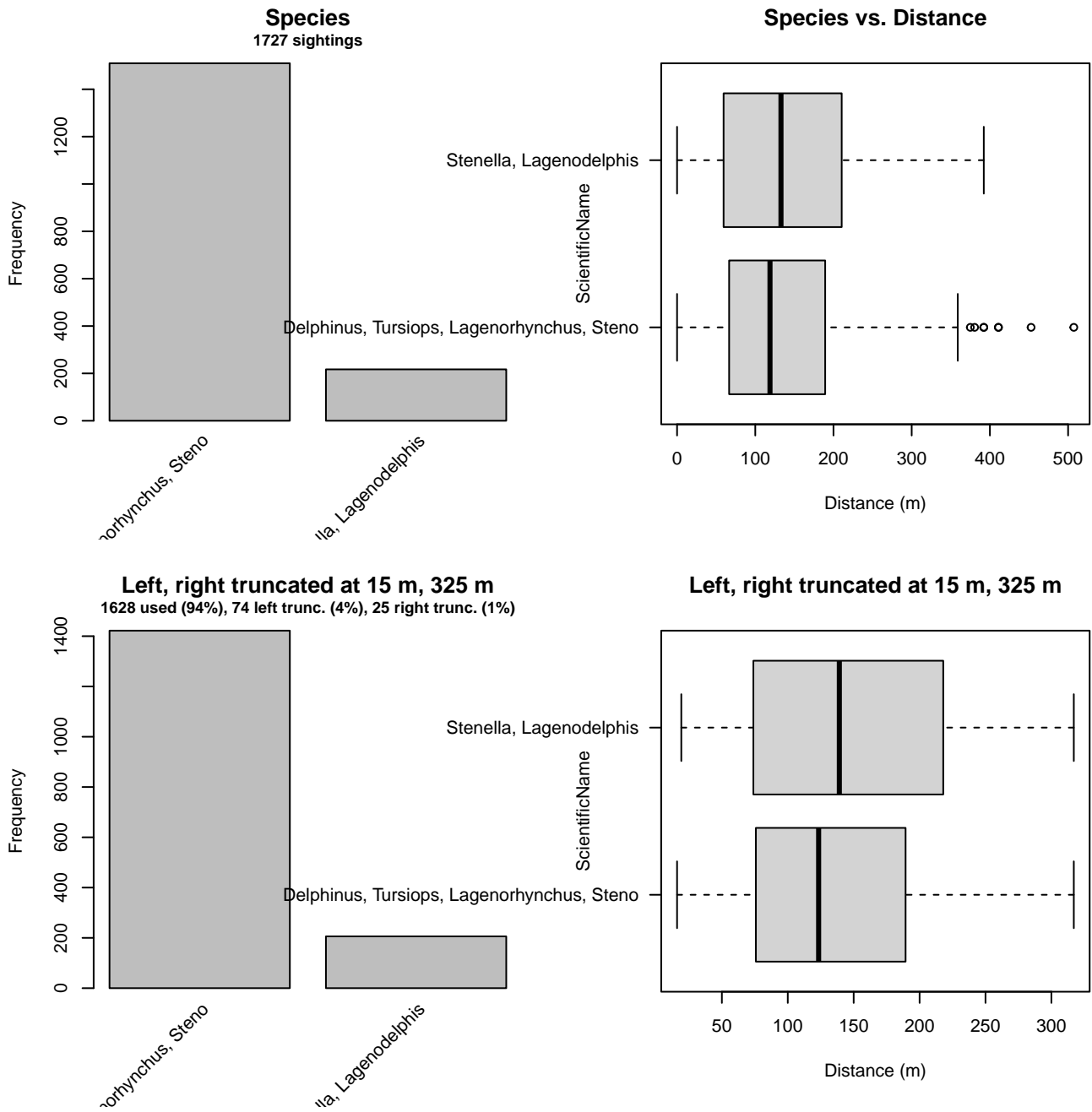


Figure 9: Distribution of the ScientificName covariate before (top row) and after (bottom row) observations were truncated to fit the SEFSC AMAPPS detection function.

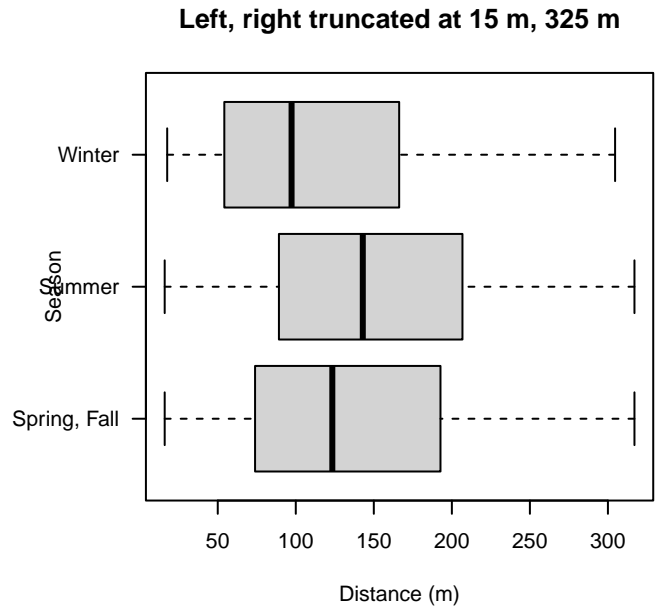
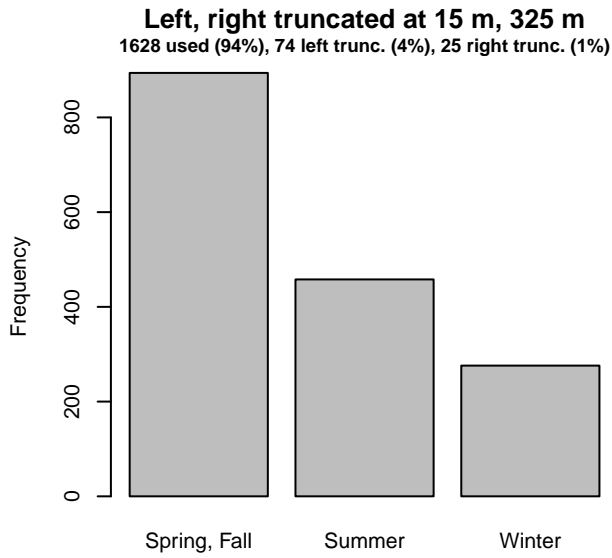
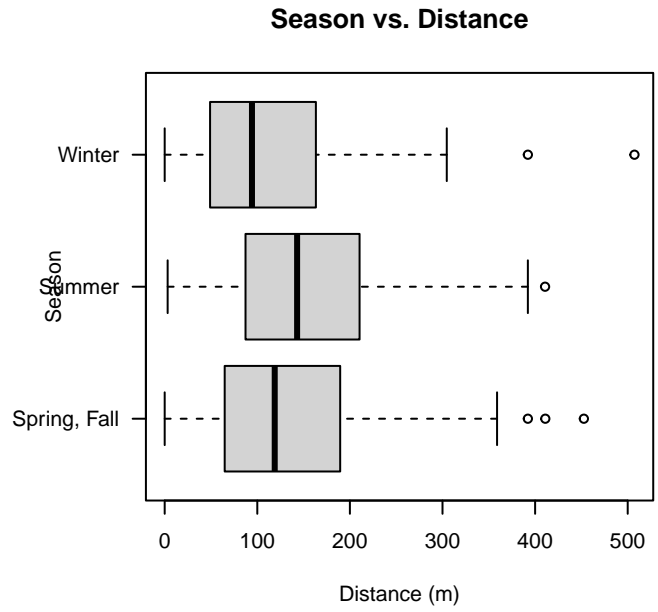
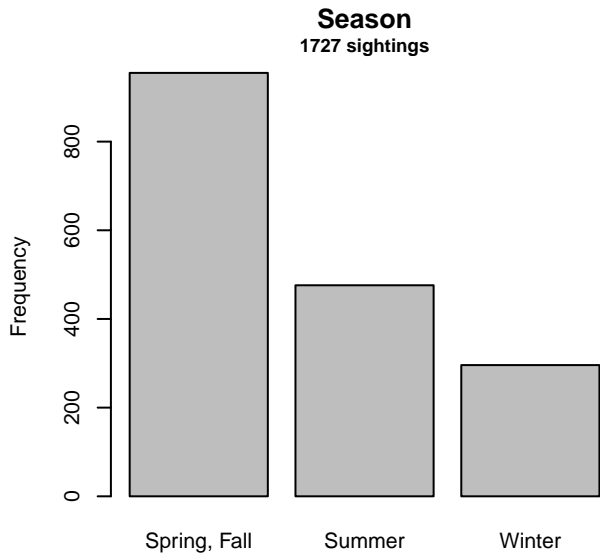


Figure 10: Distribution of the Season covariate before (top row) and after (bottom row) observations were truncated to fit the SEFSC AMAPPS detection function.

2.1.2 Shipboard Surveys

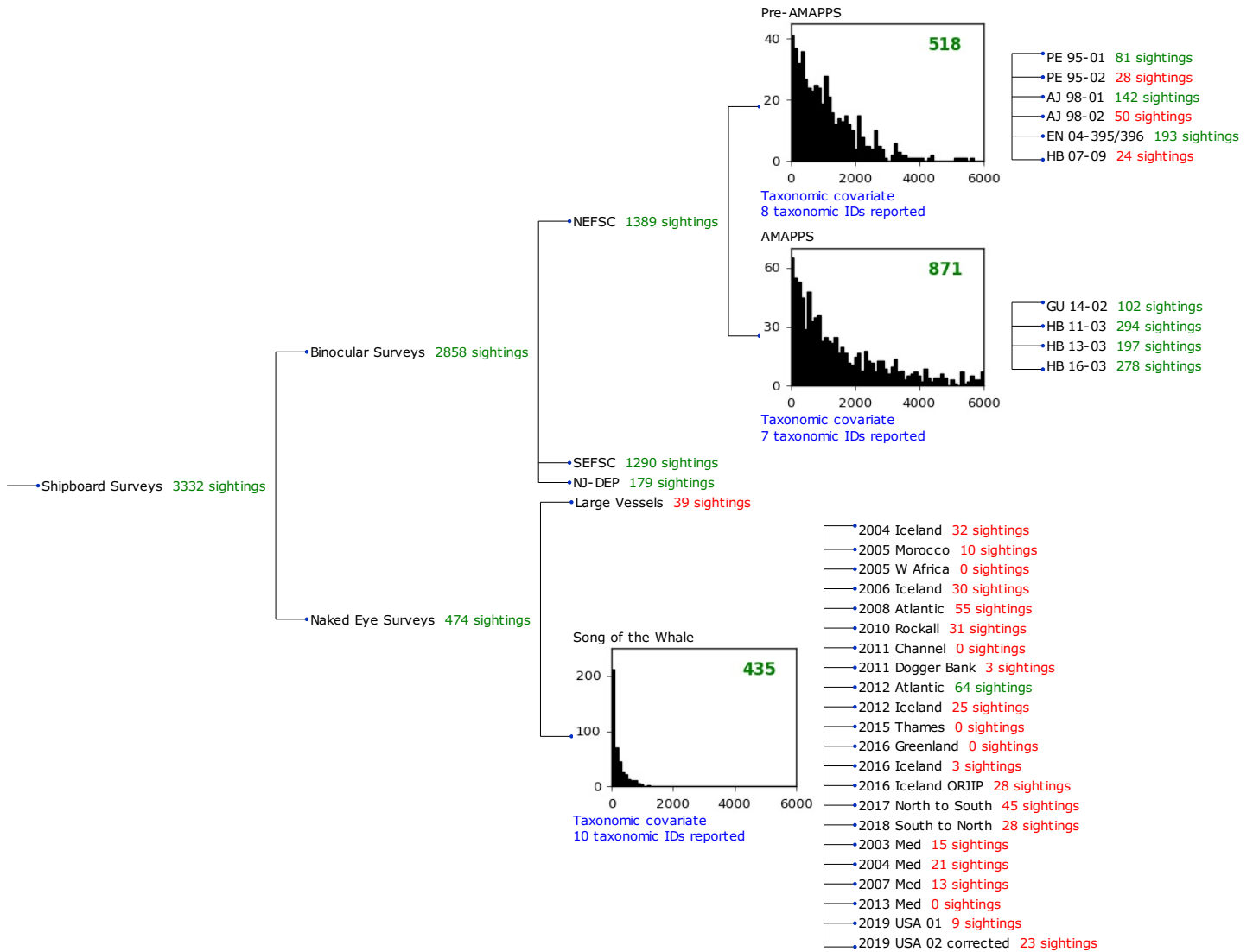


Figure 11: Detection hierarchy for shipboard surveys, showing how they were pooled during detectability modeling, for detection functions that pooled multiple taxa and used a taxonomic covariate to account for differences between them. Each histogram represents a detection function and summarizes the perpendicular distances of observations that were pooled to fit it, prior to truncation. Observation counts, also prior to truncation, are shown in green when they met the recommendation of Buckland et al. (2001) that detection functions utilize at least 60 sightings, and red otherwise. For rare taxa, it was not always possible to meet this recommendation, yielding higher statistical uncertainty. During the spatial modeling stage of the analysis, effective strip widths were computed for each survey using the closest detection function above it in the hierarchy (i.e. moving from right to left in the figure). Surveys that do not have a detection function above them in this figure were either addressed by a detection function presented in a different section of this report, or were omitted from the analysis.

2.1.2.1 NEFSC Pre-AMAPPS

After right-truncating observations greater than 4000 m, we fitted the detection function to the 508 observations that remained (Table 6). The selected detection function (Figure 12) used a hazard rate key function with Beaufort (Figure 13), ScientificName (Figure 14) and VesselName (Figure 15) as covariates.

Table 6: Observations used to fit the NEFSC Pre-AMAPPS detection function.

ScientificName	n
Delphinus, Lagenorhynchus, Tursiops, Steno	365
Other Stenella, Lagenodelphis	130
Stenella frontalis	13
Total	508

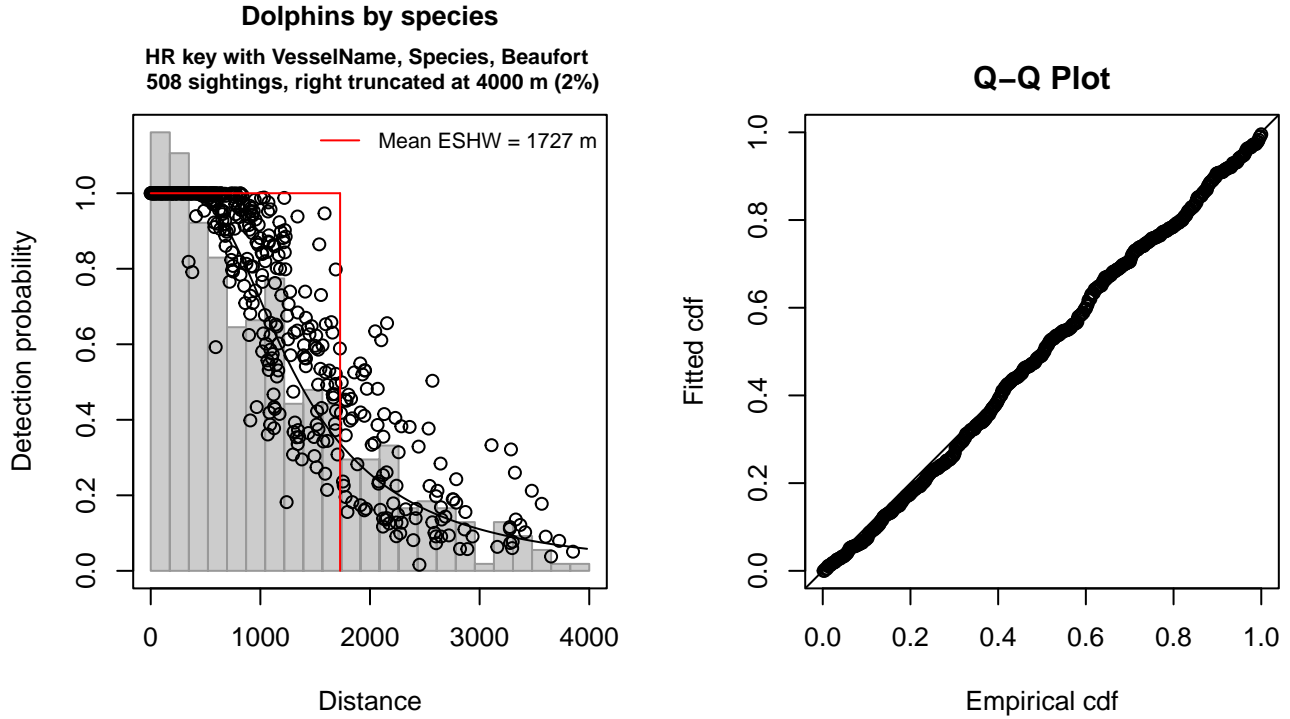


Figure 12: NEFSC Pre-AMAPPS detection function and Q-Q plot showing its goodness of fit.

Statistical output for this detection function:

Summary for ds object

Number of observations : 508
 Distance range : 0 - 4000
 AIC : 8058.614

Detection function:

Hazard-rate key function

Detection function parameters

Scale coefficient(s):

	estimate	se
(Intercept)	7.3979634	0.1986065
VesselNameEndeavor, Bigelow	0.2529041	0.1095209
ScientificNameOther Stenella, Lagenodelphis	0.3555978	0.1258179
ScientificNameStenella frontalis	-0.8556981	0.3078540
Beaufort	-0.1897812	0.0694737

Shape coefficient(s):

	estimate	se
(Intercept)	0.8752144	0.1006522

	Estimate	SE	CV
Average p	0.4071518	0.02118698	0.05203705
N in covered region	1247.6919609	78.15195776	0.06263722

Distance sampling Cramer-von Mises test (unweighted)
 Test statistic = 0.120847 p = 0.492001

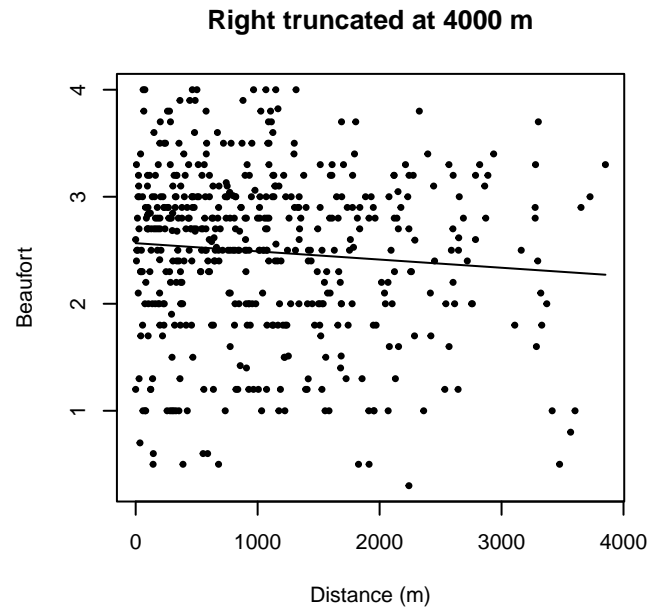
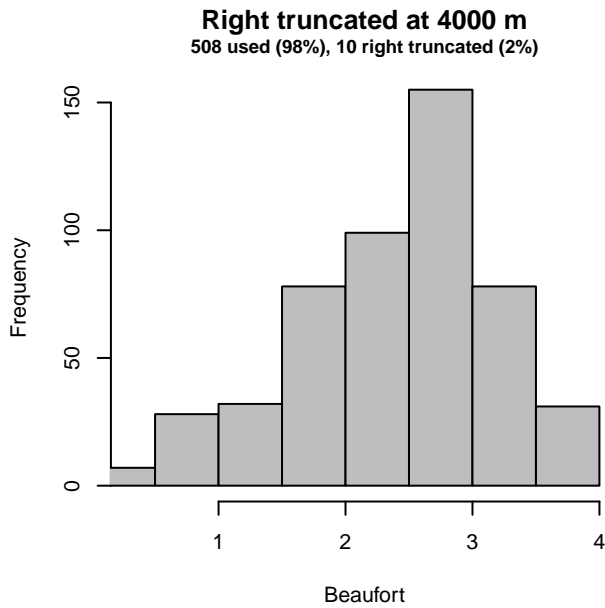
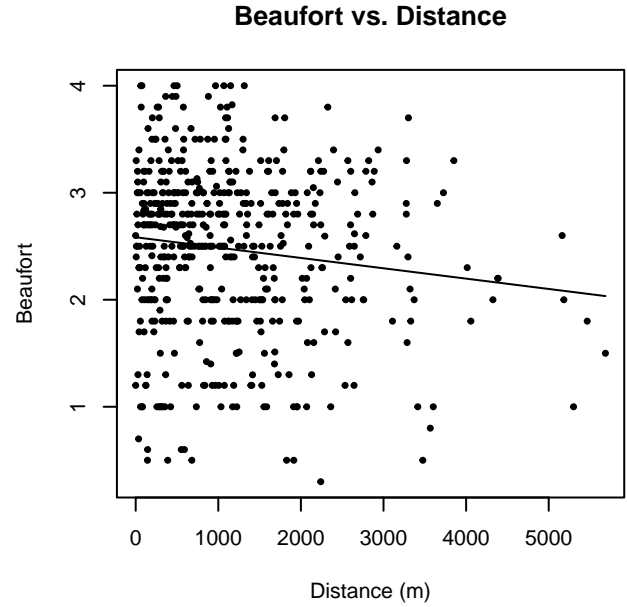
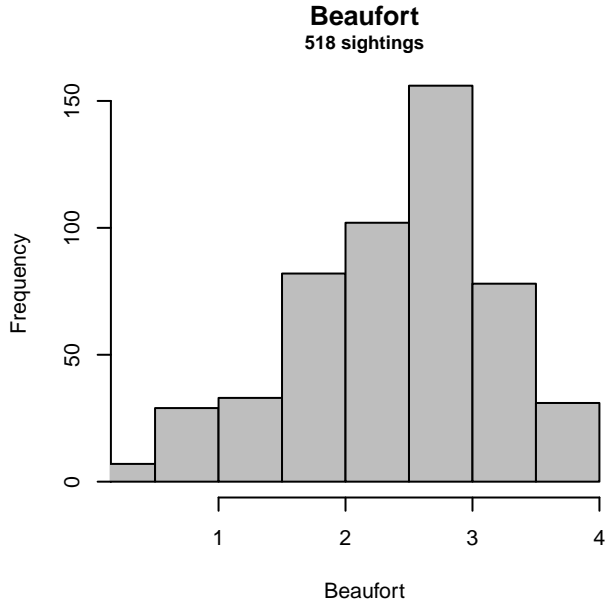


Figure 13: Distribution of the Beaufort covariate before (top row) and after (bottom row) observations were truncated to fit the NEFSC Pre-AMAPPS detection function.

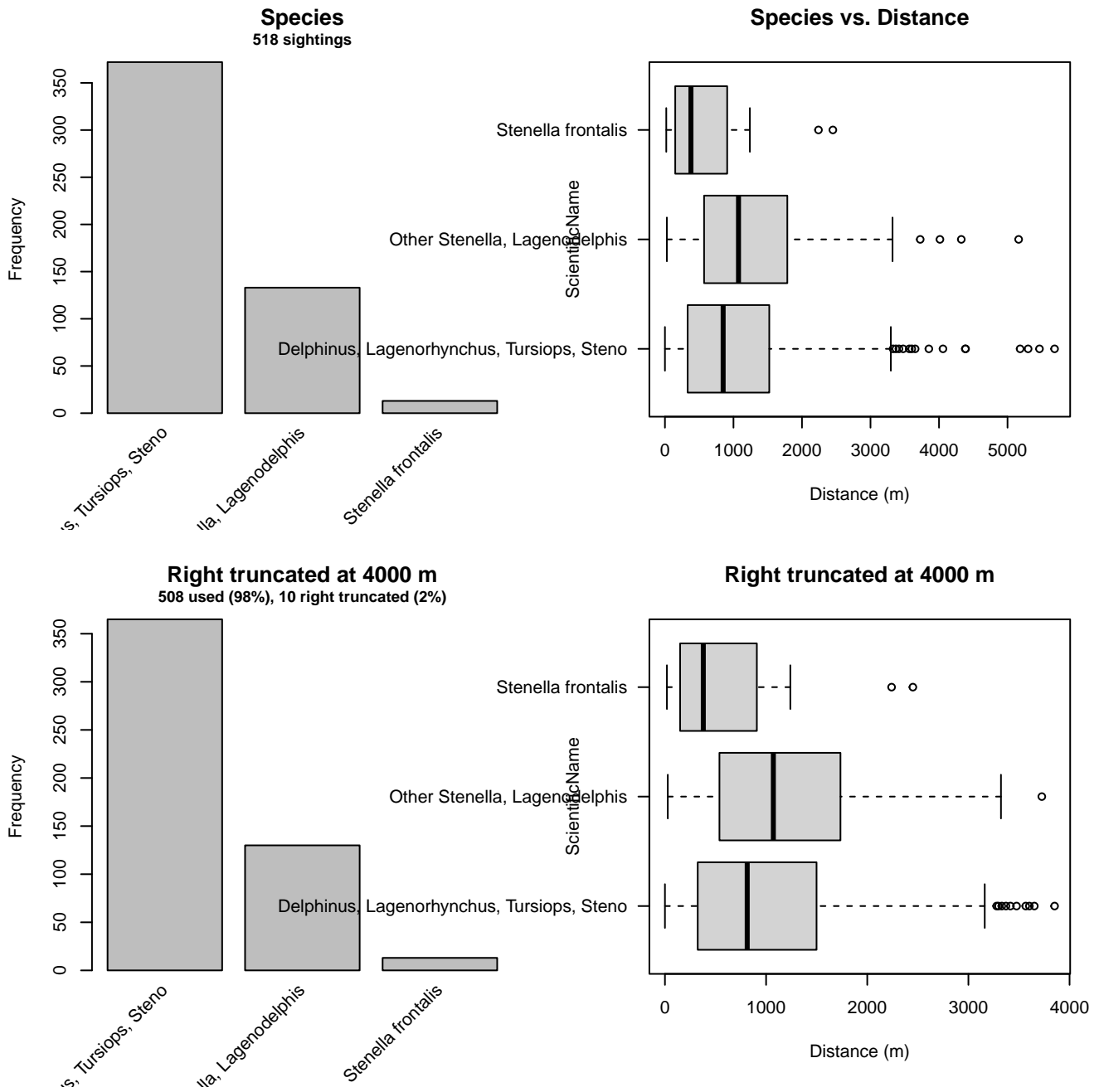


Figure 14: Distribution of the ScientificName covariate before (top row) and after (bottom row) observations were truncated to fit the NEFSC Pre-AMAPPS detection function.

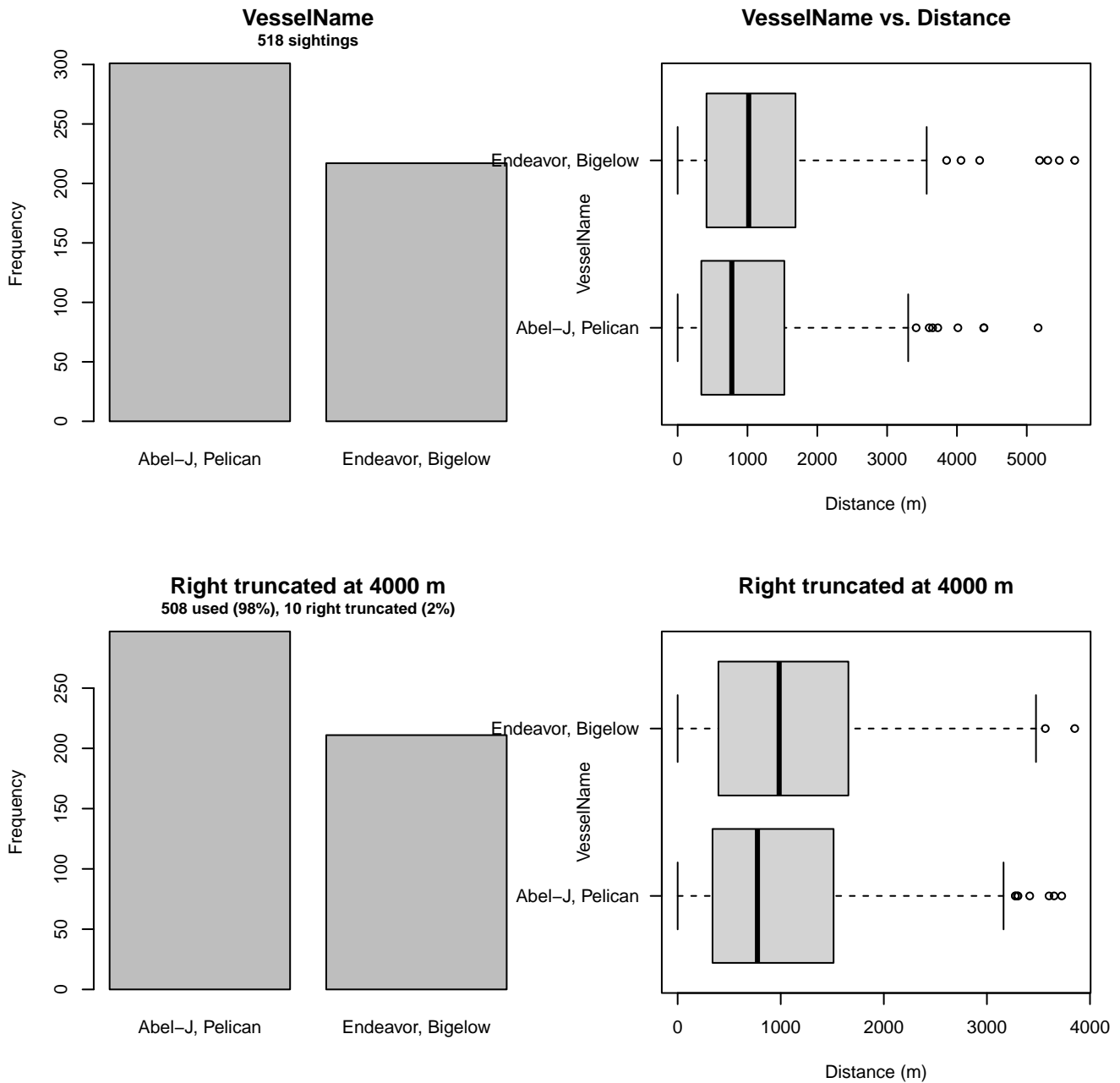


Figure 15: Distribution of the VesselName covariate before (top row) and after (bottom row) observations were truncated to fit the NEFSC Pre-AMAPPS detection function.

2.1.2.2 NEFSC AMAPPS

After right-truncating observations greater than 6000 m, we fitted the detection function to the 857 observations that remained (Table 7). The selected detection function (Figure 16) used a hazard rate key function with Beaufort (Figure 17) and ScientificName (Figure 18) as covariates.

Table 7: Observations used to fit the NEFSC AMAPPS detection function.

ScientificName	n
Delphinus, Lagenorhynchus	358
Other Stenella, Lagenodelphis	175
Stenella frontalis	53
Tursiops, Steno	271
Total	857

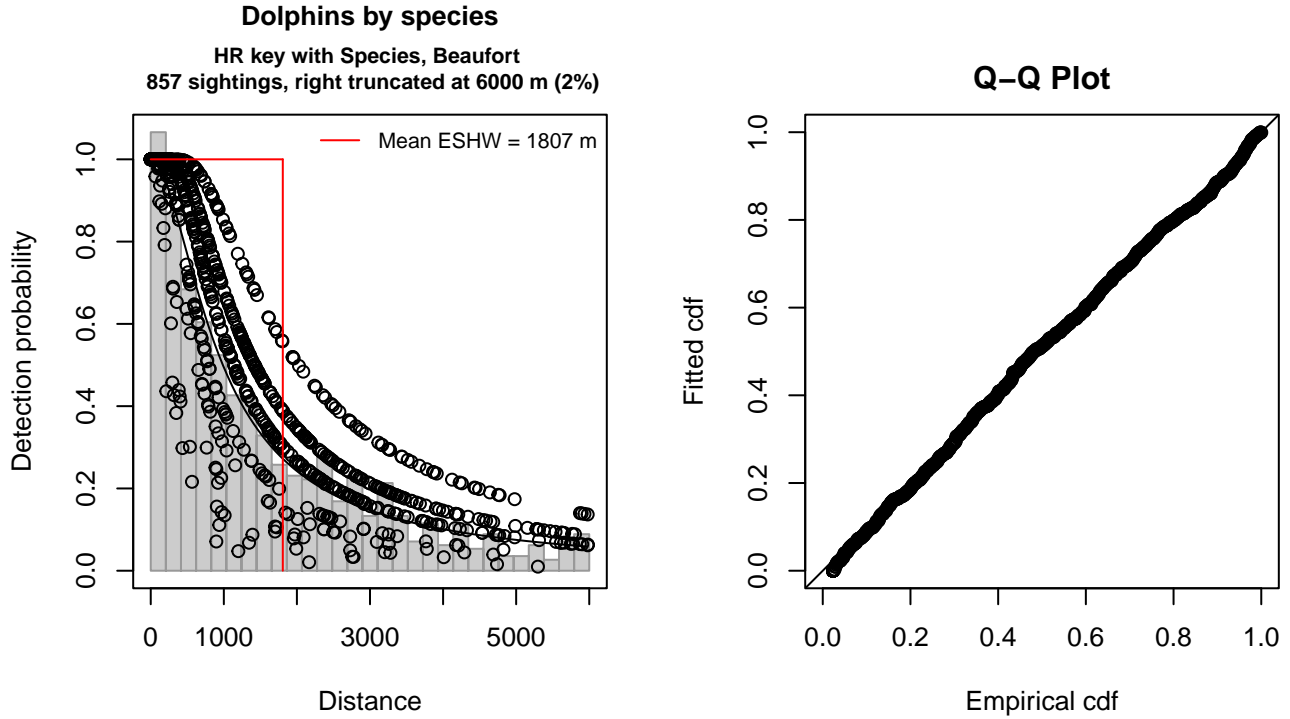


Figure 16: NEFSC AMAPPS detection function and Q-Q plot showing its goodness of fit.

Statistical output for this detection function:

Summary for ds object

Number of observations : 857
 Distance range : 0 - 6000
 AIC : 14222.66

Detection function:

Hazard-rate key function

Detection function parameters

Scale coefficient(s):

	estimate	se
(Intercept)	7.0022801	0.1342692
ScientificNameOther Stenella, Lagenodelphis	0.3515378	0.1854896
ScientificNameStenella frontalis	-0.5910499	0.3033455
ScientificNameTursiops, Steno	-0.2176361	0.1602756
Beaufort3-4	-0.5842019	0.1839783
Beaufort4-5	-1.4374209	0.2667762

Shape coefficient(s):

estimate	se
----------	----

(Intercept) 0.356339 0.0663051

	Estimate	SE	CV
Average p	0.2624967	0.01868208	0.07117073
N in covered region	3264.8026106	252.27662296	0.07727163

Distance sampling Cramer-von Mises test (unweighted)
Test statistic = 0.089267 p = 0.640081

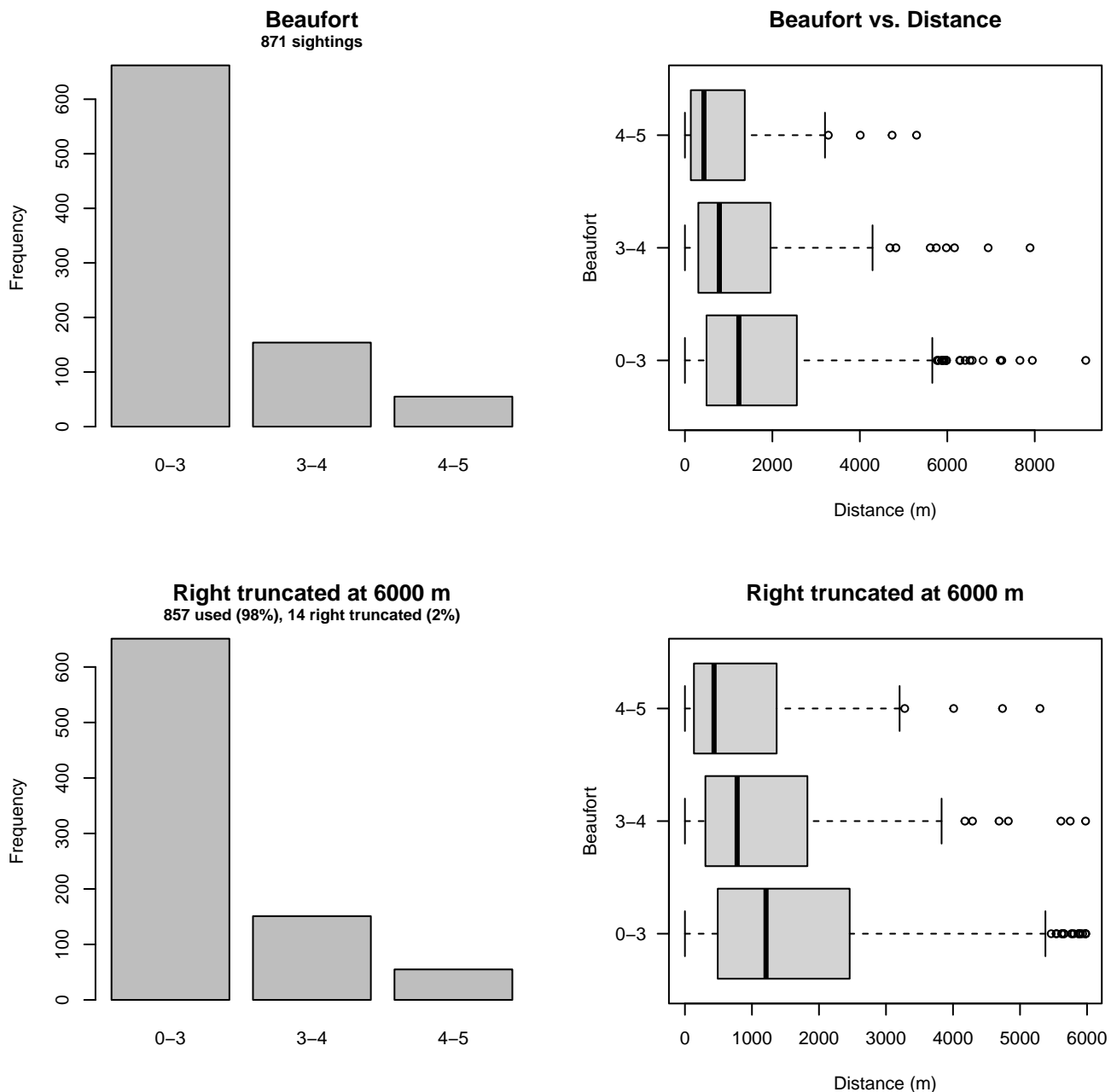


Figure 17: Distribution of the Beaufort covariate before (top row) and after (bottom row) observations were truncated to fit the NEFSC AMAPPS detection function.

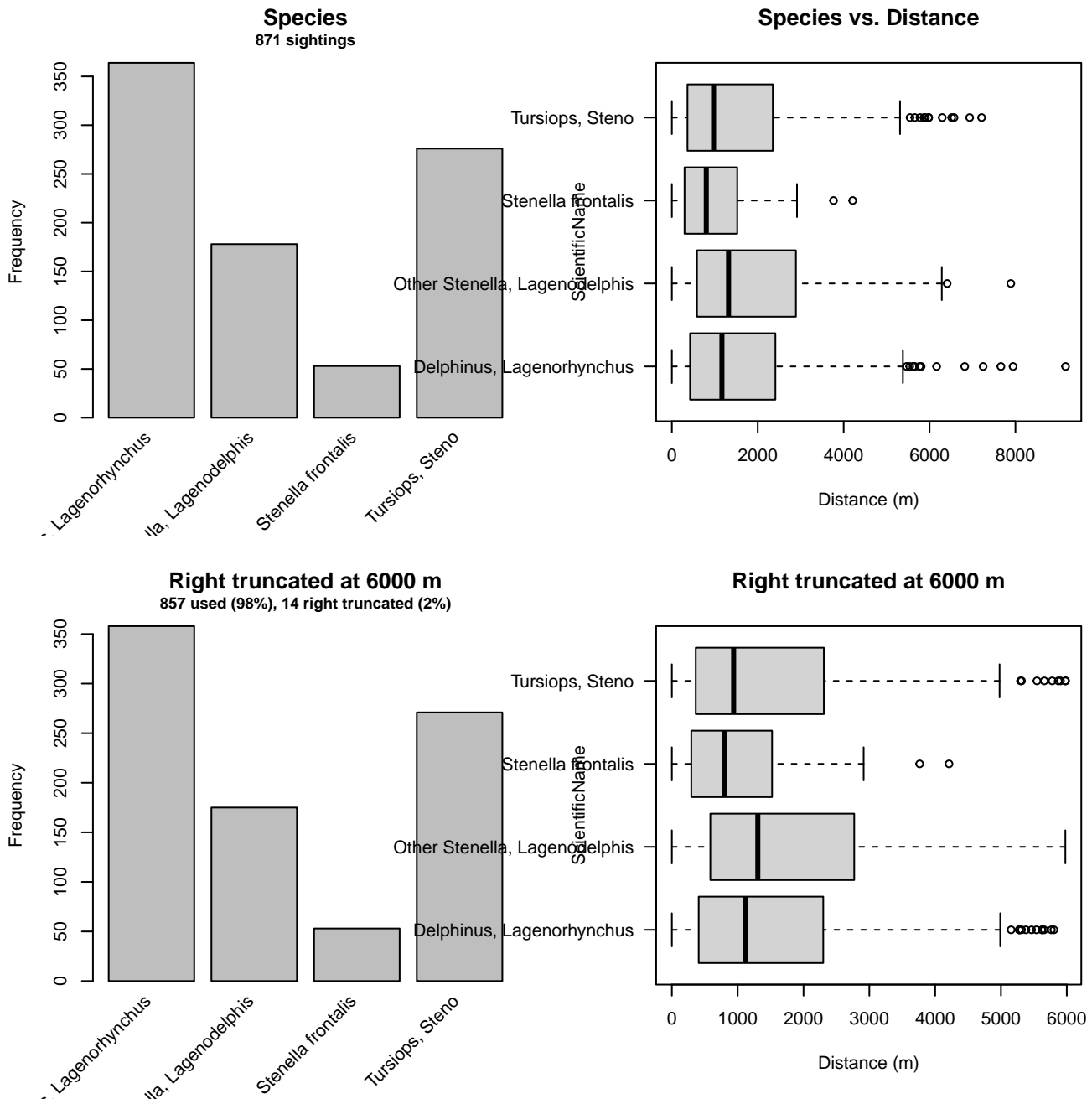


Figure 18: Distribution of the ScientificName covariate before (top row) and after (bottom row) observations were truncated to fit the NEFSC AMAPPS detection function.

2.1.2.3 Song of the Whale

After right-truncating observations greater than 700 m and left-truncating observations less than 1 m (Figure 20), we fitted the detection function to the 360 observations that remained (Table 8). The selected detection function (Figure 19) used a hazard rate key function with Beaufort (Figure 21), ScientificName (Figure 22) and Visibility (Figure 23) as covariates.

Table 8: Observations used to fit the Song of the Whale detection function.

ScientificName	n
All others	211
Delphinus	149
Total	360

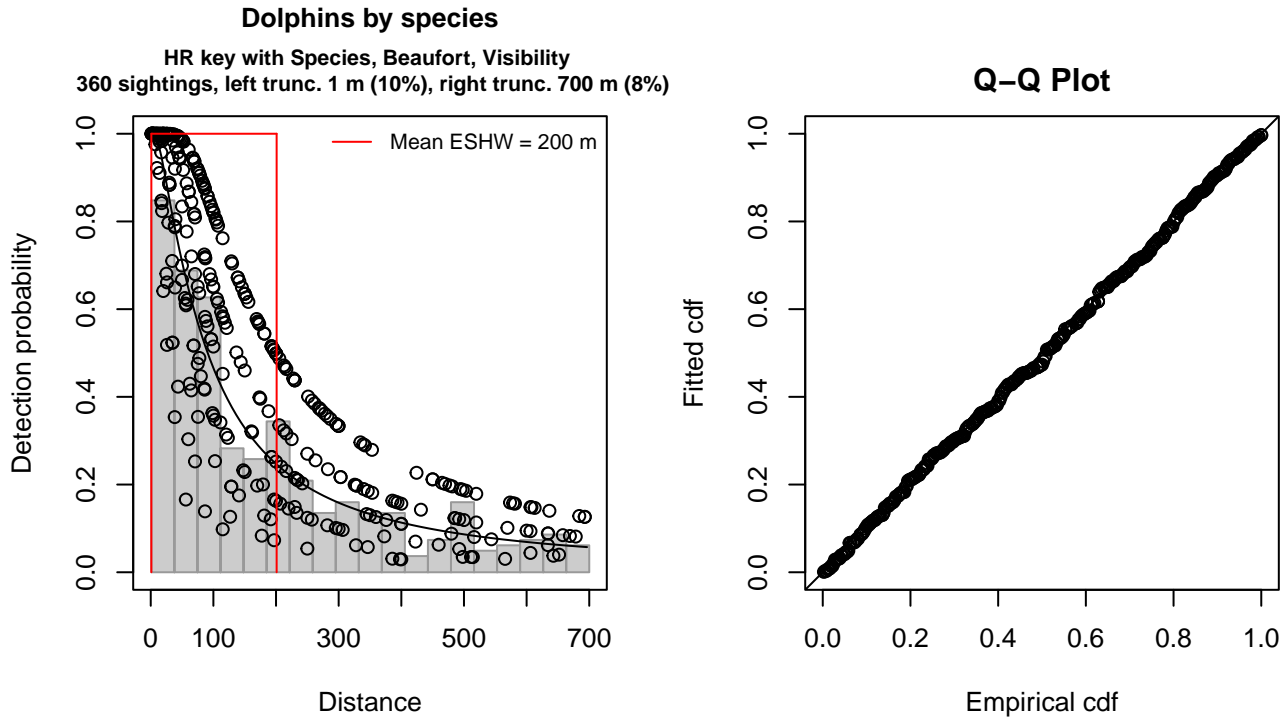


Figure 19: Song of the Whale detection function and Q-Q plot showing its goodness of fit.

Statistical output for this detection function:

Summary for ds object

Number of observations : 360
 Distance range : 1 - 700
 AIC : 4434.06

Detection function:

Hazard-rate key function

Detection function parameters

Scale coefficient(s):

	estimate	se
(Intercept)	5.0168382	0.2118228
ScientificNameDelphinus	-0.3746003	0.2526245
Beaufort3	-0.6586604	0.2922112
Beaufort3.5-4	-1.3223280	0.3841776
VisibilityModerate (2-5nmi)	-0.9687696	0.4363084

Shape coefficient(s):

	estimate	se
(Intercept)	0.2728327	0.09542948

	Estimate	SE	CV
Average p	0.232512	0.02944422	0.1266352
N in covered region	1548.306965	209.54903632	0.1353408

Distance sampling Cramer-von Mises test (unweighted)

Test statistic = 0.019198 p = 0.997687

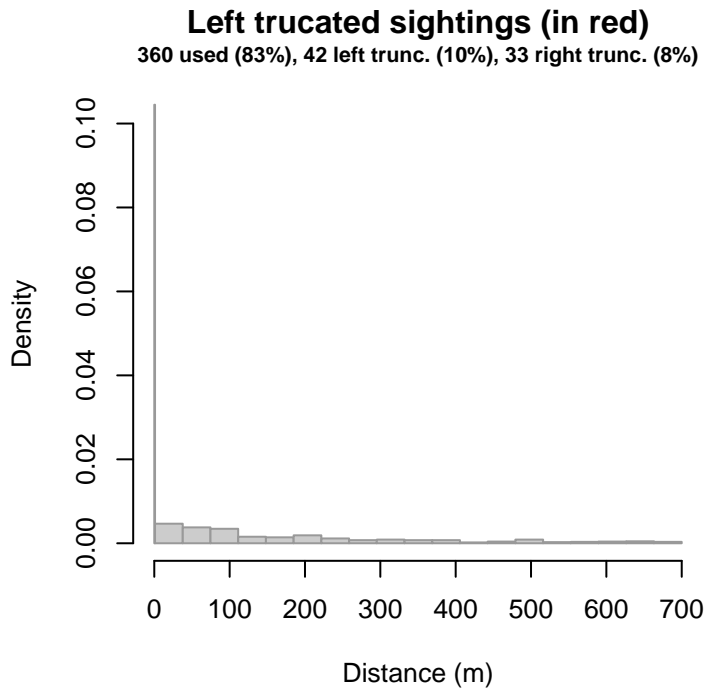


Figure 20: Density histogram of observations used to fit the Song of the Whale detection function, with the left-most bar showing observations at distances less than 1 m, which were left-truncated and not used to fit the detection function. (This bar may be very short if there were very few left-truncated sightings, or very narrow if the left truncation distance was very small; in either case it may not appear red.) These were excluded because they formed a problematic "spike" in detections close to the trackline, suggesting that animals approached the vessel (e.g. to bow-ride) prior to being detected. To address this, we fitted the detection function to the observations beyond the spike and assumed that within it, detection probability was 1, effectively treating it like a strip transect. We then added the left-truncated observations back into the analysis as if they occurred in this strip. This treatment may have resulted in an underestimation of detection probability.

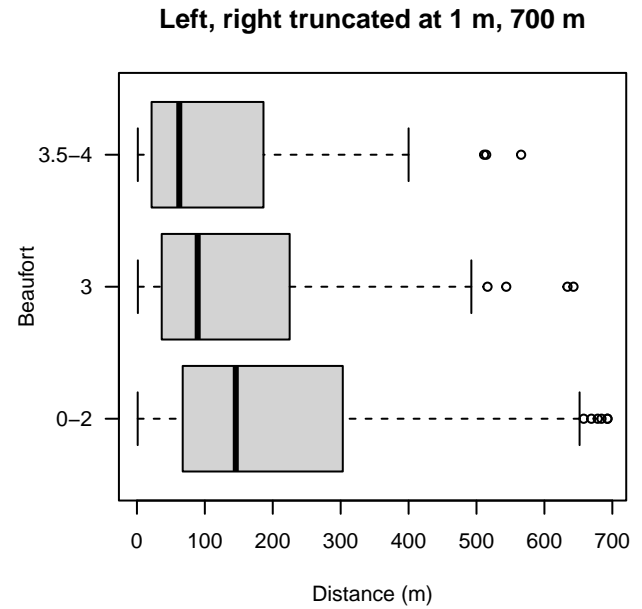
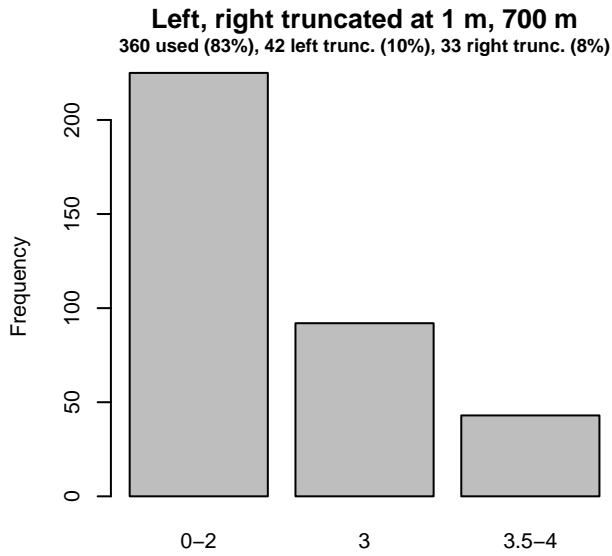
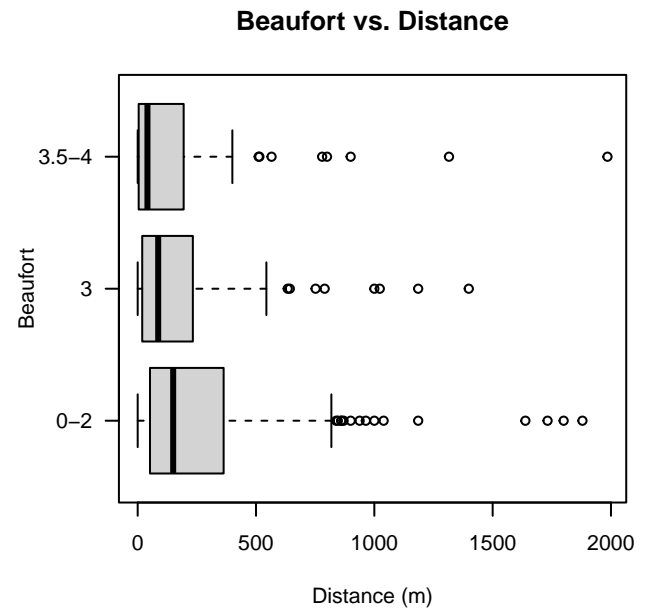
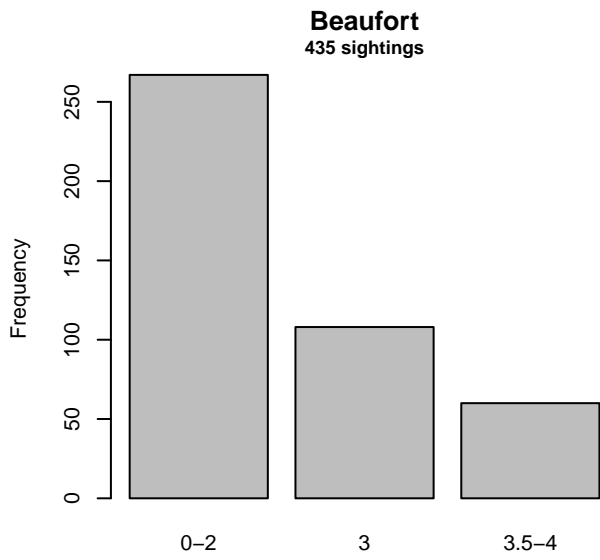


Figure 21: Distribution of the Beaufort covariate before (top row) and after (bottom row) observations were truncated to fit the Song of the Whale detection function.

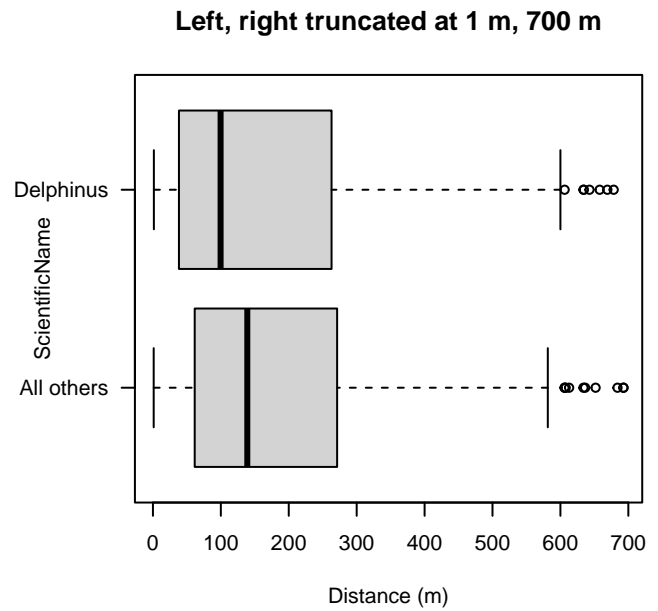
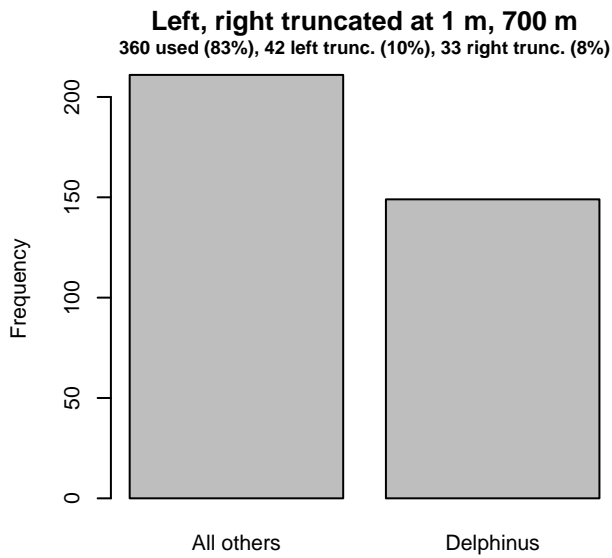
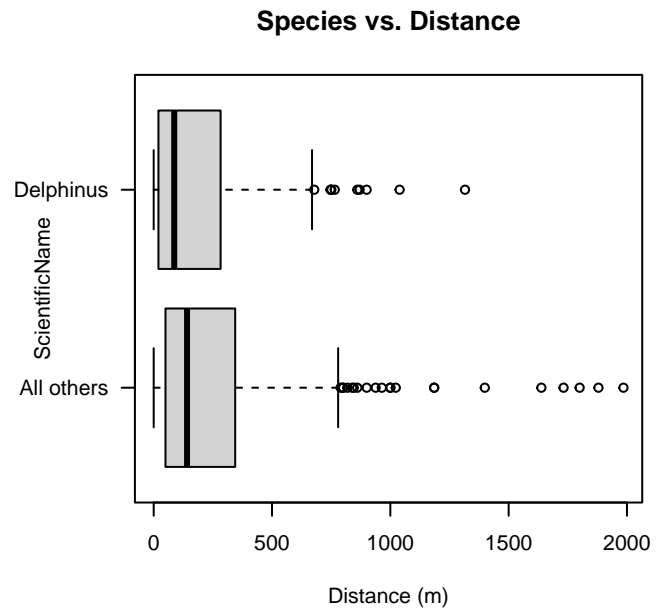
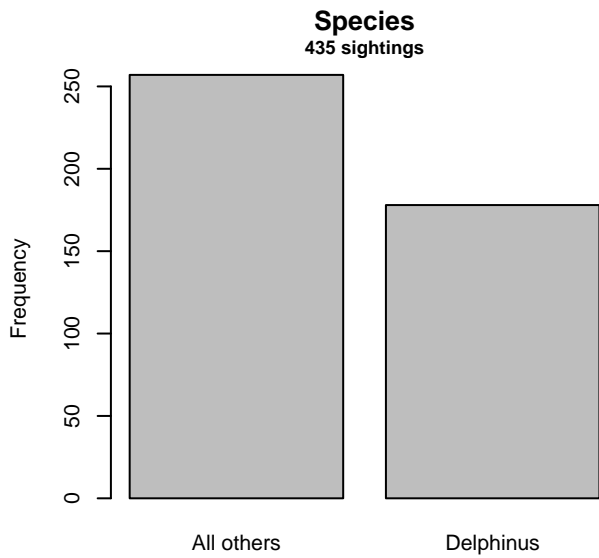


Figure 22: Distribution of the ScientificName covariate before (top row) and after (bottom row) observations were truncated to fit the Song of the Whale detection function.

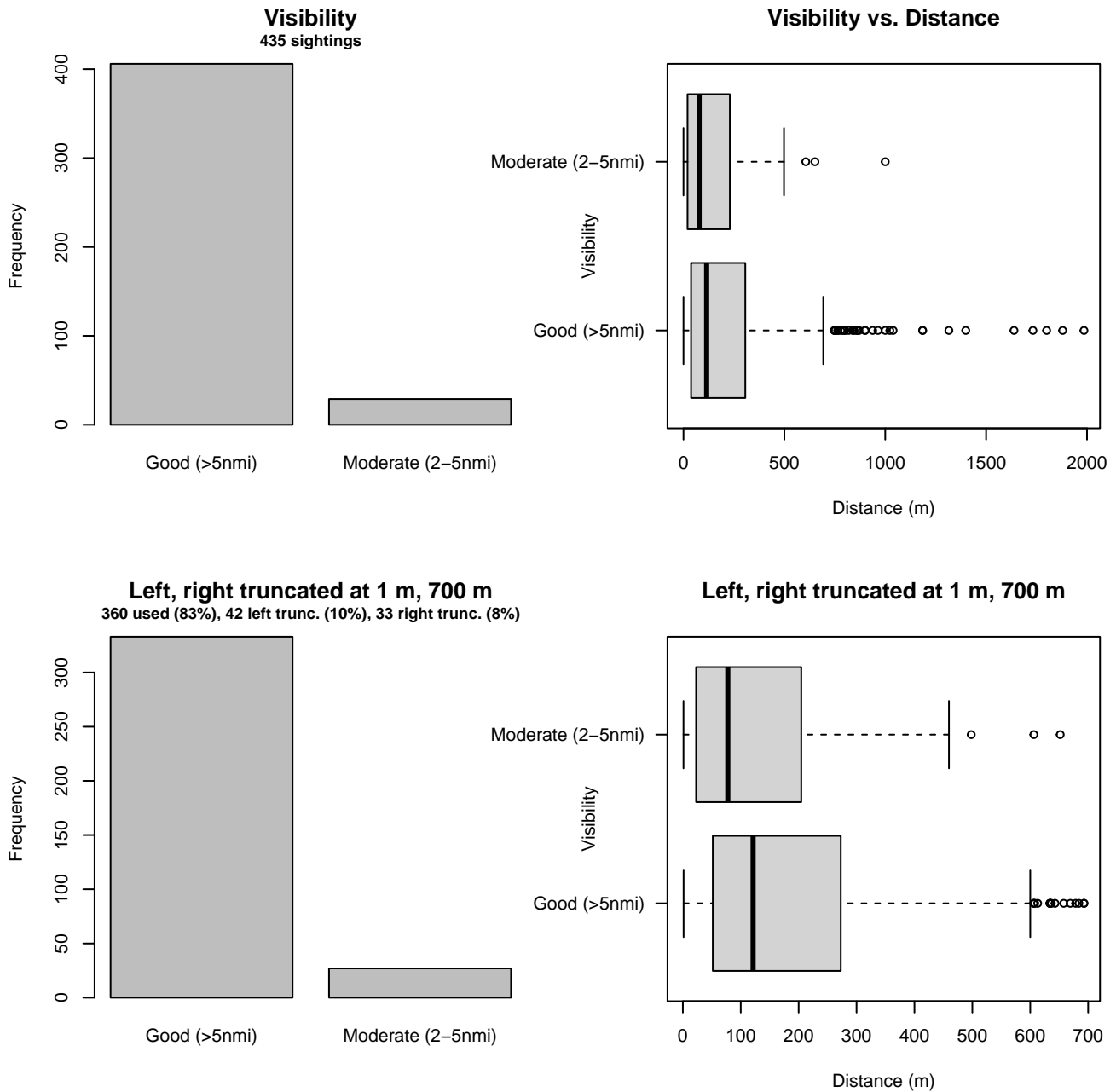


Figure 23: Distribution of the Visibility covariate before (top row) and after (bottom row) observations were truncated to fit the Song of the Whale detection function.

2.2 Without a Taxonomic Covariate

We fitted the detection functions in this section to pools of species with similar detectability characteristics but could not use a taxonomic identification as a covariate to account for differences between them. We usually took this approach after trying the taxonomic covariate and finding it had insufficient statistical power to be retained. We also resorted to it when the focal taxon being modeled had too few observations to be allocated its own taxonomic covariate level and was too poorly known for us to confidently determine which other taxa we could group it with.

2.2.1 Aerial Surveys

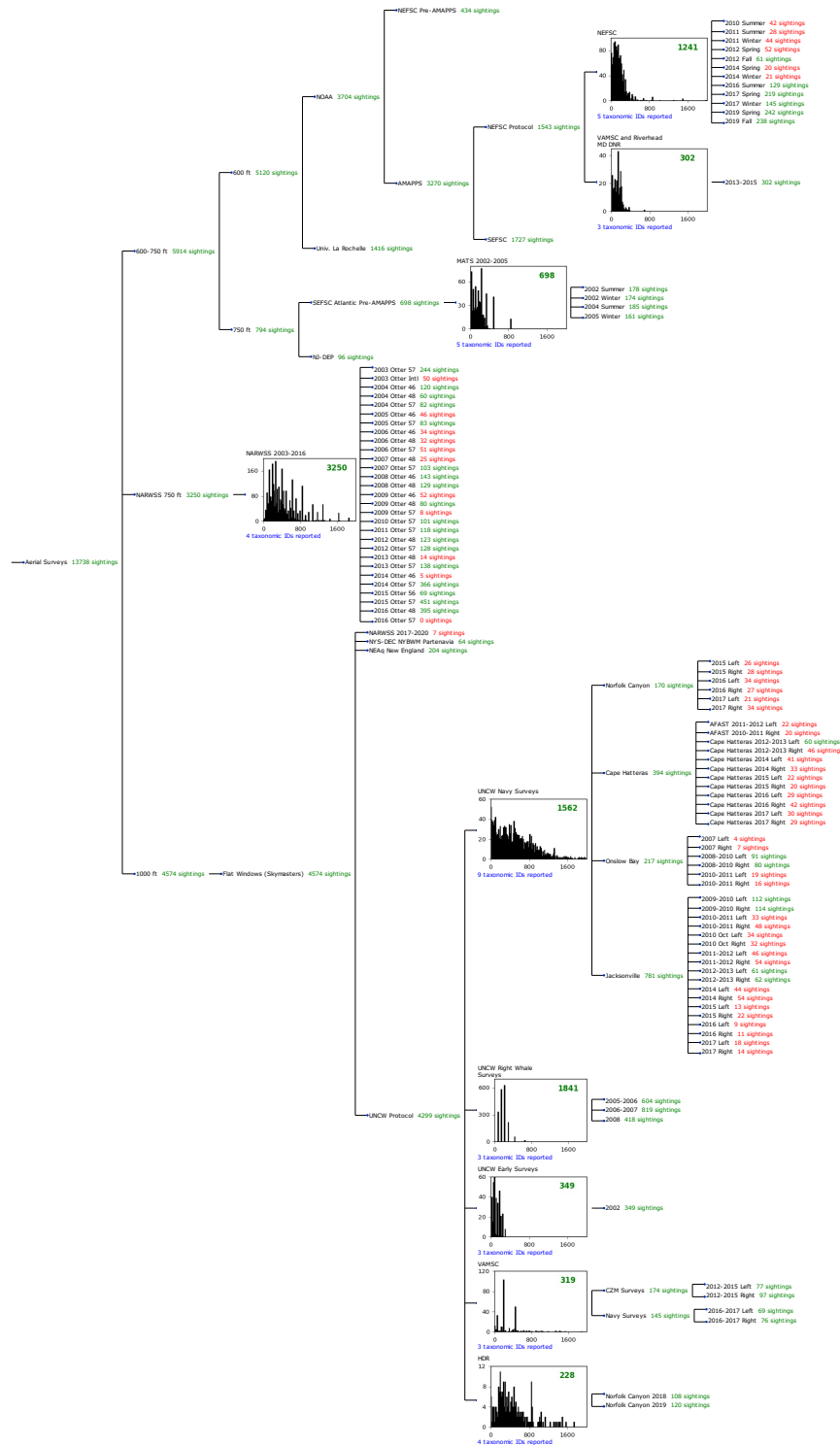


Figure 24: Detection hierarchy for aerial surveys, showing how they were pooled during detectability modeling, for detection functions that pooled multiple taxa but could not use a taxonomic covariate to account for differences between them. Each histogram represents a detection function and summarizes the perpendicular distances of observations that were pooled to fit it, prior to truncation. Observation counts, also prior to truncation, are shown in green when they met the recommendation of Buckland et al. (2001) that detection functions utilize at least 60 sightings, and red otherwise. For rare taxa, it was not always possible to meet this recommendation, yielding higher statistical uncertainty. During the spatial modeling stage of the analysis, effective strip widths were computed for each survey using the closest detection function above it in the hierarchy (i.e. moving from right to left in the figure). Surveys that do not have a detection function above them in this figure were either addressed by a detection function presented in a different section of this report, or were omitted from the analysis.

2.2.1.1 NEFSC AMAPPS

After right-truncating observations greater than 600 m, we fitted the detection function to the 1218 observations that remained (Table 9). The selected detection function (Figure 25) used a hazard rate key function with Season (Figure 26) as a covariate.

Table 9: Observations used to fit the NEFSC AMAPPS detection function.

ScientificName	n
Delphinus delphis	817
Lagenorhynchus acutus	280
Lagenorhynchus albirostris	3
Stenella coeruleoalba	13
Tursiops truncatus	105
Total	1218

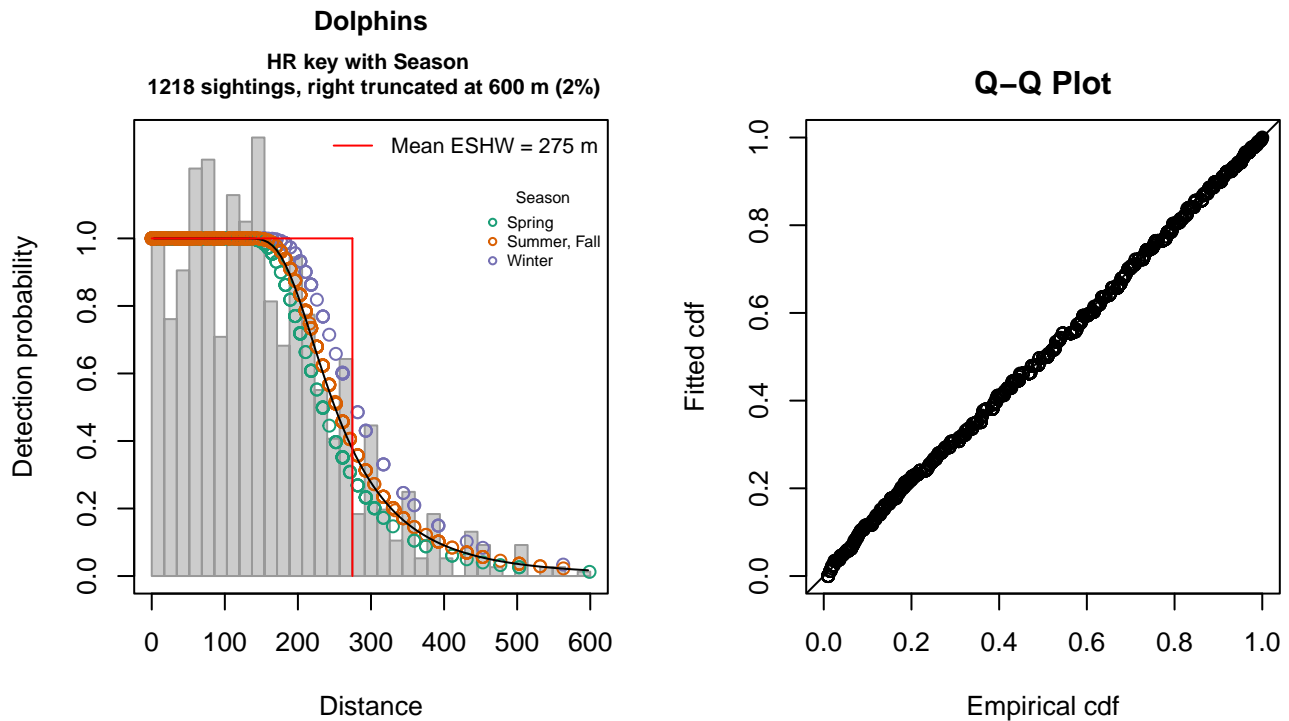


Figure 25: NEFSC AMAPPS detection function and Q-Q plot showing its goodness of fit.

Statistical output for this detection function:

Summary for ds object

Number of observations : 1218
 Distance range : 0 - 600
 AIC : 14460.69

Detection function:

Hazard-rate key function

Detection function parameters

Scale coefficient(s):

	estimate	se
(Intercept)	5.36944749	0.04422696
SeasonSummer, Fall	0.08083579	0.04638562
SeasonWinter	0.17600218	0.07702020

Shape coefficient(s):

	estimate	se
(Intercept)	1.452854	0.065484

	Estimate	SE	CV
Average p	0.456561	0.00970389	0.02125431
N in covered region	2667.770370	79.97999993	0.02998009

Distance sampling Cramer-von Mises test (unweighted)
 Test statistic = 0.126854 p = 0.468488

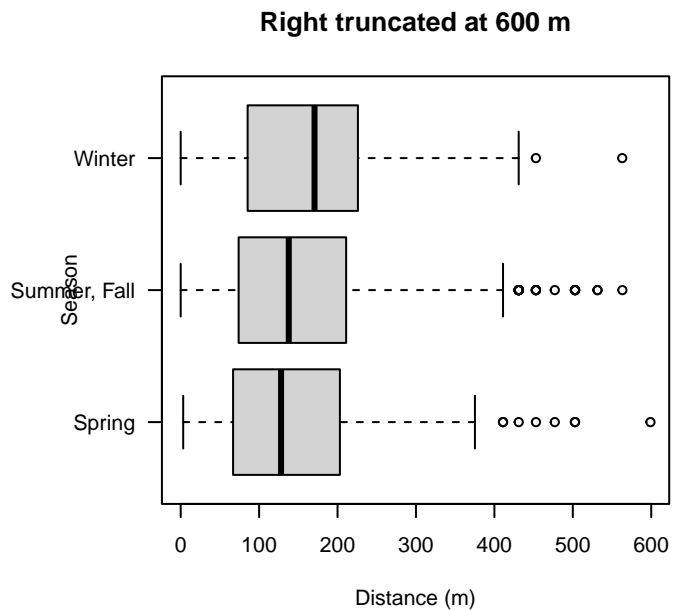
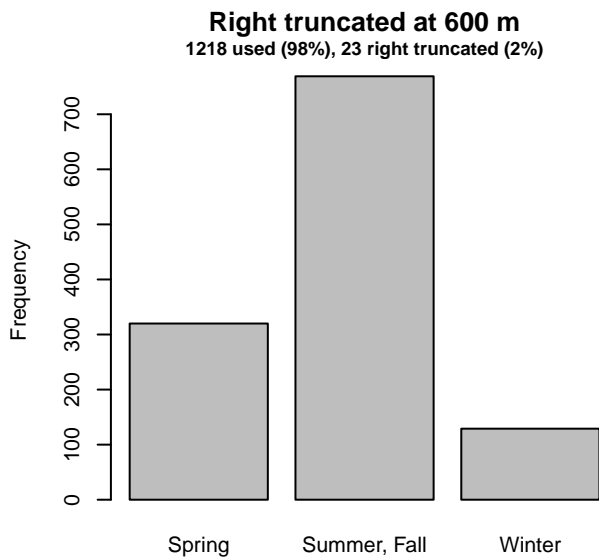
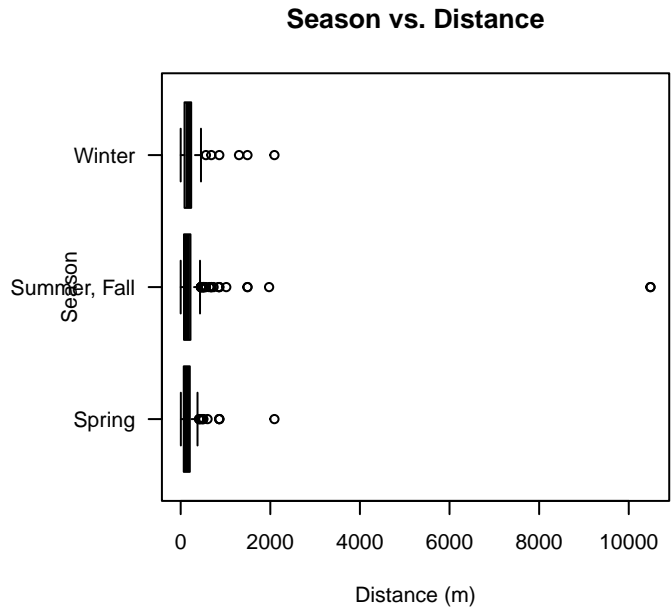
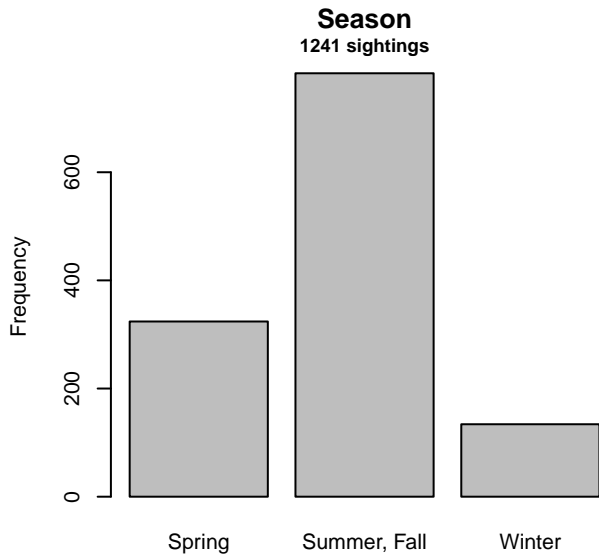


Figure 26: Distribution of the Season covariate before (top row) and after (bottom row) observations were truncated to fit the NEFSC AMAPPS detection function.

2.2.1.2 VAMSC and Riverhead MD DNR

After right-truncating observations greater than 400 m, we fitted the detection function to the 301 observations that remained (Table 10). The selected detection function (Figure 27) used a hazard rate key function with no covariates.

Table 10: Observations used to fit the VAMSC and Riverhead MD DNR detection function.

ScientificName	n
Delphinus delphis	22
Stenella frontalis	1
Tursiops truncatus	278
Total	301

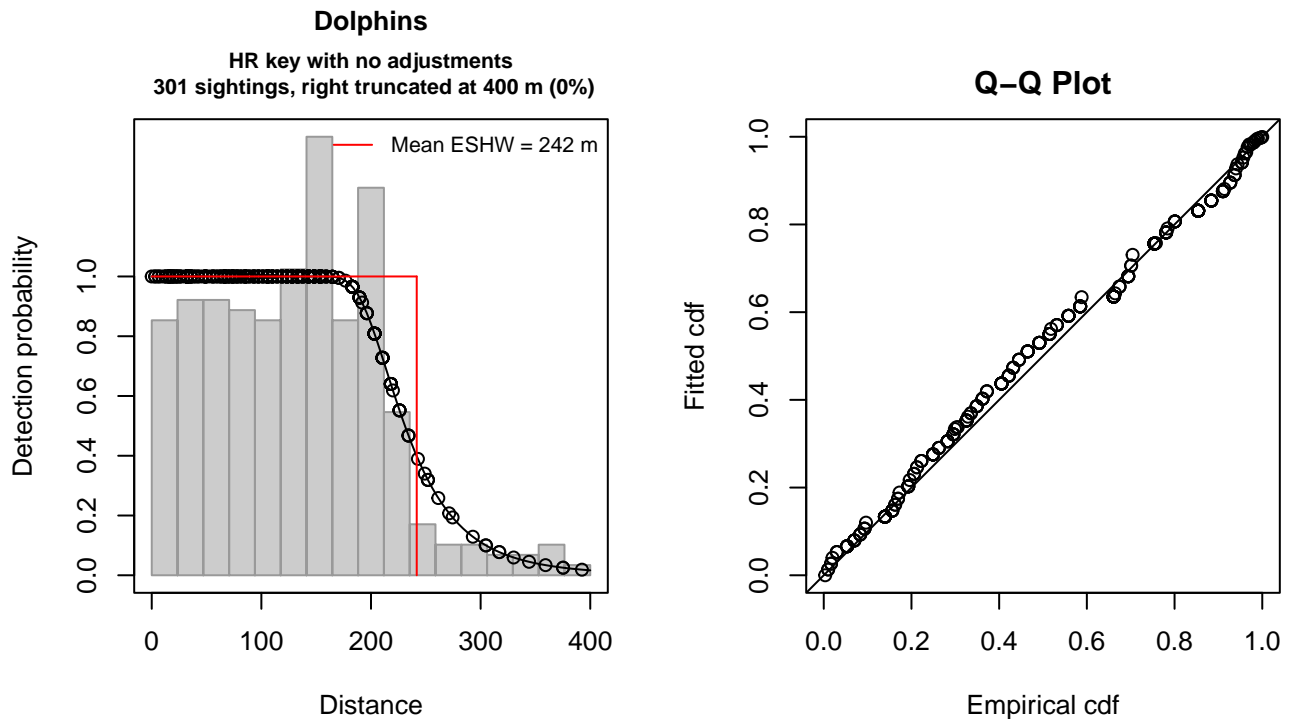


Figure 27: VAMSC and Riverhead MD DNR detection function and Q-Q plot showing its goodness of fit.

Statistical output for this detection function:

```
Summary for ds object
Number of observations : 301
Distance range       : 0 - 400
AIC                  : 3426.124
```

```
Detection function:
Hazard-rate key function
```

```
Detection function parameters
Scale coefficient(s):
      estimate      se
(Intercept) 5.388208 0.04209556
```

```
Shape coefficient(s):
      estimate      se
(Intercept) 1.91525 0.1331166
```

	Estimate	SE	CV
Average p	0.6042969	0.0203517	0.03367831
N in covered region	498.0995265	24.6489147	0.04948592

Distance sampling Cramer-von Mises test (unweighted)
 Test statistic = 0.302011 p = 0.133421

2.2.1.3 MATS 2002-2005

After right-truncating observations greater than 629 m, we fitted the detection function to the 684 observations that remained (Table 11). The selected detection function (Figure 28) used a hazard rate key function with Beaufort (Figure 29) as a covariate.

Table 11: Observations used to fit the MATS 2002-2005 detection function.

ScientificName	n
Delphinus delphis	2
Stenella attenuata	2
Stenella frontalis	104
Tursiops truncatus	576
Total	684

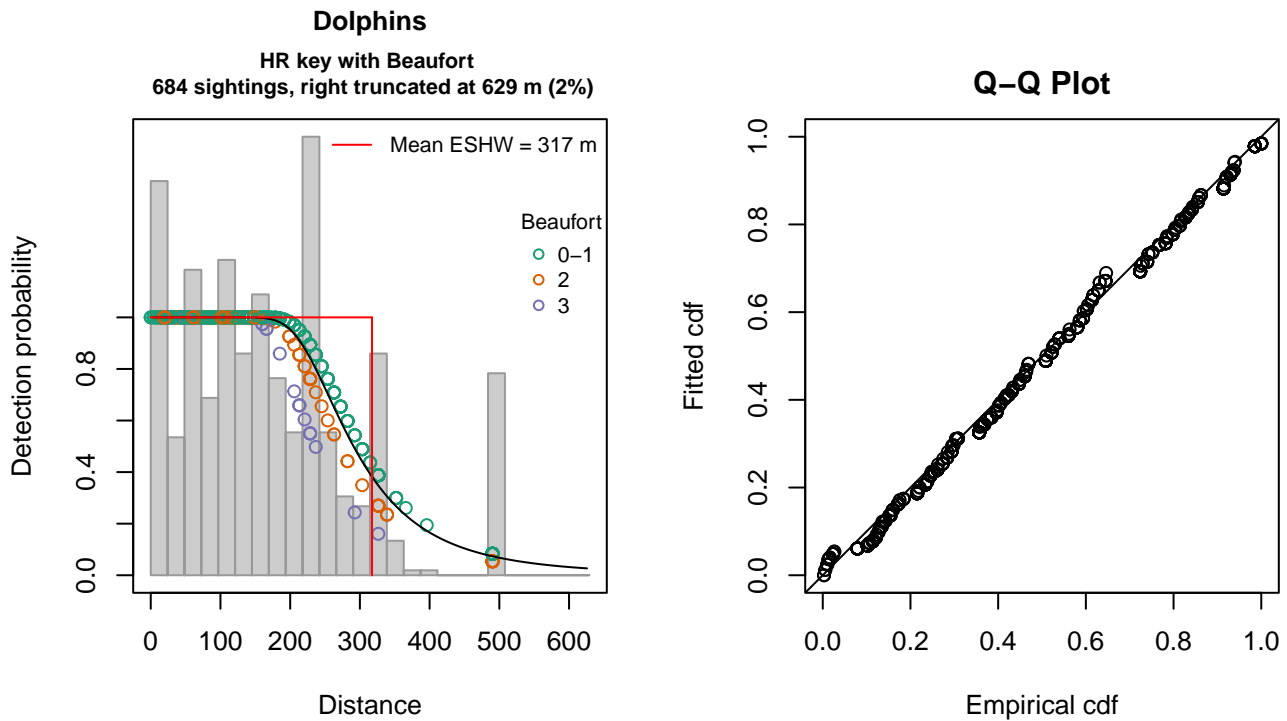


Figure 28: MATS 2002-2005 detection function and Q-Q plot showing its goodness of fit.

Statistical output for this detection function:

```
Summary for ds object
Number of observations : 684
Distance range       : 0 - 629
AIC                  : 8306.088
```

Detection function:

Hazard-rate key function

Detection function parameters

Scale coefficient(s):

	estimate	se
(Intercept)	5.6213531	0.04325709
Beaufort2	-0.1046854	0.06814971
Beaufort3	-0.2421057	0.13060115

Shape coefficient(s):

	estimate	se
(Intercept)	1.449025	0.08965229

	Estimate	SE	CV
Average p	0.5026836	0.0147185	0.02927984
N in covered region	1360.6968013	54.2106880	0.03984039

Distance sampling Cramer-von Mises test (unweighted)

Test statistic = 0.194502 p = 0.278380

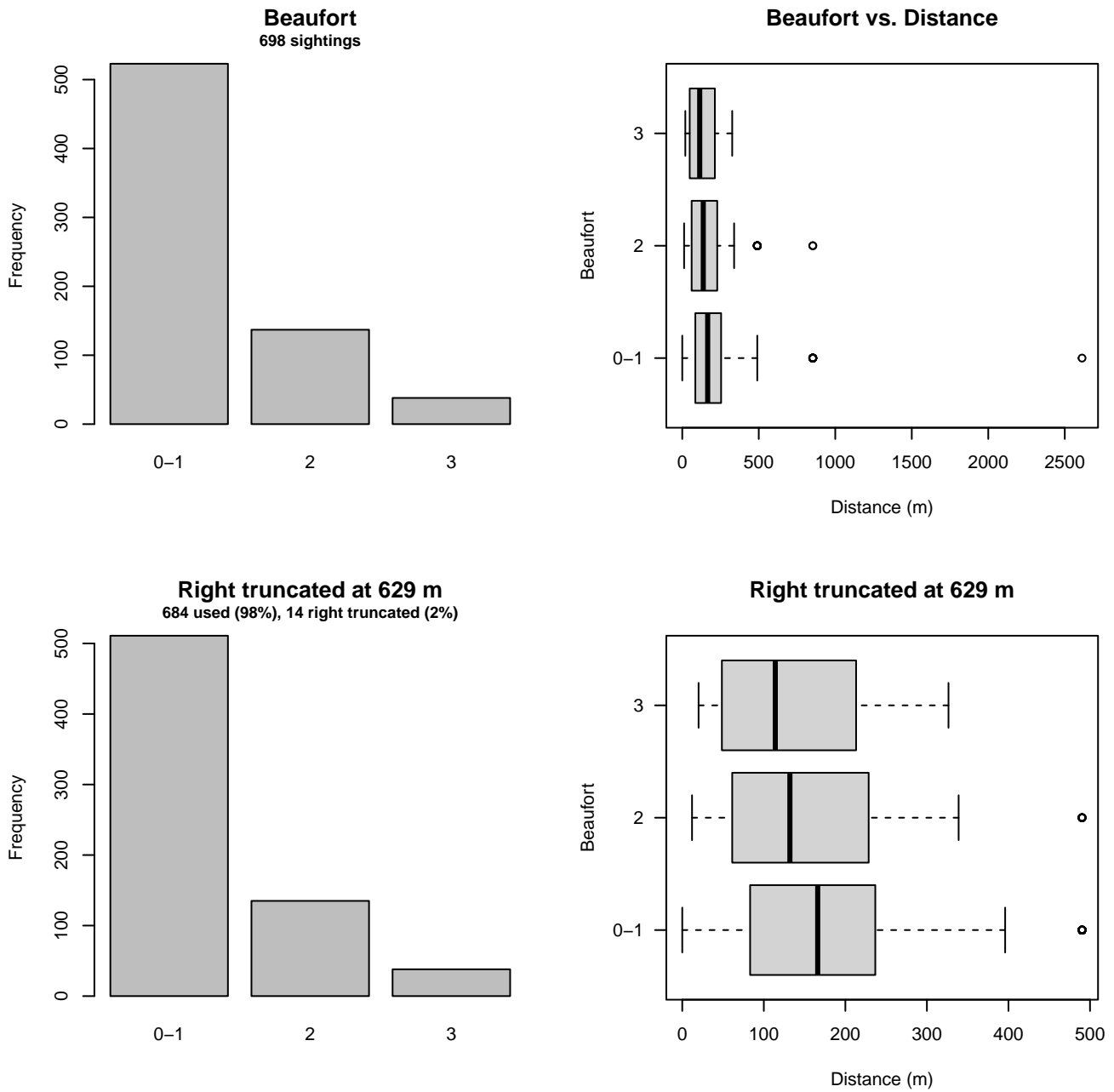


Figure 29: Distribution of the Beaufort covariate before (top row) and after (bottom row) observations were truncated to fit the MATS 2002-2005 detection function.

2.2.1.4 NARWSS 2003-2016

After right-truncating observations greater than 1367 m and left-truncating observations less than 61 m (Figure 31), we fitted the detection function to the 3073 observations that remained (Table 12). The selected detection function (Figure 30) used a hazard rate key function with Beaufort (Figure 32) and Season (Figure 33) as covariates.

Table 12: Observations used to fit the NARWSS 2003-2016 detection function.

ScientificName	n
Delphinus delphis	607
Lagenorhynchus acutus	2404
Lagenorhynchus albirostris	6
Tursiops truncatus	56
Total	3073

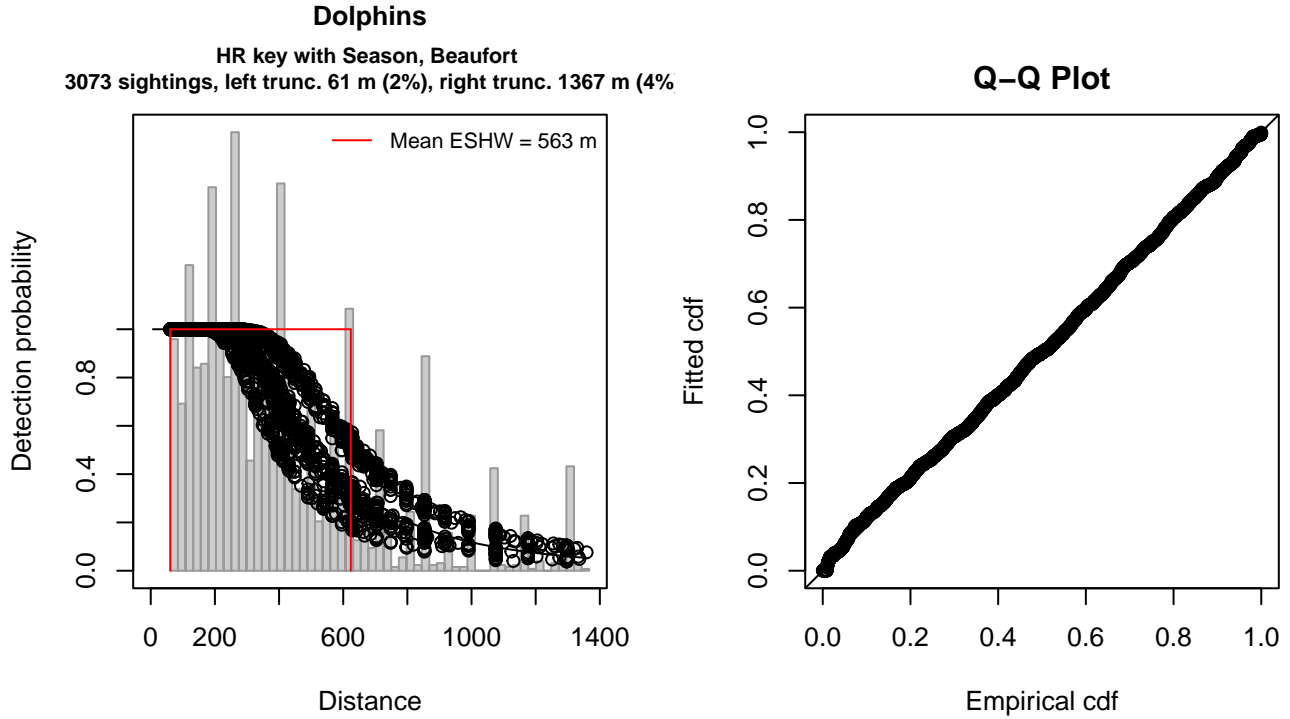


Figure 30: NARWSS 2003-2016 detection function and Q-Q plot showing its goodness of fit.

Statistical output for this detection function:

Summary for ds object

Number of observations : 3073
 Distance range : 61 - 1367
 AIC : 41850.8

Detection function:

Hazard-rate key function

Detection function parameters

Scale coefficient(s):

	estimate	se
(Intercept)	6.10469263	0.07579397
SeasonSpring	0.06689438	0.05622050
SeasonSummer	0.29278056	0.05383279
SeasonWinter	-0.15259970	0.06804643
Beaufort	-0.03572691	0.02383833

Shape coefficient(s):

	estimate	se
(Intercept)	1.009361	0.0398862

	Estimate	SE	CV
Average p	0.4196247	8.827249e-03	0.02103606
N in covered region	7323.2113220	1.845410e+02	0.02519946

Distance sampling Cramer-von Mises test (unweighted)
 Test statistic = 0.246036 p = 0.193531

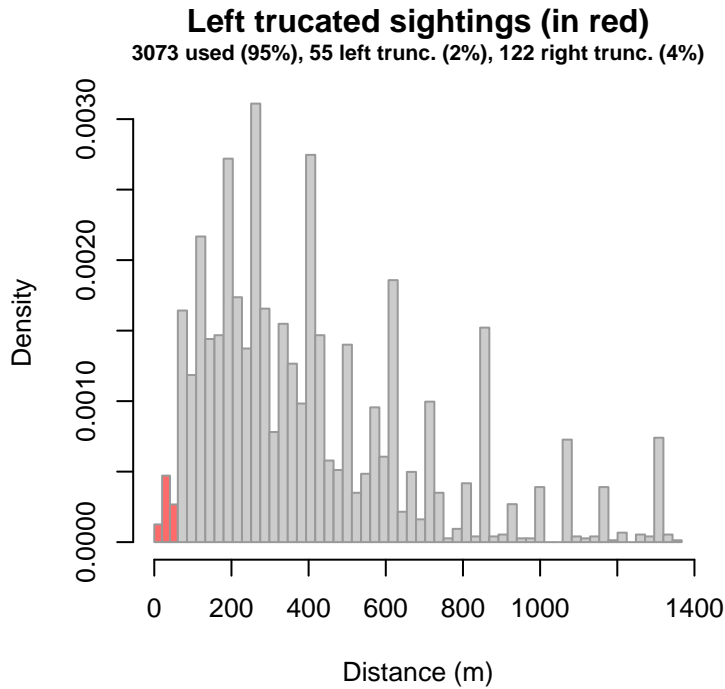


Figure 31: Density histogram of observations used to fit the NARWSS 2003-2016 detection function, with the left-most bar showing observations at distances less than 61 m, which were left-truncated and excluded from the analysis [Buckland et al. (2001)]. (This bar may be very short if there were very few left-truncated sightings, or very narrow if the left truncation distance was very small; in either case it may not appear red.)

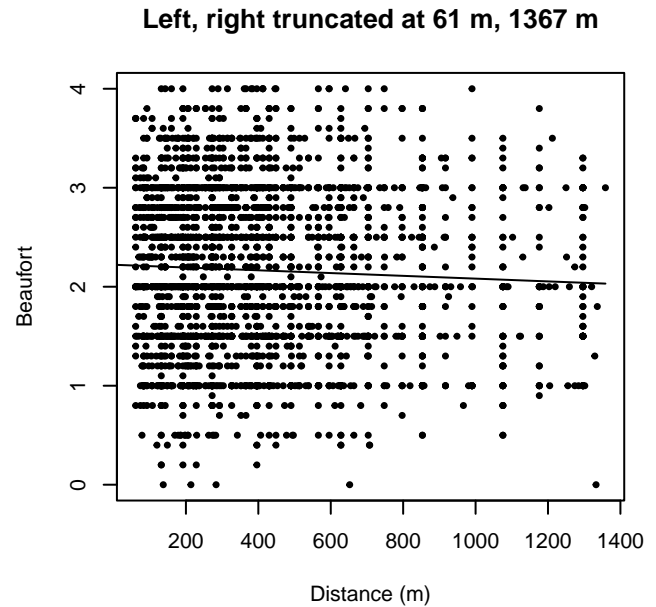
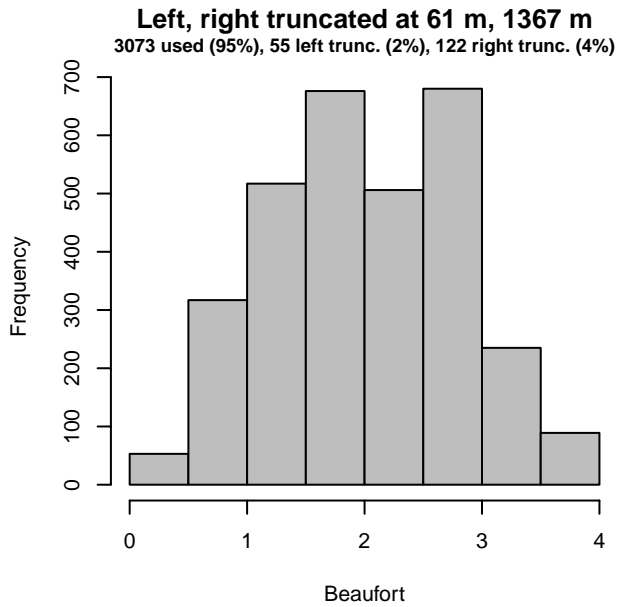
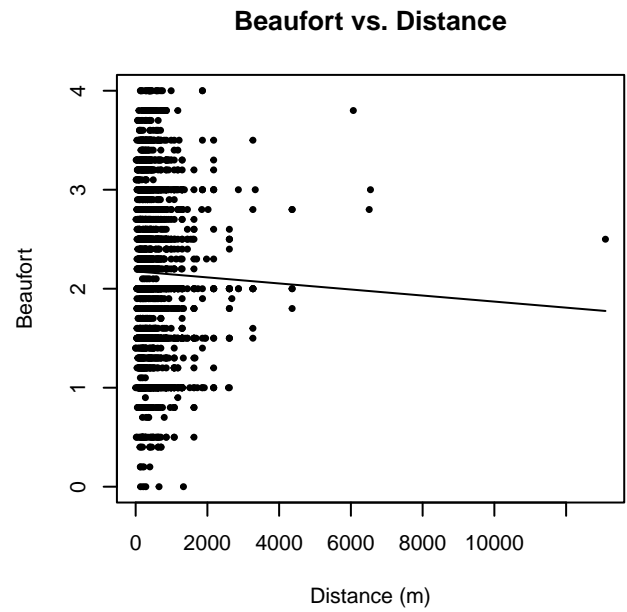
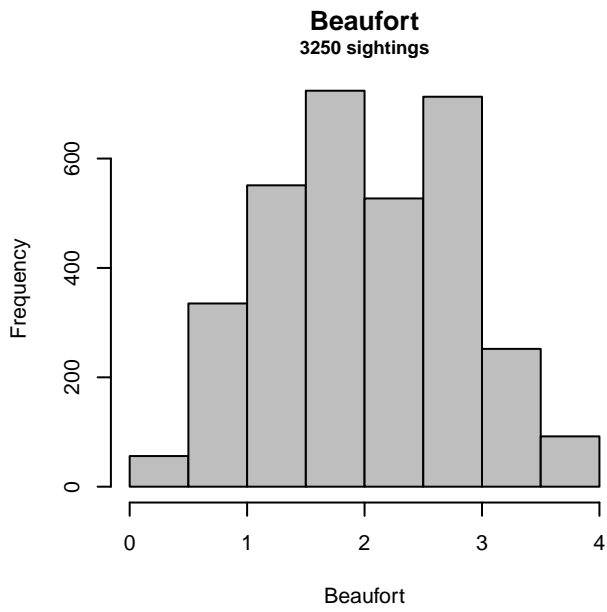


Figure 32: Distribution of the Beaufort covariate before (top row) and after (bottom row) observations were truncated to fit the NARWSS 2003-2016 detection function.

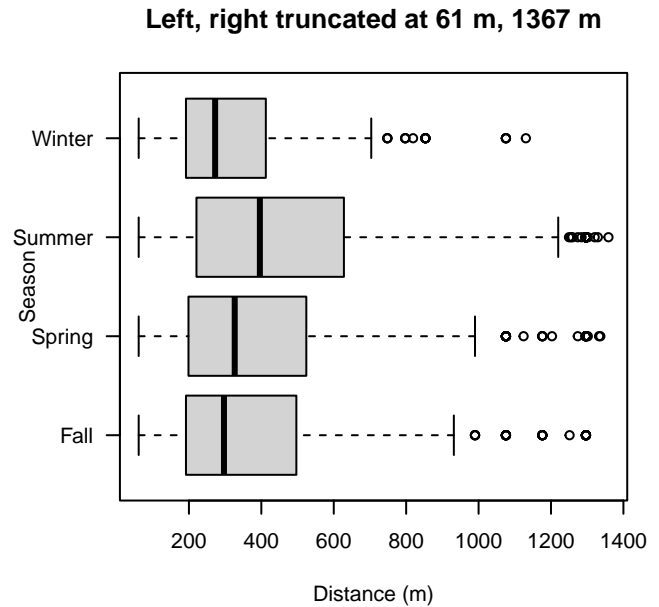
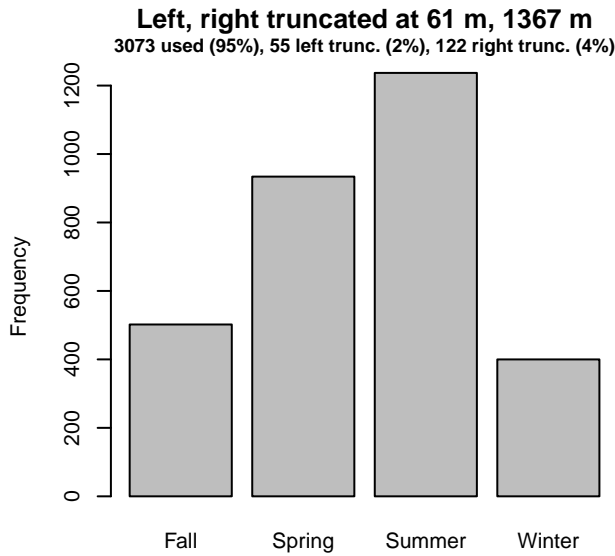
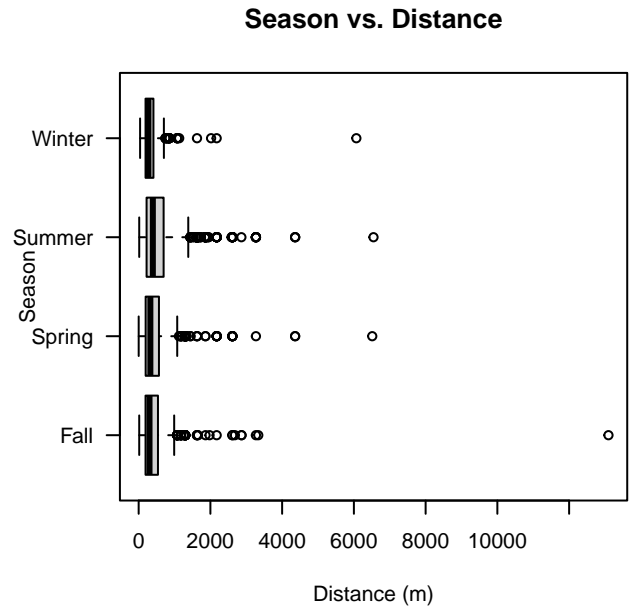
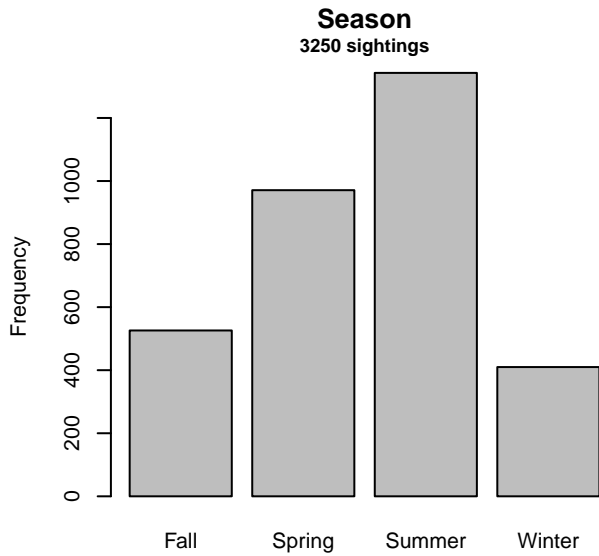


Figure 33: Distribution of the Season covariate before (top row) and after (bottom row) observations were truncated to fit the NARWSS 2003-2016 detection function.

2.2.1.5 UNCW Navy Surveys

After right-truncating observations greater than 1600 m, we fitted the detection function to the 1523 observations that remained (Table 13). The selected detection function (Figure 34) used a half normal key function with Glare (Figure 35) and Visibility (Figure 36) as covariates.

Table 13: Observations used to fit the UNCW Navy Surveys detection function.

ScientificName	n
Delphinus delphis	77
Lagenodelphis hosei	1
Stenella attenuata	2
Stenella clymene	11
Stenella coeruleoalba	19
Stenella frontalis	480
Stenella longirostris	1
Steno bredanensis	14
Tursiops truncatus	918
Total	1523

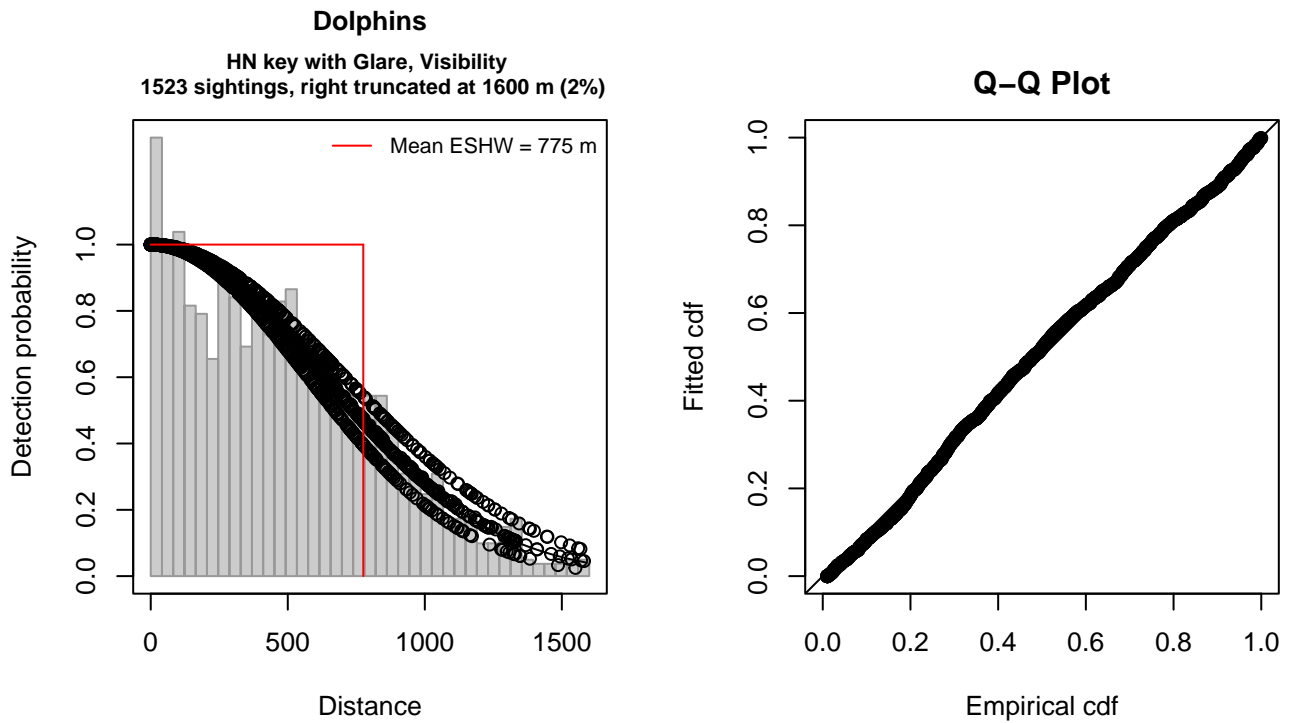


Figure 34: UNCW Navy Surveys detection function and Q-Q plot showing its goodness of fit.

Statistical output for this detection function:

Summary for ds object

Number of observations : 1523
 Distance range : 0 - 1600
 AIC : 21665.78

Detection function:

Half-normal key function

Detection function parameters

Scale coefficient(s):

	estimate	se
(Intercept)	6.55223233	0.04798577
GlareNone, 0-25%, Unk.	-0.10934970	0.05247015
VisibilityHalf	-0.09759271	0.04601702

	Estimate	SE	CV
Average p	0.4827398	0.01003395	0.02078542
N in covered region	3154.9084328	87.71221948	0.02780183

Distance sampling Cramer-von Mises test (unweighted)
 Test statistic = 0.331909 p = 0.110182

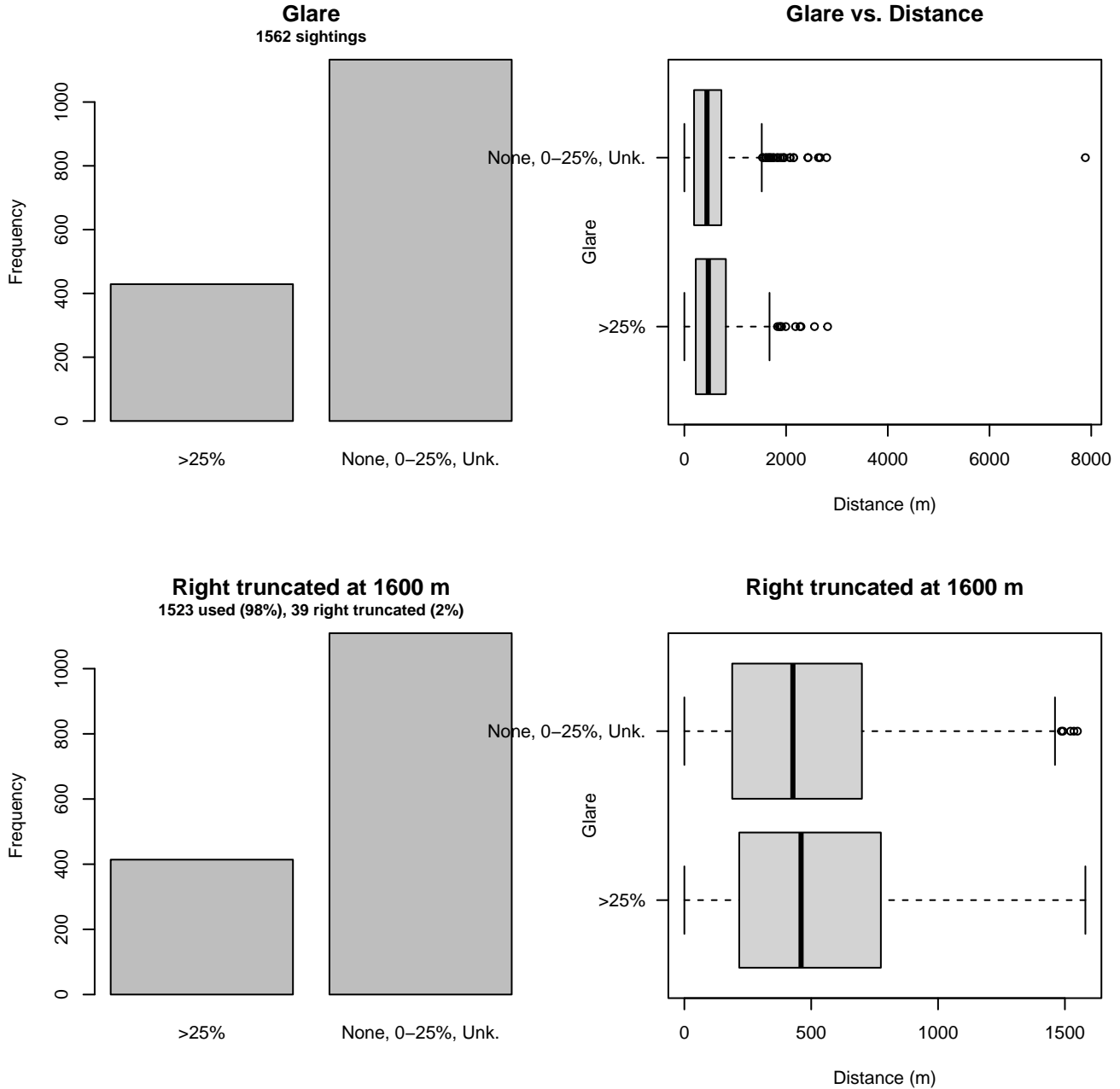


Figure 35: Distribution of the Glare covariate before (top row) and after (bottom row) observations were truncated to fit the UNCW Navy Surveys detection function.

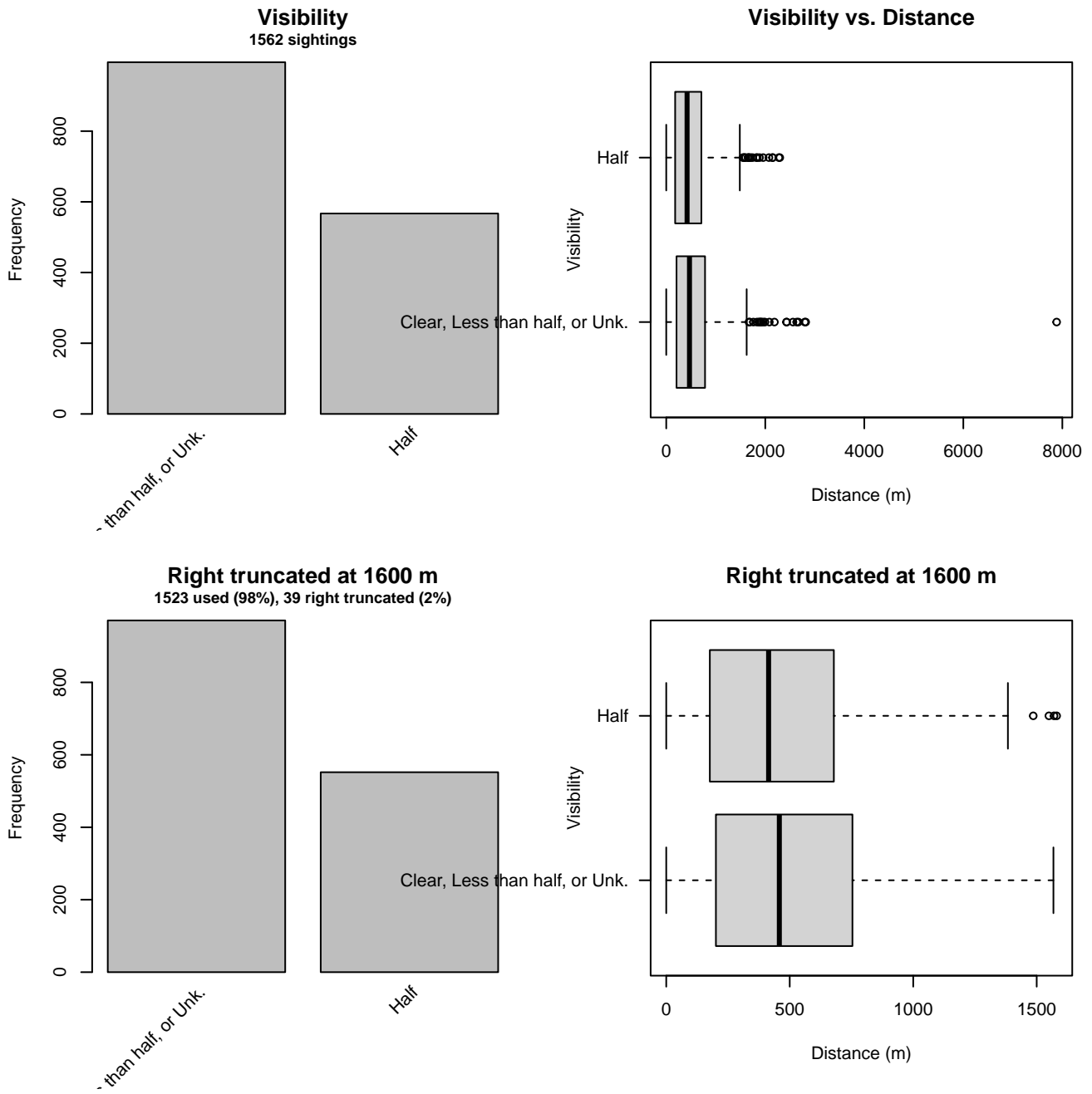


Figure 36: Distribution of the Visibility covariate before (top row) and after (bottom row) observations were truncated to fit the UNCW Navy Surveys detection function.

2.2.1.6 UNCW Right Whale Surveys

After right-truncating observations greater than 528 m and left-truncating observations less than 54 m (Figure 38), we fitted the detection function to the 1821 observations that remained (Table 14). The selected detection function (Figure 37) used a hazard rate key function with no covariates.

Table 14: Observations used to fit the UNCW Right Whale Surveys detection function.

ScientificName	n
Delphinus delphis	26
Stenella frontalis	4
Tursiops truncatus	1791
Total	1821

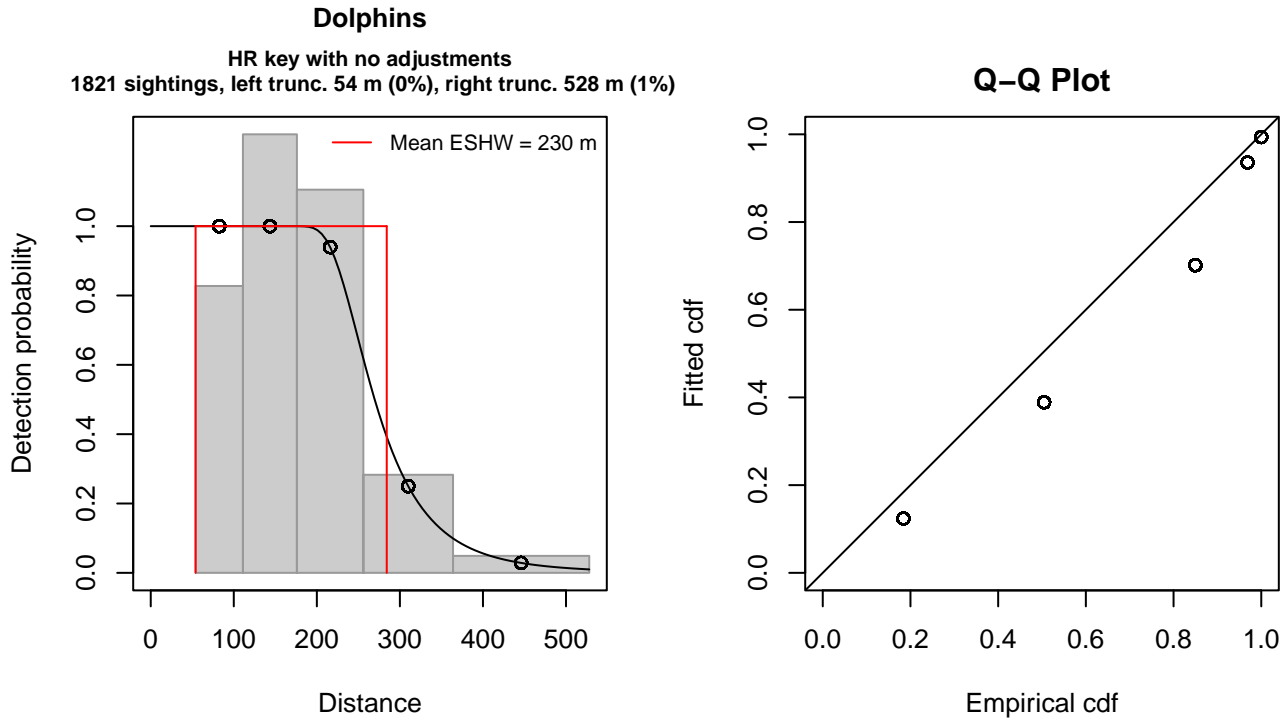


Figure 37: UNCW Right Whale Surveys detection function and Q-Q plot showing its goodness of fit.

Statistical output for this detection function:

Summary for ds object

Number of observations : 1821
 Distance range : 54 - 528
 AIC : 5176.116

Detection function:

Hazard-rate key function

Detection function parameters

Scale coefficient(s):

	estimate	se
(Intercept)	5.538954	0.02098751

Shape coefficient(s):

	estimate	se
(Intercept)	1.841299	0.06464608

	Estimate	SE	CV
Average p	0.4855453	0.009233858	0.01901750
N in covered region	3750.4226341	95.188173832	0.02538065

Distance sampling Cramer-von Mises test (unweighted)
 Test statistic = 14.468539 p = 0.010416

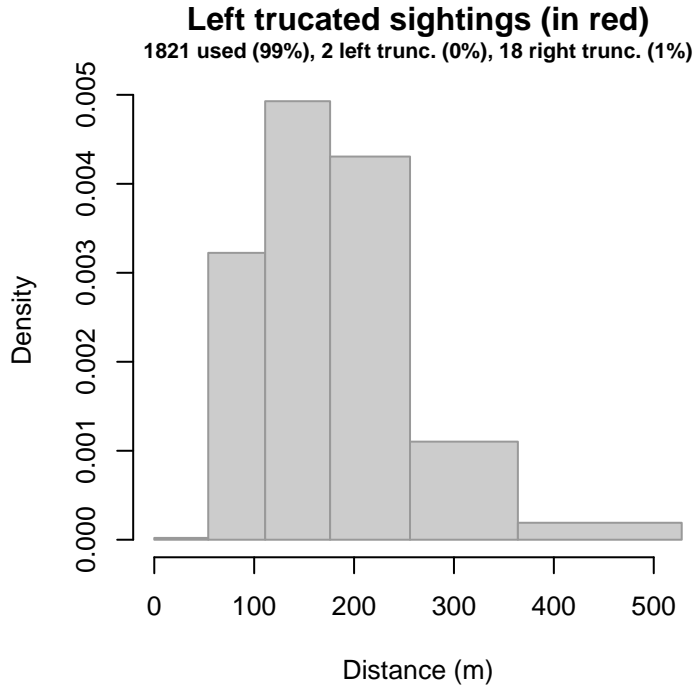


Figure 38: Density histogram of observations used to fit the UNCW Right Whale Surveys detection function, with the left-most bar showing observations at distances less than 54 m, which were left-truncated and excluded from the analysis [Buckland et al. (2001)]. (This bar may be very short if there were very few left-truncated sightings, or very narrow if the left truncation distance was very small; in either case it may not appear red.)

2.2.1.7 UNCW Early Surveys

After right-truncating observations greater than 333 m and left-truncating observations less than 14 m (Figure 40), we fitted the detection function to the 349 observations that remained (Table 15). The selected detection function (Figure 39) used a half normal key function with Beaufort (Figure 41) as a covariate.

Table 15: Observations used to fit the UNCW Early Surveys detection function.

ScientificName	n
Delphinus delphis	5
Stenella frontalis	1
Tursiops truncatus	343
Total	349

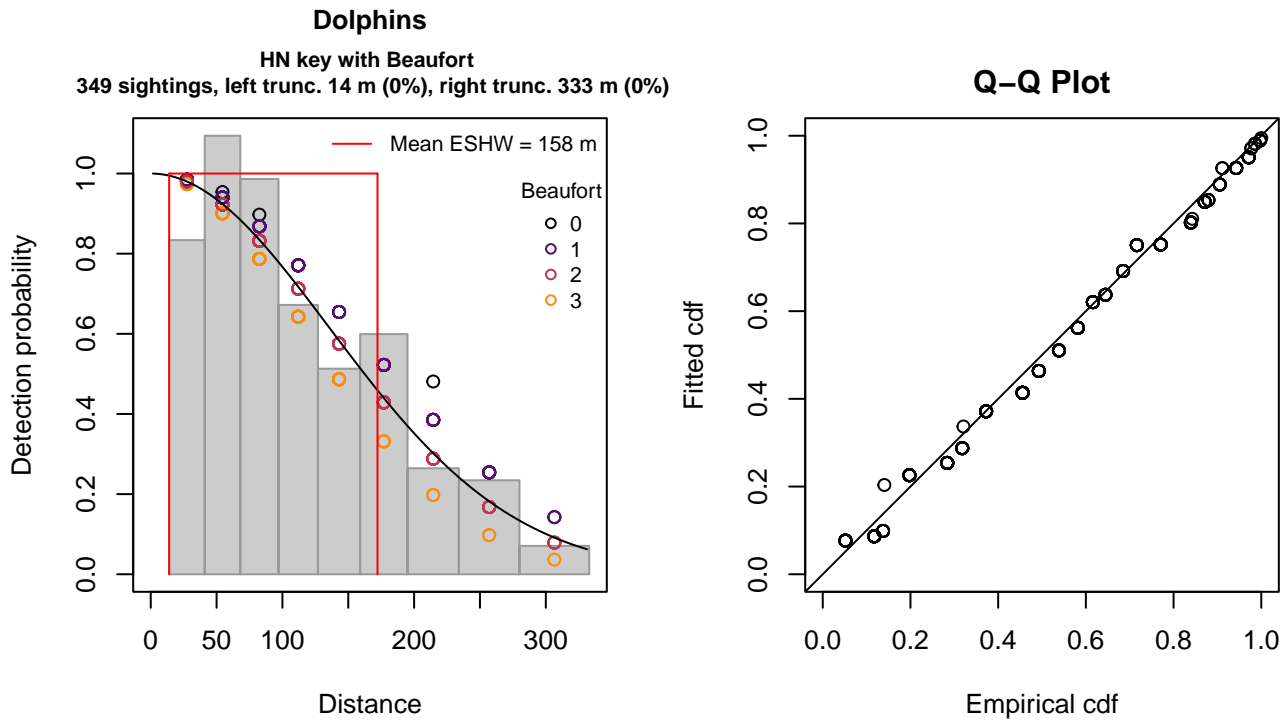


Figure 39: UNCW Early Surveys detection function and Q-Q plot showing its goodness of fit.

Statistical output for this detection function:

Summary for ds object

Number of observations : 349
 Distance range : 14 - 333
 AIC : 1464.597

Detection function:

Half-normal key function

Detection function parameters

Scale coefficient(s):

	estimate	se
(Intercept)	5.1778911	0.14575211
Beaufort	-0.1325498	0.07066838

	Estimate	SE	CV
Average p	0.4915207	0.02352103	0.04785360
N in covered region	710.0413079	43.53534195	0.06131382

Distance sampling Cramer-von Mises test (unweighted)

Test statistic = 0.278162 p = 0.155953

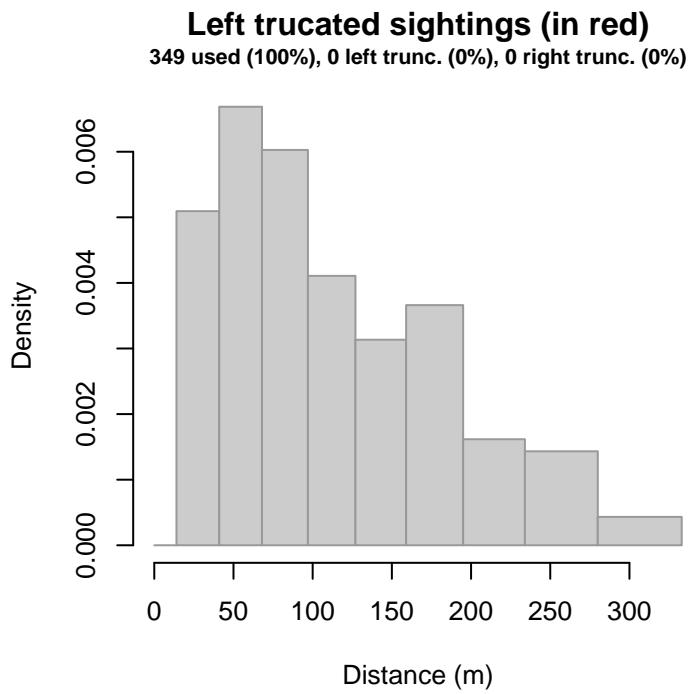


Figure 40: Density histogram of observations used to fit the UNCW Early Surveys detection function, with the left-most bar showing observations at distances less than 14 m, which were left-truncated and excluded from the analysis [Buckland et al. (2001)]. (This bar may be very short if there were very few left-truncated sightings, or very narrow if the left truncation distance was very small; in either case it may not appear red.)

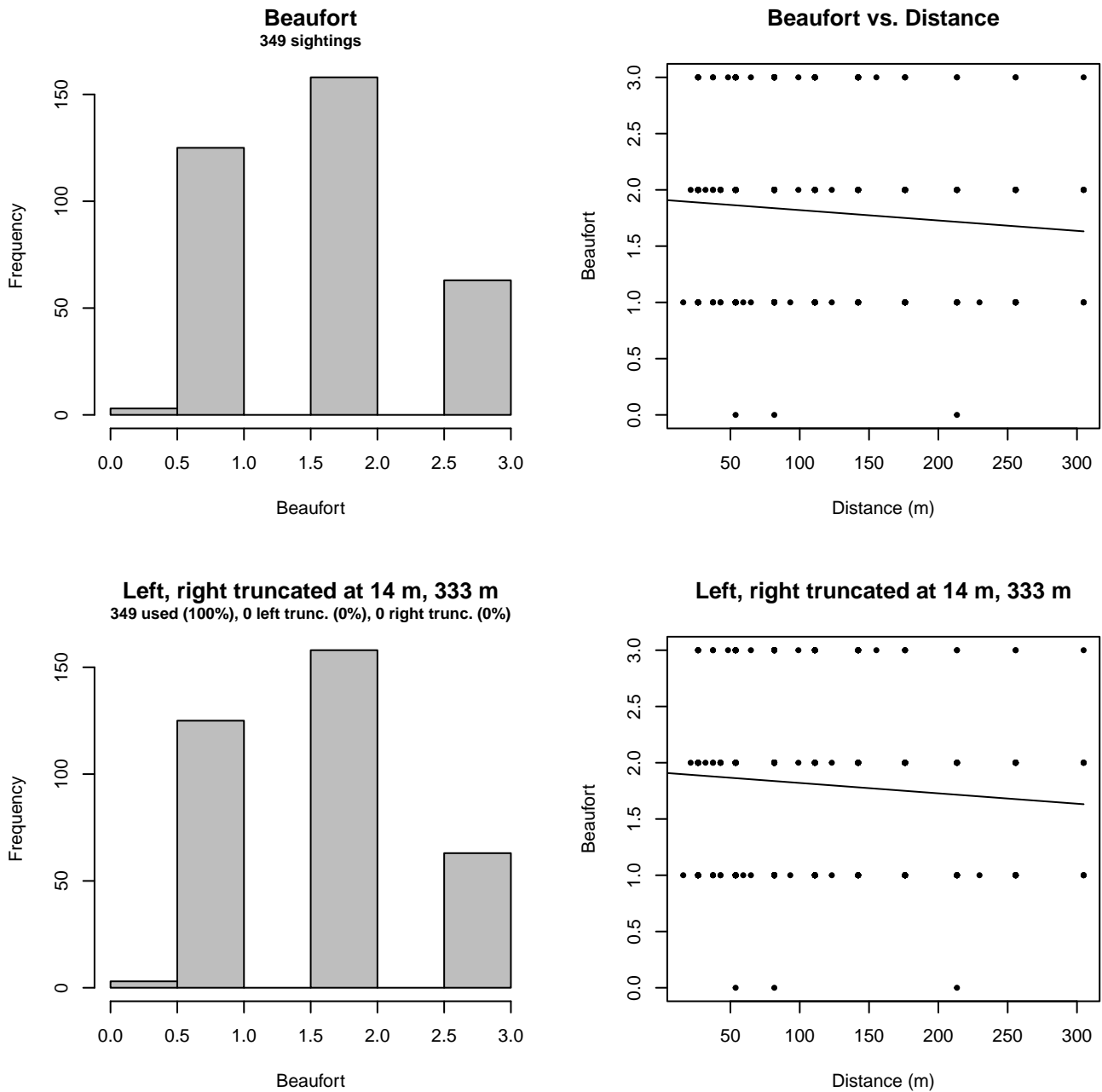


Figure 41: Distribution of the Beaufort covariate before (top row) and after (bottom row) observations were truncated to fit the UNCW Early Surveys detection function.

2.2.1.8 VAMSC

After right-truncating observations greater than 1000 m, we fitted the detection function to the 303 observations that remained (Table 16). The selected detection function (Figure 42) used a hazard rate key function with no covariates.

Table 16: Observations used to fit the VAMSC detection function.

ScientificName	n
Delphinus delphis	30
Stenella frontalis	4
Tursiops truncatus	269
Total	303

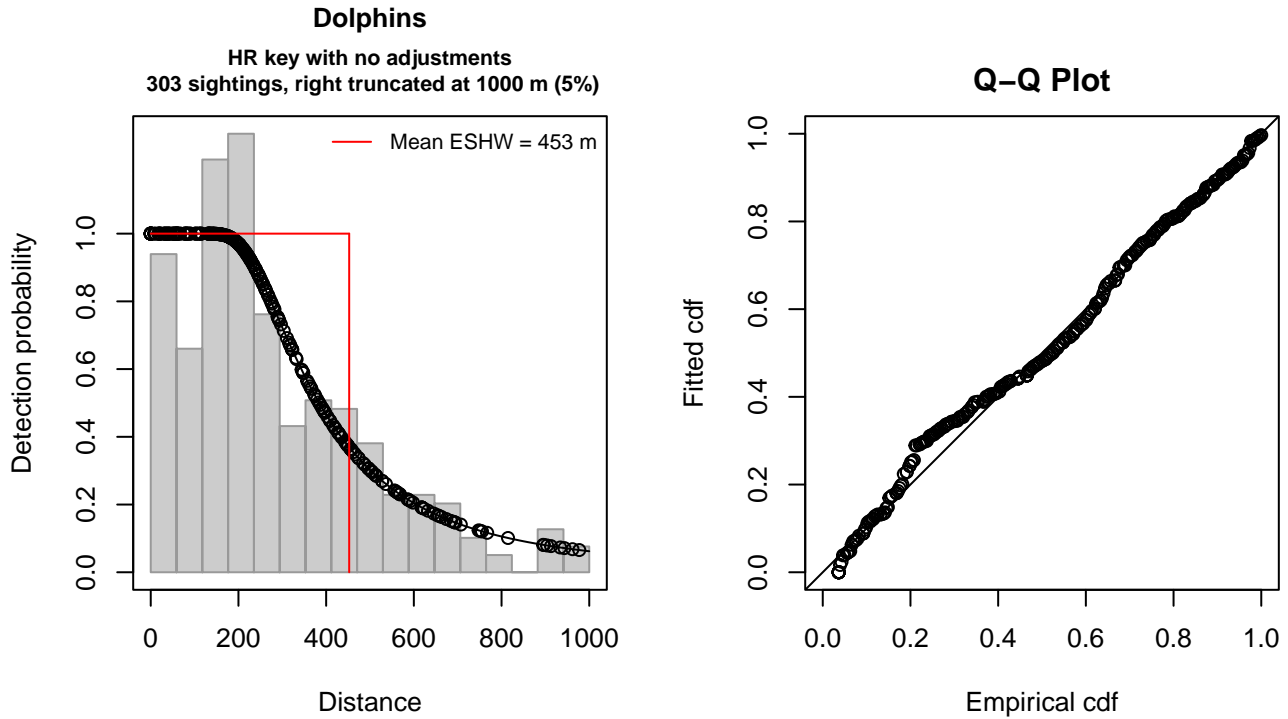


Figure 42: VAMSC detection function and Q-Q plot showing its goodness of fit.

Statistical output for this detection function:

Summary for ds object

Number of observations : 303
 Distance range : 0 - 1000
 AIC : 3992.632

Detection function:

Hazard-rate key function

Detection function parameters

Scale coefficient(s):

	estimate	se
(Intercept)	5.803823	0.1019737

Shape coefficient(s):

	estimate	se
(Intercept)	0.9119562	0.1438459

	Estimate	SE	CV
Average p	0.4525805	0.02853931	0.06305908
N in covered region	669.4942067	50.91287837	0.07604678

Distance sampling Cramer-von Mises test (unweighted)
 Test statistic = 0.212402 p = 0.244680

2.2.1.9 HDR

After right-truncating observations greater than 1500 m and left-truncating observations less than 111 m (Figure 44), we fitted the detection function to the 203 observations that remained (Table 17). The selected detection function (Figure 43) used a hazard rate key function with Season (Figure 45) and Swell (Figure 46) as covariates.

Table 17: Observations used to fit the HDR detection function.

ScientificName	n
Delphinus delphis	47
Stenella coeruleoalba	14
Stenella frontalis	19
Tursiops truncatus	123
Total	203

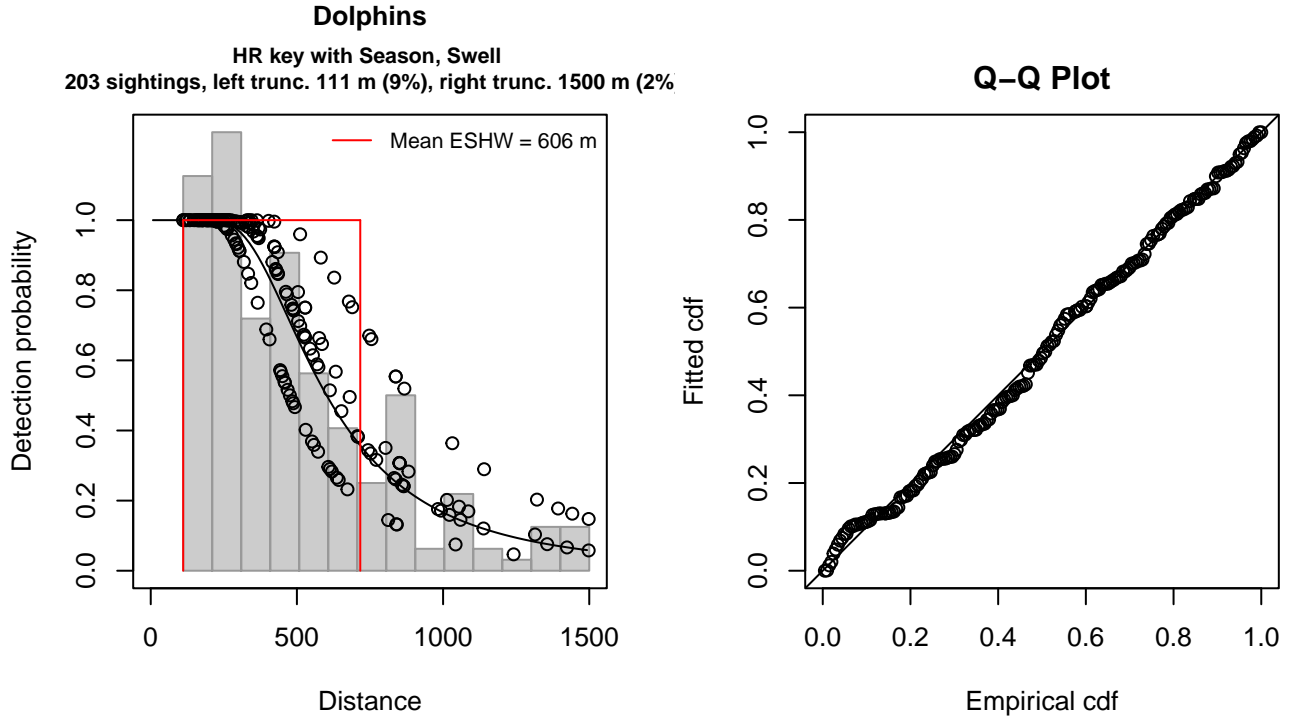


Figure 43: HDR detection function and Q-Q plot showing its goodness of fit.

Statistical output for this detection function:

Summary for ds object

Number of observations : 203
 Distance range : 111 - 1500
 AIC : 2802.845

Detection function:

Hazard-rate key function

Detection function parameters

Scale coefficient(s):

	estimate	se
(Intercept)	6.3015171	0.1328018
SeasonWinter, Spring	-0.2671651	0.1458664
Swell3-4	0.3527933	0.1530784

Shape coefficient(s):

	estimate	se
(Intercept)	1.026101	0.1620057

Estimate	SE	CV
----------	----	----

Average p 0.419883 0.03654238 0.08702991
N in covered region 483.467993 49.56848062 0.10252691

Distance sampling Cramer-von Mises test (unweighted)
Test statistic = 0.059652 p = 0.816171

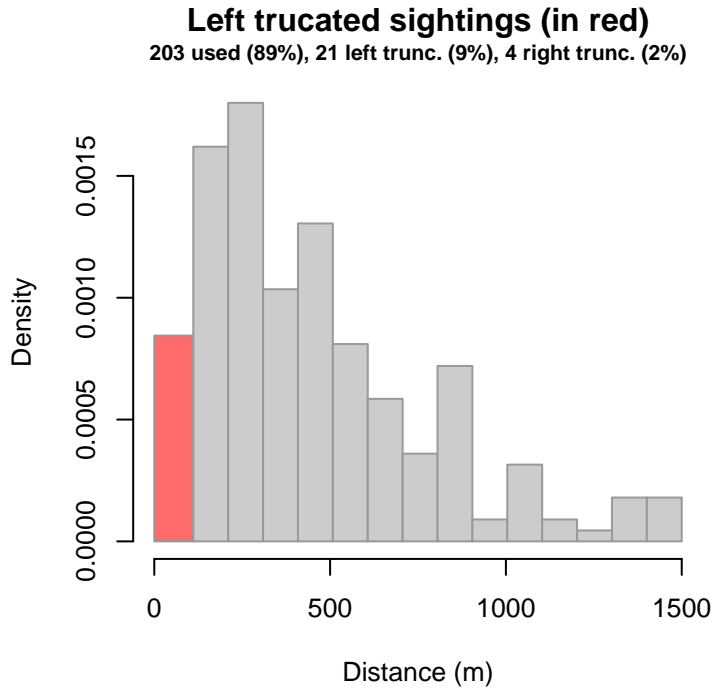


Figure 44: Density histogram of observations used to fit the HDR detection function, with the left-most bar showing observations at distances less than 111 m, which were left-truncated and excluded from the analysis [Buckland et al. (2001)]. (This bar may be very short if there were very few left-truncated sightings, or very narrow if the left truncation distance was very small; in either case it may not appear red.)

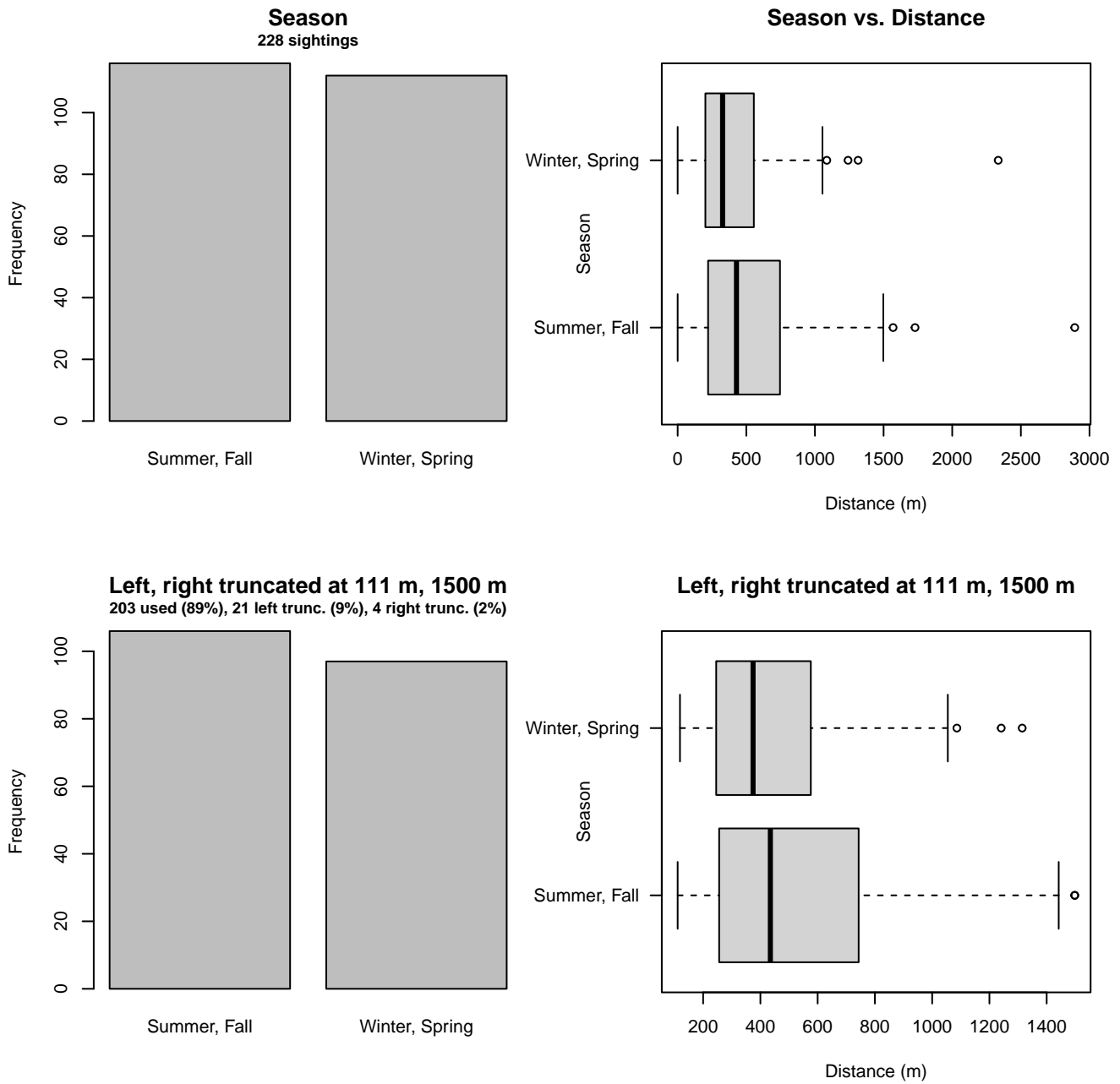


Figure 45: Distribution of the Season covariate before (top row) and after (bottom row) observations were truncated to fit the HDR detection function.

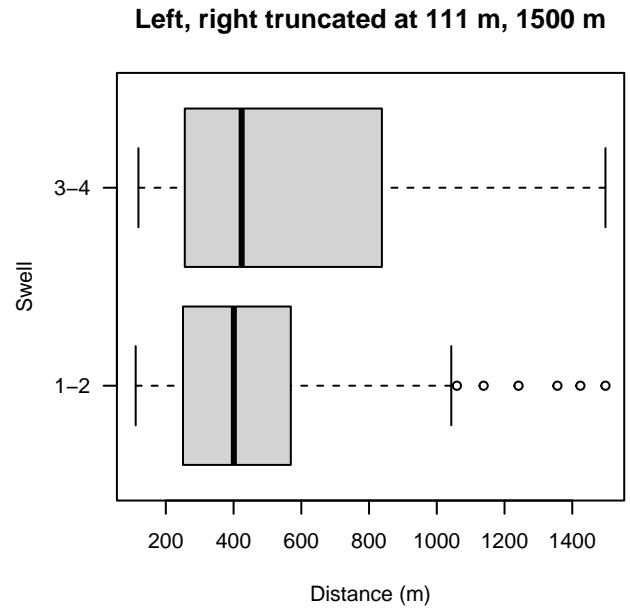
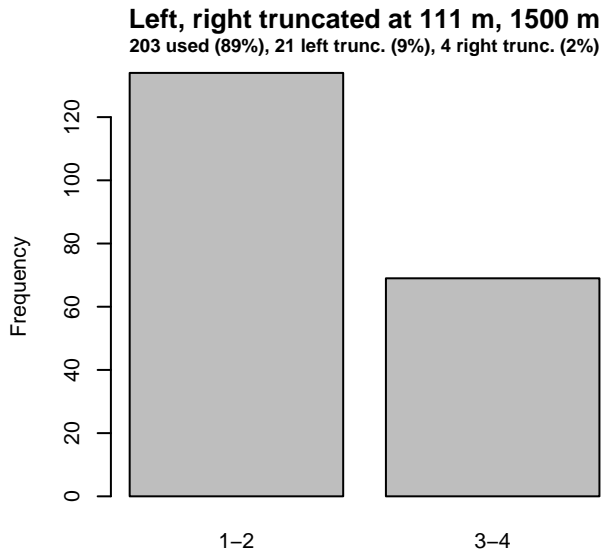
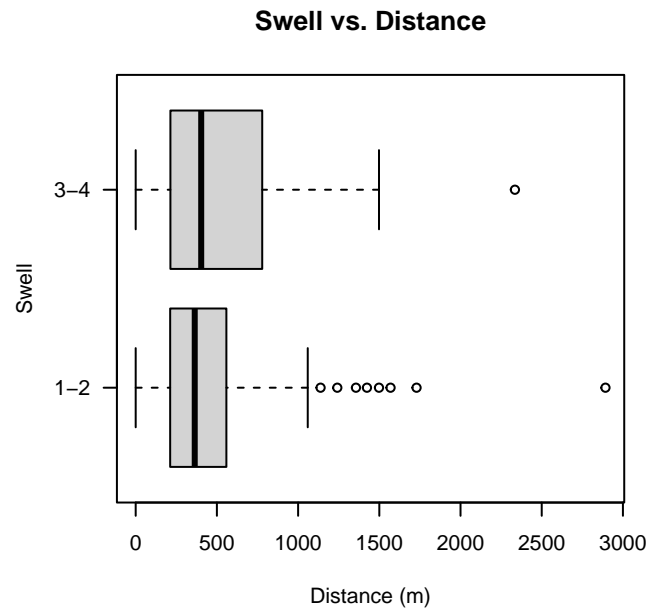
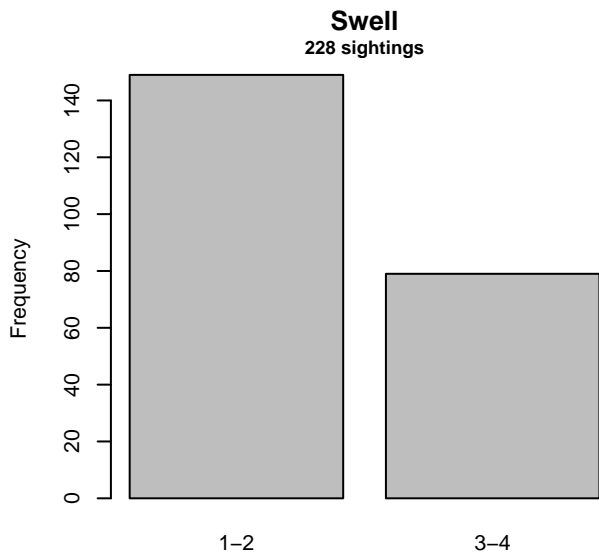


Figure 46: Distribution of the Swell covariate before (top row) and after (bottom row) observations were truncated to fit the HDR detection function.

2.2.2 Shipboard Surveys

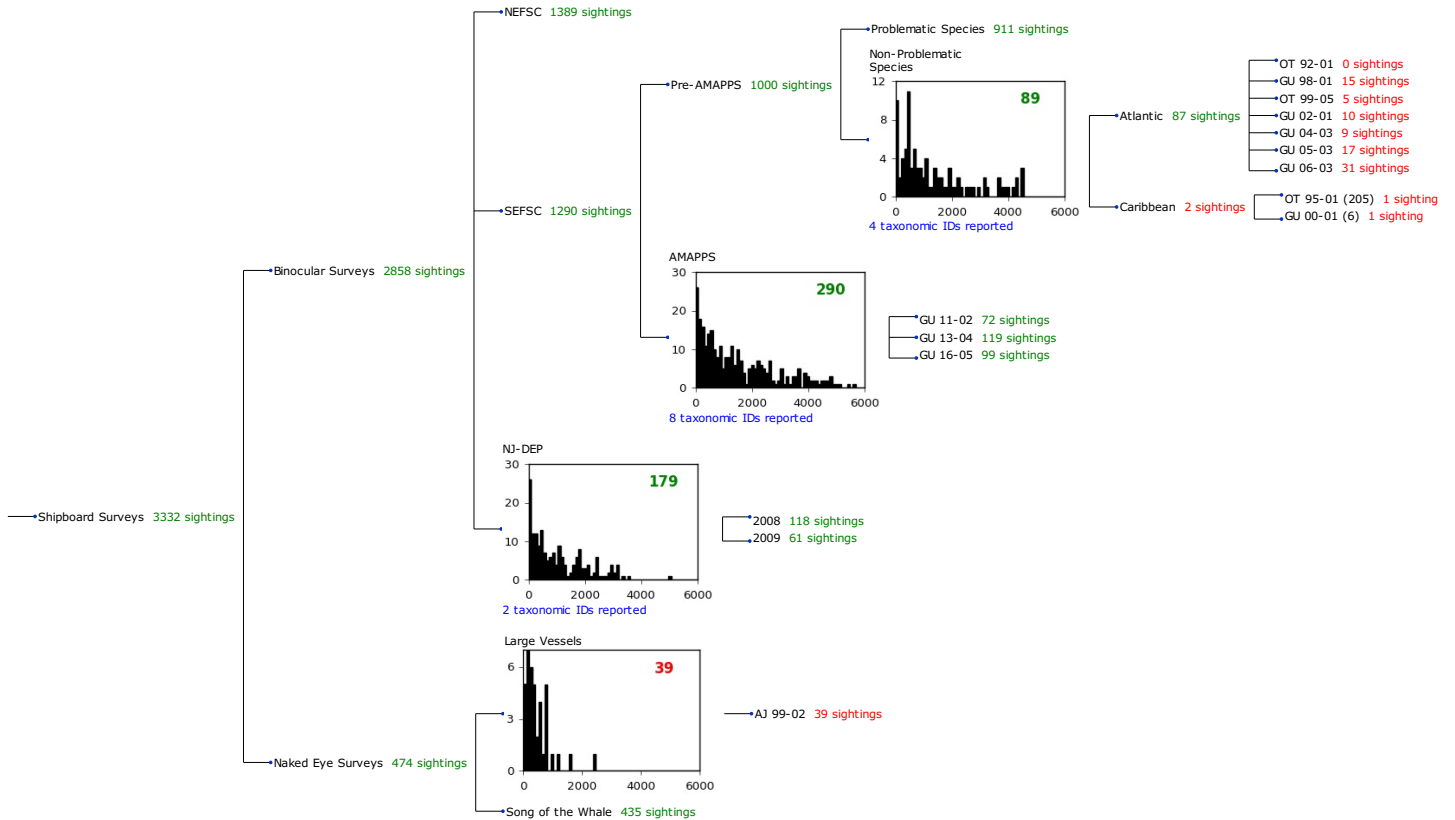


Figure 47: Detection hierarchy for shipboard surveys, showing how they were pooled during detectability modeling, for detection functions that pooled multiple taxa but could not use a taxonomic covariate to account for differences between them. Each histogram represents a detection function and summarizes the perpendicular distances of observations that were pooled to fit it, prior to truncation. Observation counts, also prior to truncation, are shown in green when they met the recommendation of Buckland et al. (2001) that detection functions utilize at least 60 sightings, and red otherwise. For rare taxa, it was not always possible to meet this recommendation, yielding higher statistical uncertainty. During the spatial modeling stage of the analysis, effective strip widths were computed for each survey using the closest detection function above it in the hierarchy (i.e. moving from right to left in the figure). Surveys that do not have a detection function above them in this figure were either addressed by a detection function presented in a different section of this report, or were omitted from the analysis.

2.2.2.1 SEFSC Pre-AMAPPS Non-Problematic Species

After right-truncating observations greater than 4700 m, we fitted the detection function to the 89 observations that remained (Table 18). The selected detection function (Figure 48) used a hazard rate key function with no covariates.

Table 18: Observations used to fit the SEFSC Pre-AMAPPS Non-Problematic Species detection function.

ScientificName	n
Lagenodelphis hosei	1
Stenella clymene	10
Stenella coeruleoalba	75
Stenella longirostris	3
Total	89

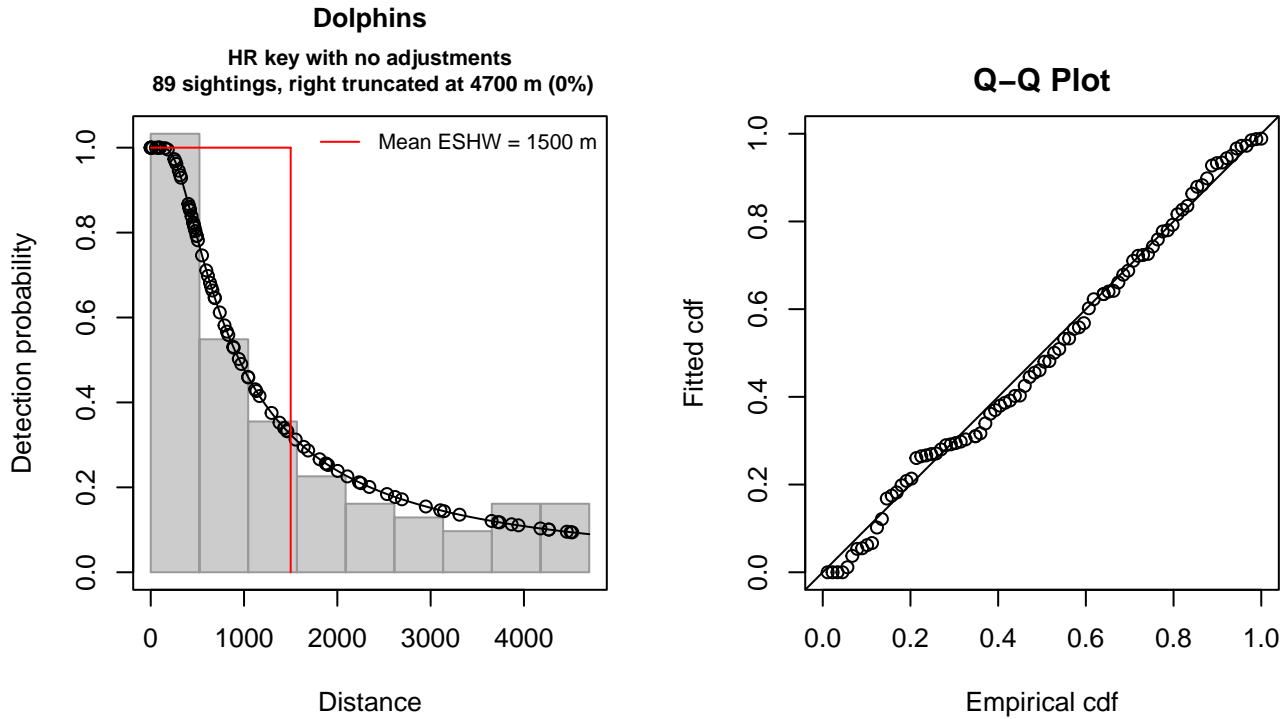


Figure 48: SEFSC Pre-AMAPPS Non-Problematic Species detection function and Q-Q plot showing its goodness of fit.

Statistical output for this detection function:

Summary for ds object

Number of observations : 89
 Distance range : 0 - 4700
 AIC : 1457.185

Detection function:

Hazard-rate key function

Detection function parameters

Scale coefficient(s):
 estimate se
 (Intercept) 6.562458 0.4314852

Shape coefficient(s):
 estimate se
 (Intercept) 0.2225386 0.2209014

	Estimate	SE	CV
Average p	0.319168	0.07146324	0.2239048
N in covered region	278.850035	67.03032811	0.2403813

Distance sampling Cramer-von Mises test (unweighted)
 Test statistic = 0.048231 p = 0.886935

2.2.2.2 SEFSC AMAPPS

After right-truncating observations greater than 5000 m, we fitted the detection function to the 284 observations that remained (Table 19). The selected detection function (Figure 49) used a hazard rate key function with Beaufort (Figure 50) as a covariate.

Table 19: Observations used to fit the SEFSC AMAPPS detection function.

ScientificName	n
Delphinus delphis	2
Stenella attenuata	10
Stenella clymene	3
Stenella coeruleoalba	11
Stenella frontalis	84
Stenella longirostris	1
Steno bredanensis	2
Tursiops truncatus	171
Total	284

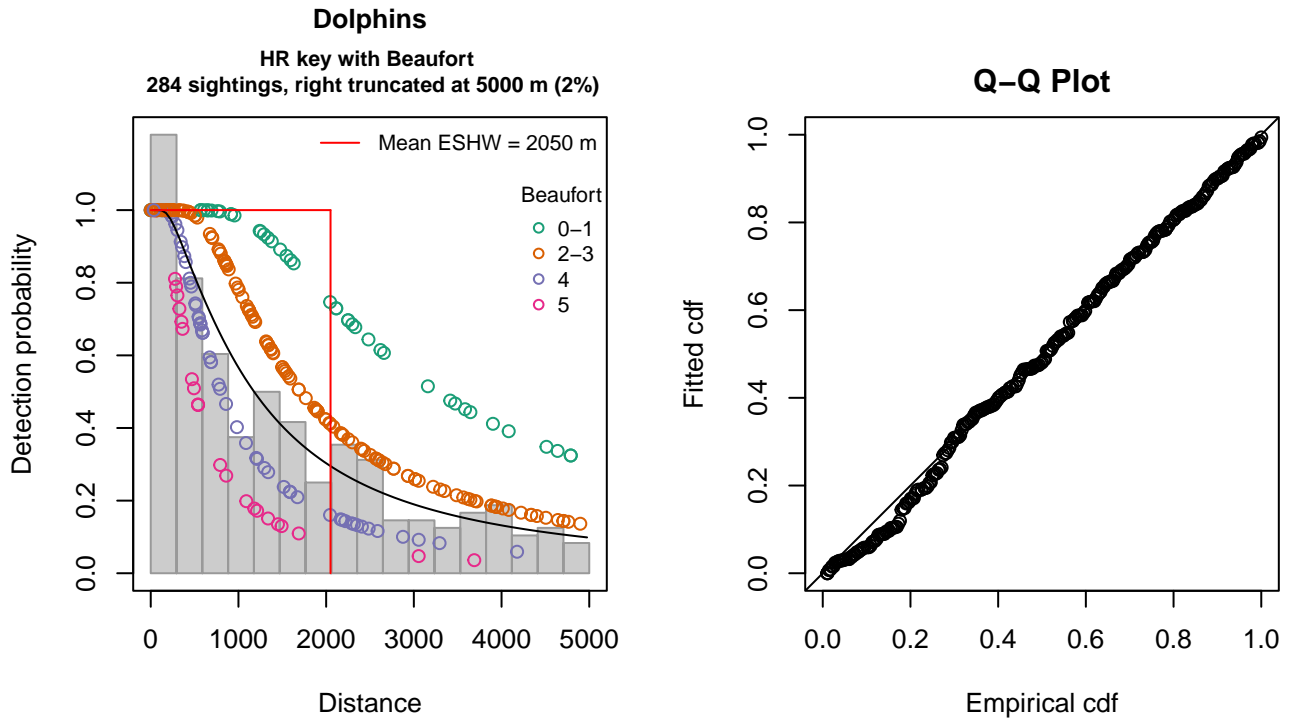


Figure 49: SEFSC AMAPPS detection function and Q-Q plot showing its goodness of fit.

Statistical output for this detection function:

```
Summary for ds object
Number of observations : 284
Distance range       : 0 - 5000
AIC                  : 4678.464
```

```
Detection function:
Hazard-rate key function
```

```
Detection function parameters
Scale coefficient(s):
      estimate      se
(Intercept) 7.8386611 0.3487749
Beaufort2-3 -0.6450433 0.3816484
Beaufort4   -1.3990617 0.4441169
Beaufort5   -1.8689041 0.5186901
```

Shape coefficient(s):

	estimate	se
(Intercept)	0.3878689	0.1380351

	Estimate	SE	CV
Average p	0.3478259	0.03965009	0.1139941
N in covered region	816.5004271	101.68622285	0.1245391

Distance sampling Cramer-von Mises test (unweighted)

Test statistic = 0.107898 p = 0.547527

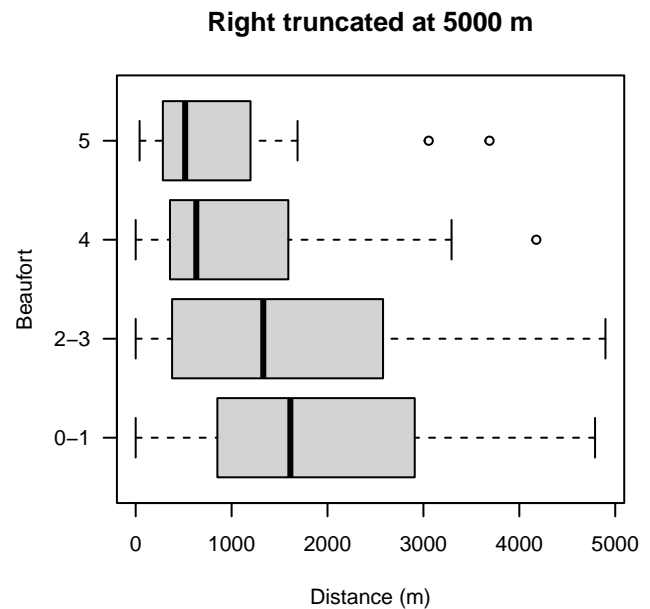
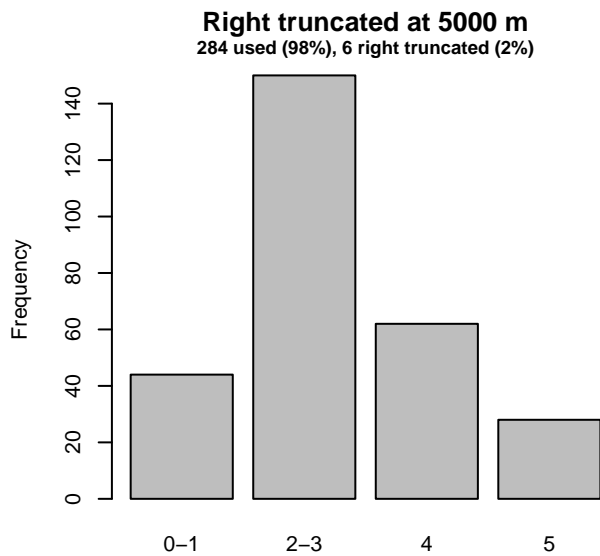
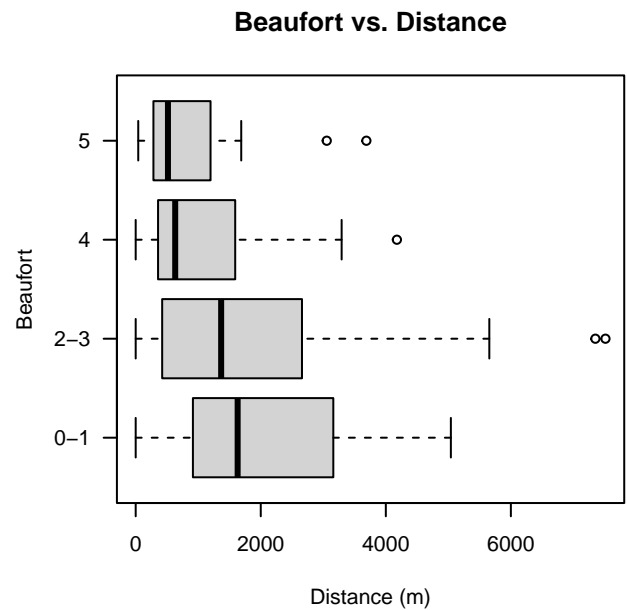
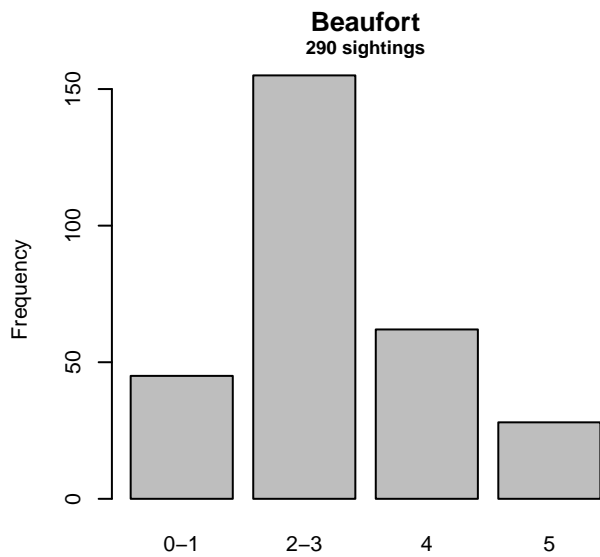


Figure 50: Distribution of the Beaufort covariate before (top row) and after (bottom row) observations were truncated to fit the SEFSC AMAPPS detection function.

2.2.2.3 NJ-DEP

After right-truncating observations greater than 3200 m, we fitted the detection function to the 175 observations that remained (Table 20). The selected detection function (Figure 51) used a hazard rate key function with no covariates.

Table 20: Observations used to fit the NJ-DEP detection function.

ScientificName	n
Delphinus delphis	19
Tursiops truncatus	156
Total	175

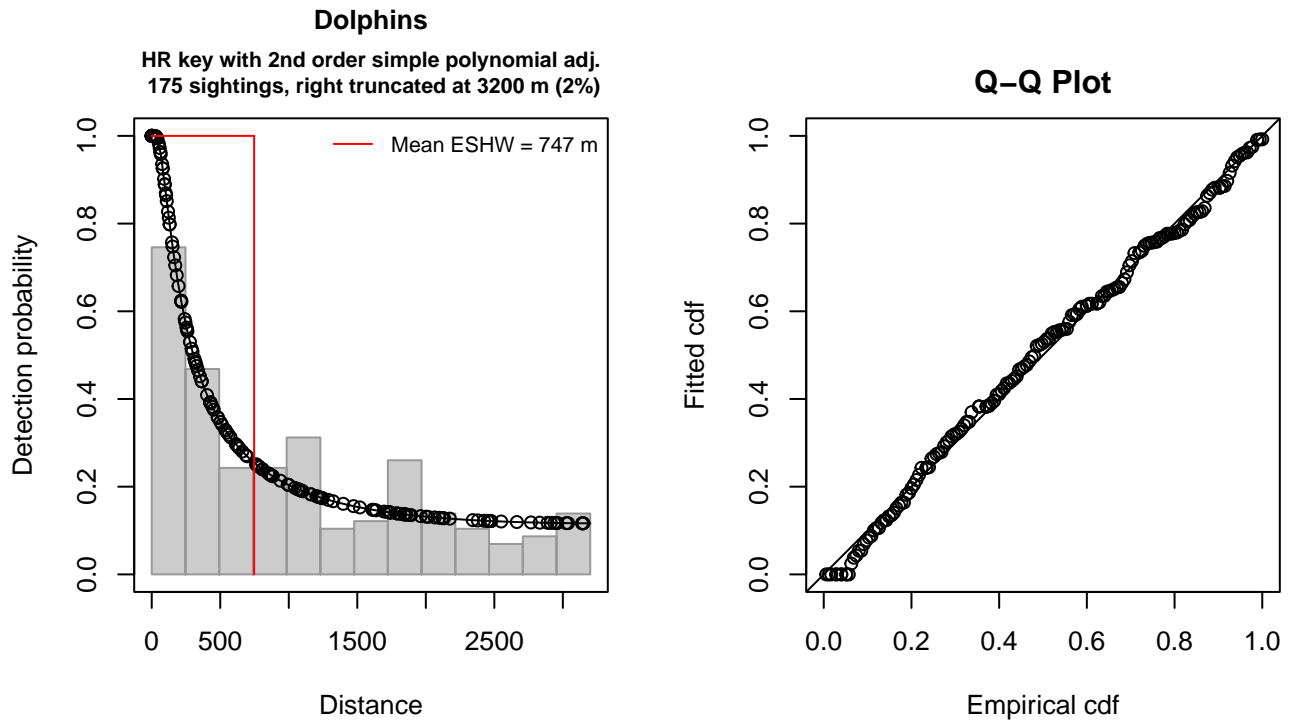


Figure 51: NJ-DEP detection function and Q-Q plot showing its goodness of fit.

Statistical output for this detection function:

Summary for ds object

Number of observations : 175
 Distance range : 0 - 3200
 AIC : 2750.547

Detection function:

Hazard-rate key function with simple polynomial adjustment term of order 2

Detection function parameters

Scale coefficient(s):
 estimate se
 (Intercept) 5.340225 0.502875

Shape coefficient(s):

estimate se
 (Intercept) 2.663565e-07 0.3025183

Adjustment term coefficient(s):
 estimate se
 poly, order 2 0.8448098 1.306568

Monotonicity constraints were enforced.

	Estimate	SE	CV
Average p	0.2335197	0.05159473	0.2209438
N in covered region	749.4013460	172.84391894	0.2306427

Monotonicity constraints were enforced.

Distance sampling Cramer-von Mises test (unweighted)
 Test statistic = 0.069450 p = 0.754942

2.2.2.4 Large Vessels

After right-truncating observations greater than 1100 m, we fitted the detection function to the 36 observations that remained (Table 21). The selected detection function (Figure 52) used a half normal key function with no covariates.

Table 21: Observations used to fit the Large Vessels detection function.

ScientificName	n
Lagenorhynchus acutus	36
Total	36

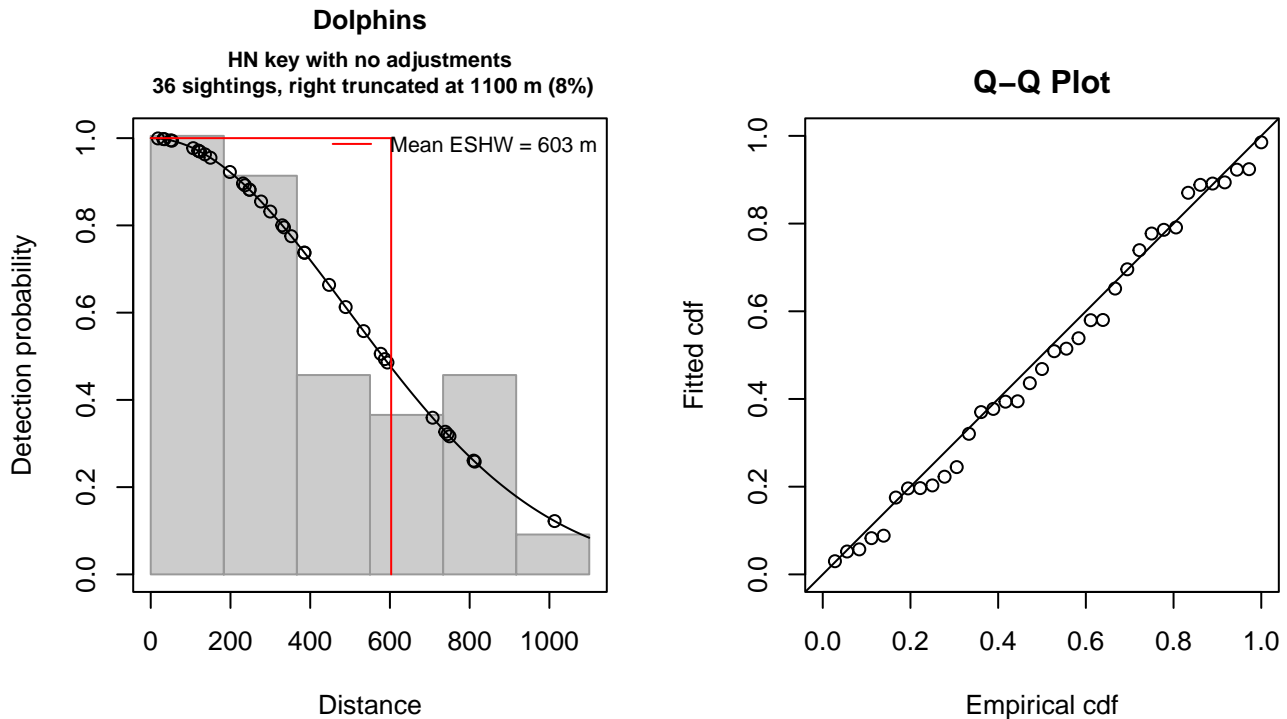


Figure 52: Large Vessels detection function and Q-Q plot showing its goodness of fit.

Statistical output for this detection function:

```
Summary for ds object
Number of observations : 36
Distance range         : 0 - 1100
```

AIC : 493.4472

Detection function:
Half-normal key function

Detection function parameters
Scale coefficient(s):
 estimate se
(Intercept) 6.202683 0.1646341

	Estimate	SE	CV
Average p	0.5483057	0.07646146	0.1394504
N in covered region	65.6568085	11.74385160	0.1788672

Distance sampling Cramer-von Mises test (unweighted)
Test statistic = 0.026241 p = 0.986825

3 Bias Corrections

Density surface modeling methodology uses *distance sampling* (Buckland et al. 2001) to model the probability that an observer on a line transect survey will detect an animal given the perpendicular distance to it from the transect line. Distance sampling assumes that detection probability is 1 when perpendicular distance is 0. When this assumption is not met, detection probability is biased high, leading to an underestimation of density and abundance. This is known as the $g_0 < 1$ problem, where g_0 refers to the detection probability at distance 0. Modelers often try to address this problem by estimating g_0 empirically and dividing it into estimated density or abundance, thereby correcting those estimates to account for the animals that were presumed missed.

Two important sources of bias for visual surveys are known as *availability bias*, in which an animal was present on the transect line but impossible to detect, e.g. because it was under water, and *perception bias*, in which an animal was present and available but not noticed, e.g. because of its small size or cryptic coloration or behavior (Marsh and Sinclair 1989). Modelers often estimate the influence of these two sources of bias on detection probability independently, yielding two estimates of g_0 , hereafter referred to as g_{0A} and g_{0P} , and multiply them together to obtain a final, combined estimate: $g_0 = g_{0A} \cdot g_{0P}$.

Our overall approach was to perform this correction on a per-observation basis, to have the flexibility to account for many factors such as platform type, surveyor institution, group size, group composition (e.g. singleton, mother-calf pair, or surface active group), and geographic location (e.g. feeding grounds vs. calving grounds). The level of complexity of the corrections varied by species according to the amount of information available, with North Atlantic right whale having the most elaborate corrections, derived from a substantial set of publications documenting its behavior, and various lesser known odontocetes having corrections based only on platform type (aerial or shipboard), derived from comparatively sparse information. Here we document the corrections used for striped dolphin.

3.1 Aerial Surveys

Palka et al. (2021) developed perception bias corrections using two team, mark recapture distance sampling (MRDS) methodology (Burt et al. 2014) for aerial surveys conducted in 2010-2017 by NOAA NEFSC and SEFSC during the AMAPPS program. These were the only extant perception bias estimates developed from aerial surveys used in our analysis, aside from estimates developed earlier by Palka and colleagues (Palka 2006; Palka et al. 2017). Those earlier efforts utilized older methods and less data than their 2021 analysis, so we applied the Palka et al. (2021) estimates to all aerial survey programs (Table 22).

We applied Palka's estimate for SEFSC to all programs other than NEFSC, as those programs mainly occurred to the south of NEFSC's study area, and overlapped more with SEFSC's. Also, striped dolphin group sizes were larger in the southerly programs, better matching SEFSC's group sizes than NEFSC's (Table 1). Given that larger groups are easier to detect than smaller groups, it was appropriate to apply SEFSC's weaker correction. However, for all surveys, to account for the influence of large group sizes on perception bias, we followed Carretta et al. (2000) and set the perception bias correction factor for sightings of more than 25 animals to $g_{0P} = 0.994$.

We caution that it is possible that perception bias was different on the other aerial programs, as they often used different aircraft, flew at different altitudes, and were staffed by different personnel. Of particular concern are that many programs flew Cessna 337 Skymasters, which had flat windows, while NOAA flew de Havilland Twin Otters, which had bubble windows,

which likely afforded a better view of the transect line and therefore might have required less of a correction than the Skymasters. Correcting the other programs using NOAA’s estimate as we have done is likely to yield less bias than leaving them uncorrected, but we urge all programs to undertake their own efforts to estimate perception bias, as resources allow.

We estimated availability bias corrections using the Laake et al. (1997) estimator and dive intervals reported by Palka et al. (2017) (Table 23). To estimate time in view, needed by the Laake estimator, we used results reported by Robertson et al. (2015), rescaled linearly for each survey program according to its target altitude and speed. We caution that Robertson’s analysis was done for a de Havilland Twin Otter, which may have a different field of view than that of the other aircraft used here, which mainly comprised Cessna 337 Skymasters with flat windows. However, we note that McLellan et al. (2018) conducted a sensitivity analysis on the influence of the length of the “window of opportunity” to view beaked whales from a Cessna Skymaster on their final density estimates and found that they varied by only a few thousandths of an animal per kilometer when the window of opportunity more than doubled. Still, we urge additional program-specific research into estimation of availability bias.

To address the influence of group size on availability bias, we applied the group availability estimator of McLellan et al. (2018) on a per-observation basis. Following Palka et al. (2021), who also used that method, we assumed that individuals in the group dived asynchronously. The resulting g_{0A} corrections ranged from about 0.94 to 1 (Figure 53), with the large majority of observations having a correction of 0.98 or higher, owing to large group sizes. We caution that the assumption of asynchronous diving can lead to an underestimation of density and abundance if diving is actually synchronous; see McLellan et al. (2018) for an exploration of this effect. However, if future research finds that this species conducts synchronous dives and characterizes the degree of synchronicity, the model can be updated to account for this knowledge.

Table 22: Perception bias corrections for striped dolphin applied to aerial surveys.

Surveys	Group Size	g_{0P}	g_{0P} Source
SEFSC	≤ 25	0.78	Palka et al. (2021): SEFSC
All others	≤ 25	0.56	Palka et al. (2021): NEFSC
All	> 25	0.99	Caretta et al. 2000

Table 23: Surface and dive intervals for striped dolphin used to estimate availability bias corrections.

Surface Interval (s)	Dive Interval (s)	Source
44	59.4	Palka et al. (2017)

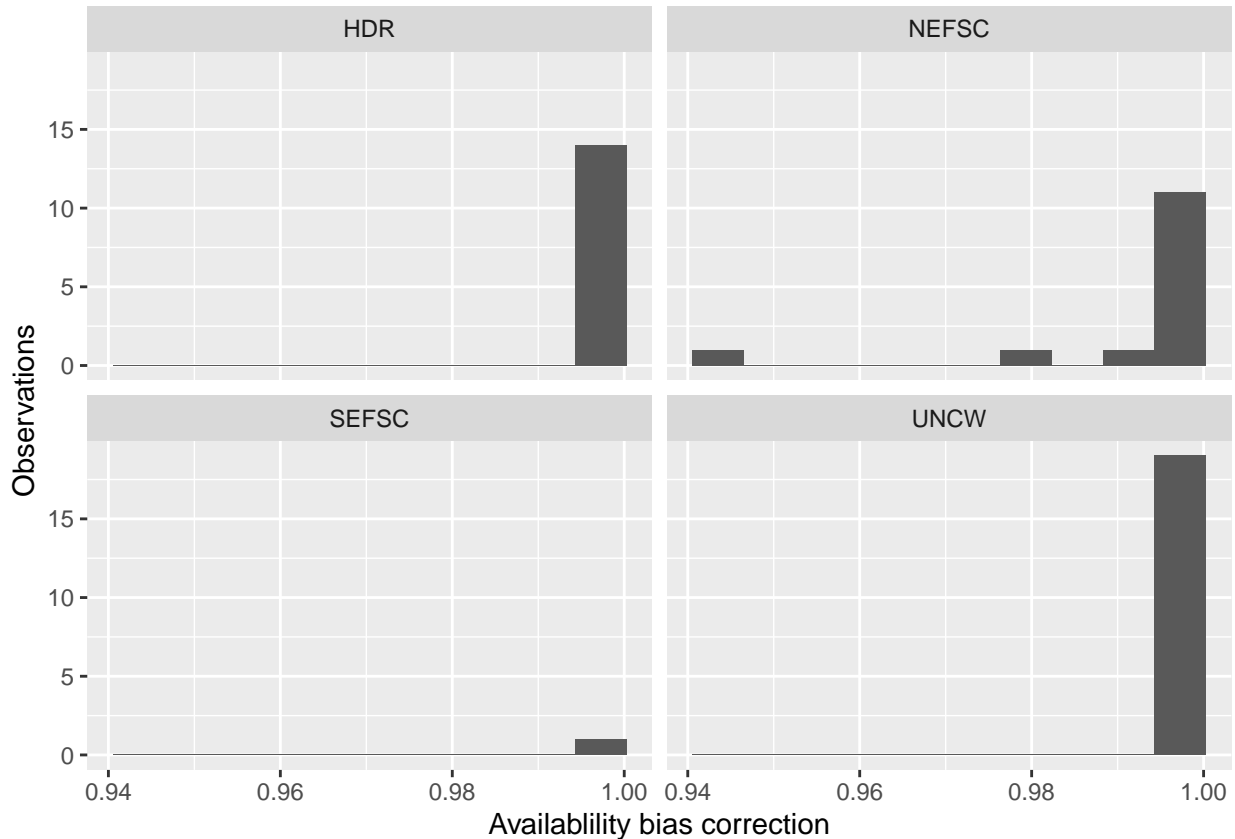


Figure 53: Availability bias corrections for striped dolphin for aerial surveys, by institution.

3.2 Shipboard Surveys

Most of the shipboard surveys in our analysis used high-power (25x150), pedestal-mounted binoculars. Similar to aerial surveys, Palka et al. (2021) developed perception bias corrections using two team, MRDS methodology (Burt et al. 2014) for high-power binocular surveys conducted in 2010-2017 by NOAA NEFSC and SEFSC during the AMAPPS program. These were the only extant perception bias estimates developed from high-power binocular surveys used in our analysis, aside from estimates developed earlier by Palka and colleagues (Palka 2006; Palka et al. 2017). Those earlier efforts utilized older methods and less data than their 2021 analysis, so we applied the Palka et al. (2021) estimates to all shipboard surveys that searched with high-power binoculars (Table 24).

A few surveys used naked eyes rather than high-power binoculars, but none of these programs prepared perception bias estimates for striped dolphin. So as a proxy, we used the estimate for Atlantic white-sided dolphins from AJ 99-02 estimate for the AJ 99-02 survey from Palka (2006) (Table 24).

For all surveys, to account for the influence of large group sizes on perception bias, we followed Barlow and Forney (2007) and set the perception bias correction factor for sightings of more than 20 animals to $g_{0P} = 0.97$. Given that the dive interval of this species (Table 23) was short relative to the amount of time a given patch of water remained in view to shipboard observers, we assumed that no availability bias correction was needed ($g_{0A} = 1$), following Palka et al. (2021).

Table 24: Perception and availability bias corrections for striped dolphin applied to shipboard surveys.

Surveys	Searching Method	Group Size	g_{0P}	g_{0P} Source	g_{0A}	g_{0A} Source
NEFSC	Binoculars	≤ 20	0.72	Palka et al. (2021): NEFSC	1	Assumed
SEFSC	Binoculars	≤ 20	0.62	Palka et al. (2021): SEFSC	1	Assumed
MCR	Naked Eye	≤ 20	0.27	Palka (2006)	1	Assumed
All	All	> 20	0.97	Barlow and Forney (2007)	1	Assumed

4 Density Model

Striped dolphins are found throughout the world in tropical and warm-temperate waters (Archer and Perrin 1999). In the western North Atlantic striped dolphins are reported to primarily occur along the shelf edge from Cape Hatteras to the southern edge of Georges Bank as well as offshore over the mid-Atlantic slope region (Winn 1982; Fulling et al. 2003; Hayes et al. 2020). The northern range of the species is not well-established, with some studies reporting that the northern limit is a function of water temperature (Bloch et al. 1996; Doksæter et al. 2008) and affected by processes such as meanderings of the Gulf Stream (Archer and Perrin 1999). Sightings and strandings occur occasionally along the east coast of Canada (Baird et al. 1993; Hooker et al. 1999). While striped dolphins are considered rare in Canadian Atlantic waters (Baird et al. 1997), Gowans and Whitehead (1995) reported 26 summer sightings in the deeper (>800m) and warmer waters (13-22°C) of the Gully during four survey years between 1989-1994, which suggests that this region may be an important part of their range. There has been a single live stranding of striped dolphin in Newfoundland and Labrador (Ledwell et al. 2018). This evidence reinforces the uncertainty in understanding the northern limits of the striped dolphin range.

Despite being described as a warm water species, the sightings of striped dolphin reported by the surveys utilized in our study occurred mainly north of the Gulf Stream. The coldest sighting occurred in 9°C and the warmest sighting occurred in 29°C. However, over 82% of the sightings occurred in waters warmer than 20°C. Nearly all of the sightings occurred over the continental slope or abyssal waters, with only 26 sightings occurring at depths less than 900 m. This corresponds well with Palka et al. (1997) who reported striped dolphin sightings associated with waters that were between 20°C and 27°C and deeper than 900 m. In oceanic waters, striped dolphins were reported to be associated with the north wall of the Gulf Stream and warm-core rings (Waring et al. 2014) and, at the mid-Atlantic Ridge, with warm, saline waters over steeper slopes than non-dolphin species. Additionally, shelf-edge sightings have been reportedly centered along the 1,000 m isobath in all seasons (Winn 1982).

The model selection procedure was straightforward. When ranked by REML score (Wood 2011), the highest ranked models with contemporaneous covariates outranked those with climatological covariates, and explained over 3% more deviance. This is perhaps unsurprising given the known relationships of striped dolphins with dynamic habitat features, such as SST and eddies. The striped dolphin model contained over 1 million km of segments with 397 total sightings of groups. The top contemporaneous model selected with the highest explained deviance and lowest AIC and REML scores retained 8 covariates (Table 25) (Figure 57), including an xy bivariate smooth. The relationship to xy showed that the highest abundance of animals was predicted north of Cape Hatteras in primarily offshore regions. The inclusion of the xy term arguably may have led to overfitting in this model, but without it the predictions included portions of the southern study area where no observations have historically occurred. Additionally, models that included xy resulted in lower REML and AIC scores and higher explained deviance in all cases.

The other covariates retained in the top model included another bivariate term, SST and distance to shore and univariate terms; depth, bottom temperature, epipelagic micronekton, distance to canyons, total kinetic energy (TKE), and distance to cyclonic eddies. The relationship to the bivariate term SST and distance to shore, showed that more animals were predicted between 50 and 200 km from shore in temperate waters as well as far from shore in warmer waters. The relationship to depth showed that the number of animals increases with increasing depth. The relationship to bottom temperature showed declining numbers of animals predicted at bottom temperatures of about 12°C or greater. There was a generally positive relationship with epipelagic micronekton, whereby greater numbers of animals were predicted at higher epipelagic micronekton biomass. Striped dolphins are considered opportunistic feeders who primarily consume fish (namely lanternfish), cephalopods and crustaceans (Ringelstein et al. 2006). Ringelstein et al. (2006). who examined the stomach contents of 60 striped dolphins caught in the albacore drift-net fishery throughout the summer months of 1992 and 1993 in the Bay of Biscay suggest that most of the foraging activity of the dolphins examined took place at dusk or early night, when deep sea organisms move up to the surface layer. Given this evidence, the relationship between striped dolphins and epipelagic micronekton biomass makes sense. There was a negative relationship to distance to canyons, with fewer animals predicted far from canyons, suggesting that these features are important habitat for striped dolphins in the study region. There was also a negative relationship to total kinetic energy, so as total kinetic energy increases, the number of animals predicted decrease. In the East Coast study area, places of highest total kinetic energy are in the Gulf Stream and high numbers of sightings occur near and are predicted in or near the north wall of the Gulf Stream, where TKE is higher than outside the Gulf Stream but lower than in the southern Gulf Stream. The relationship between striped dolphins and the northern wall of the Gulf Stream has been previously described in the literature (Hayes et al. 2020). Finally, there was an ecological envelope shown for the relationship to distance to cyclonic eddies, showing a peak between 300 and 500 km of cyclonic eddies, indicating that striped dolphins may have a preference for waters far from cold-core rings. This may also indicate a north/south divide in preferred habitat in the study area. North of the Gulf Stream there are more warm-core rings than cold-core rings, and conversely in the south there are more cold-core rings. As such, this relationship may be related to striped dolphins preference for staying out of the area south of the Gulf Stream.

4.1 Final Model

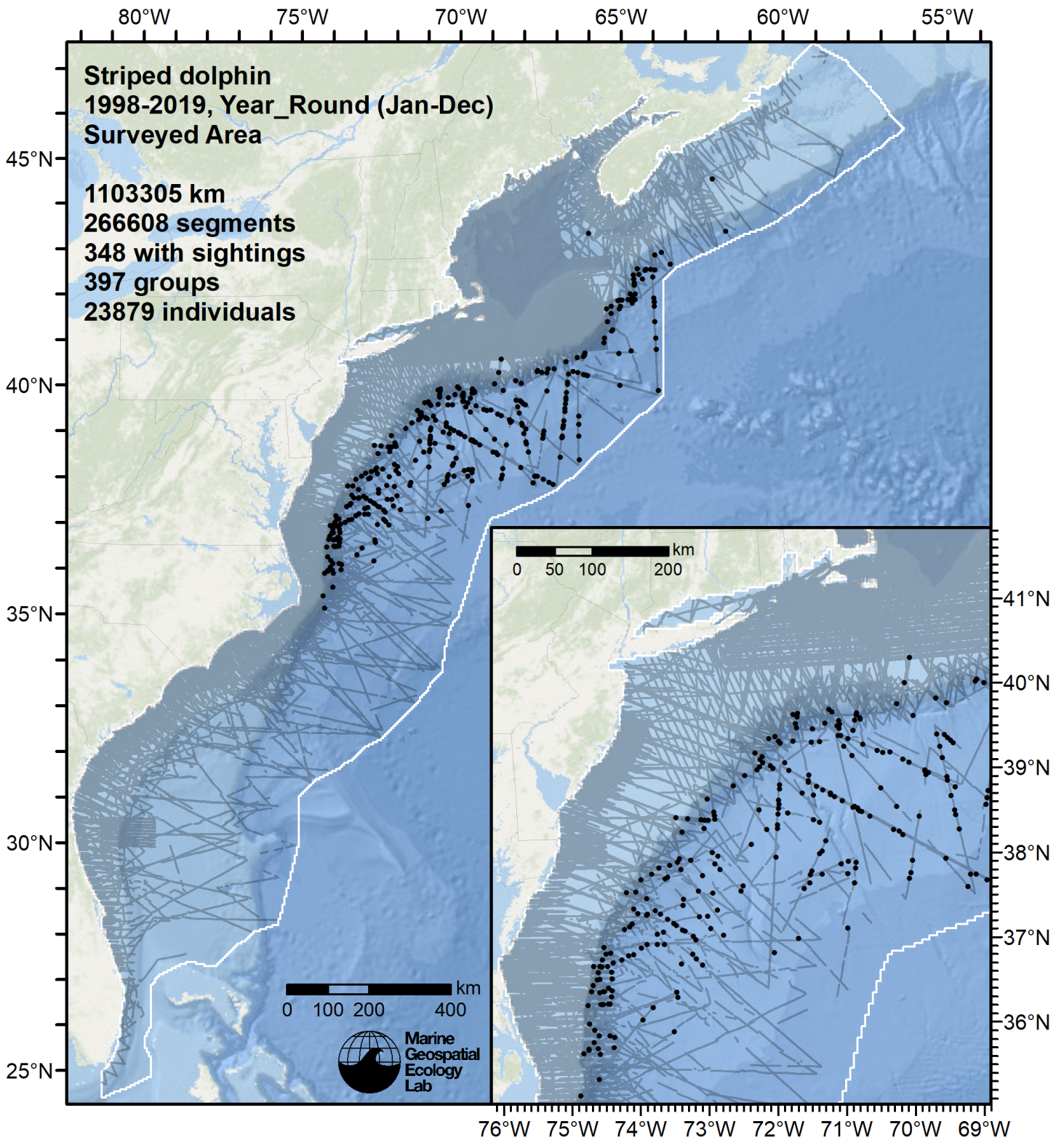


Figure 54: Survey segments used to fit the model. Black points indicate segments with observations.

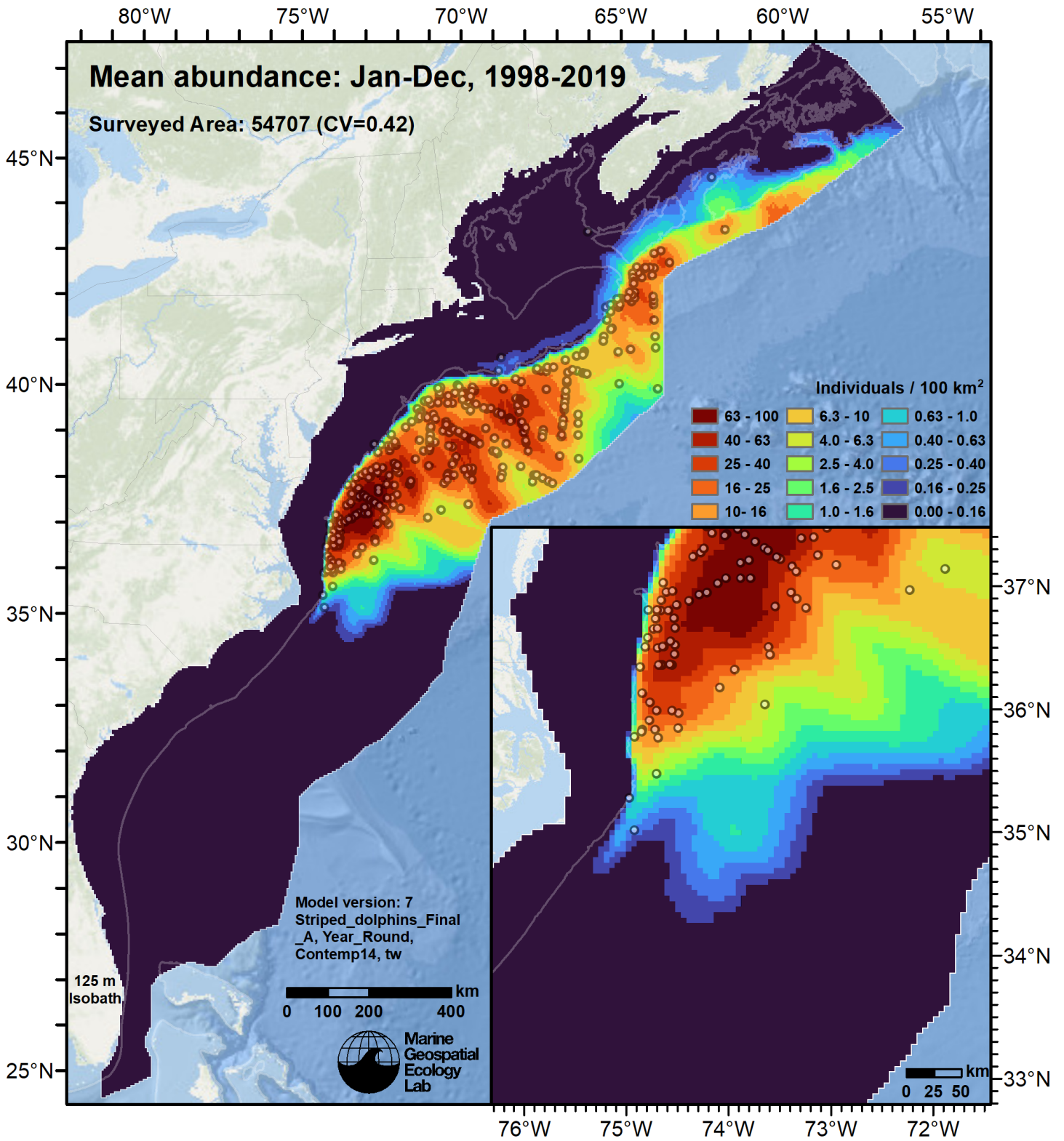


Figure 55: Striped dolphin mean density for the indicated period, as predicted by the model. Open circles indicate segments with observations. Mean total abundance and its coefficient of variation (CV) are given in the subtitle. Variance was estimated with the analytic approach given by Miller et al. (2022), Appendix S1, and accounts both for uncertainty in model parameter estimates and for seasonal and interannual variability in dynamic covariates.

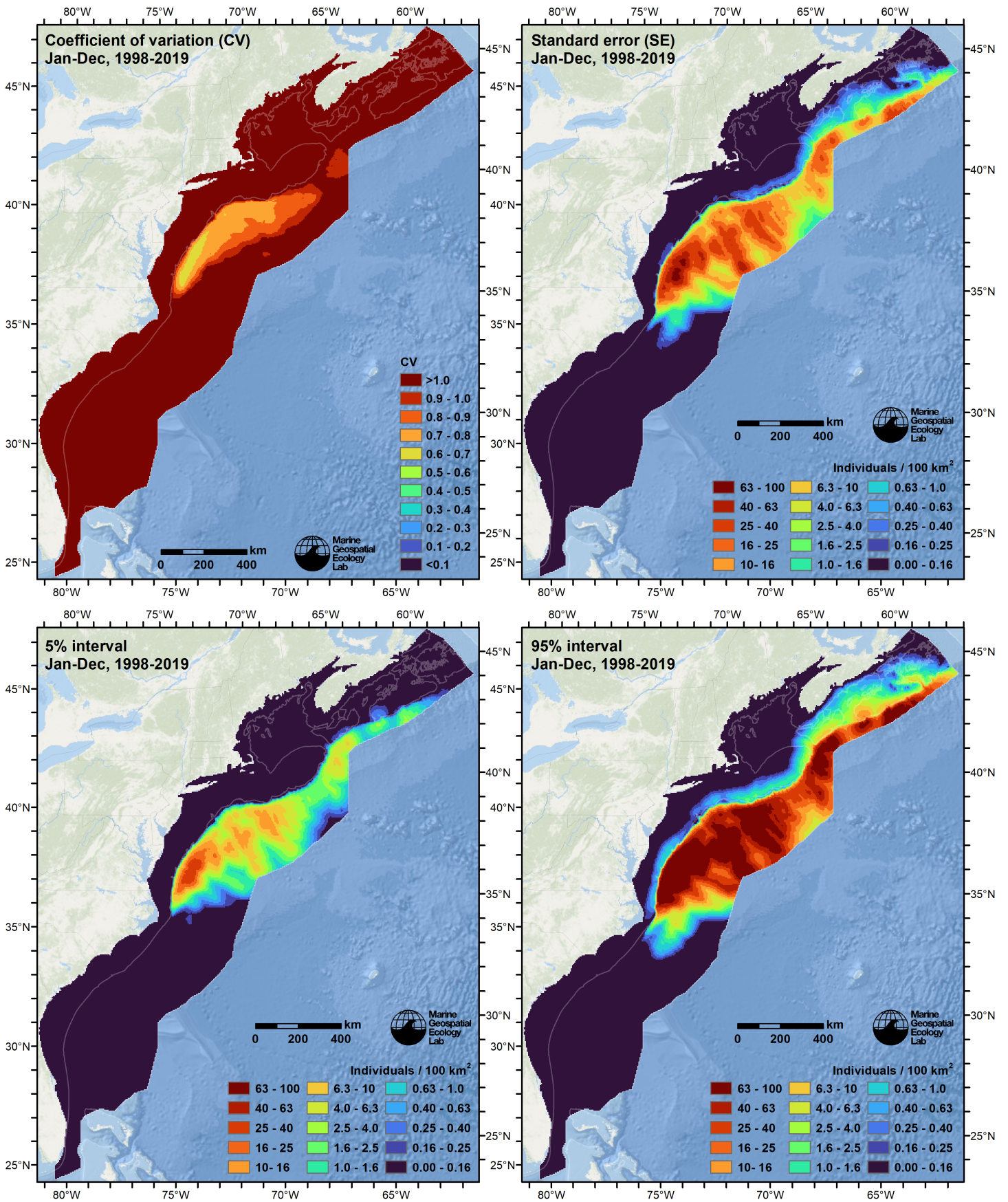


Figure 56: Uncertainty statistics for the striped dolphin mean density surface (Figure 55) predicted by the model. Variance was estimated with the analytic approach given by Miller et al. (2022), Appendix S1, and accounts both for uncertainty in model parameter estimates and for seasonal and interannual variability in dynamic covariates.

Statistical output for this model:

Family: Tweedie(p=1.308)

Link function: log

Formula:

```
IndividualsCorrected ~ offset(log(SegmentArea)) + s(I(x/1000),
  I(y/1000), bs = "ts", k = 50) + te(pmax(50, pmin(I(DistToShore/1000),
  450)), pmax(2.5, SST_CMC), bs = "ts") + s(log10(pmax(10,
  Depth)), bs = "ts") + s(pmax(3, pmin(BotT_HYCOM, 28)), bs = "ts") +
  s(log10((pmax(0.01, pmin(MnkEpi, 29))))) , bs = "ts") + s(pmin(I(DistToCan/1000),
  450), bs = "ts") + s(log10(pmax(0.002, TKE)), bs = "ts") +
  s(pmin(I(DistToCEddy90/1000), 700), bs = "ts")
```

Parametric coefficients:

	Estimate	Std. Error	t value	Pr(> t)
(Intercept)	-31.951	3.496	-9.139	<2e-16 ***

Signif. codes: 0 '***' 0.001 '**' 0.01 '*' 0.05 '.' 0.1 ' ' 1

Approximate significance of smooth terms:

	edf	Ref.df
s(I(x/1000),I(y/1000))	19.2043	49
te(pmax(50, pmin(I(DistToShore/1000), 450)),pmax(2.5, SST_CMC))	11.4092	24
s(log10(pmax(10, Depth)))	0.9539	9
s(pmax(3, pmin(BotT_HYCOM, 28)))	2.3681	9
s(log10((pmax(0.01, pmin(MnkEpi, 29)))))	3.4675	9
s(pmin(I(DistToCan/1000), 450))	1.0007	9
s(log10(pmax(0.002, TKE)))	1.0607	9
s(pmin(I(DistToCEddy90/1000), 700))	3.4210	9
	F	p-value
s(I(x/1000),I(y/1000))	1.819	< 2e-16
te(pmax(50, pmin(I(DistToShore/1000), 450)),pmax(2.5, SST_CMC))	2.208	< 2e-16
s(log10(pmax(10, Depth)))	0.855	0.001986
s(pmax(3, pmin(BotT_HYCOM, 28)))	1.535	0.000351
s(log10((pmax(0.01, pmin(MnkEpi, 29)))))	2.057	0.000123
s(pmin(I(DistToCan/1000), 450))	2.171	1.79e-06
s(log10(pmax(0.002, TKE)))	1.642	4.50e-05
s(pmin(I(DistToCEddy90/1000), 700))	2.145	0.000125

s(I(x/1000),I(y/1000))	***
te(pmax(50, pmin(I(DistToShore/1000), 450)),pmax(2.5, SST_CMC))	***
s(log10(pmax(10, Depth)))	**
s(pmax(3, pmin(BotT_HYCOM, 28)))	***
s(log10((pmax(0.01, pmin(MnkEpi, 29)))))	***
s(pmin(I(DistToCan/1000), 450))	***
s(log10(pmax(0.002, TKE)))	***
s(pmin(I(DistToCEddy90/1000), 700))	***

Signif. codes: 0 '***' 0.001 '**' 0.01 '*' 0.05 '.' 0.1 ' ' 1

R-sq.(adj) = 0.0388 Deviance explained = 67.2%

-REML = 3389.5 Scale est. = 73.698 n = 266608

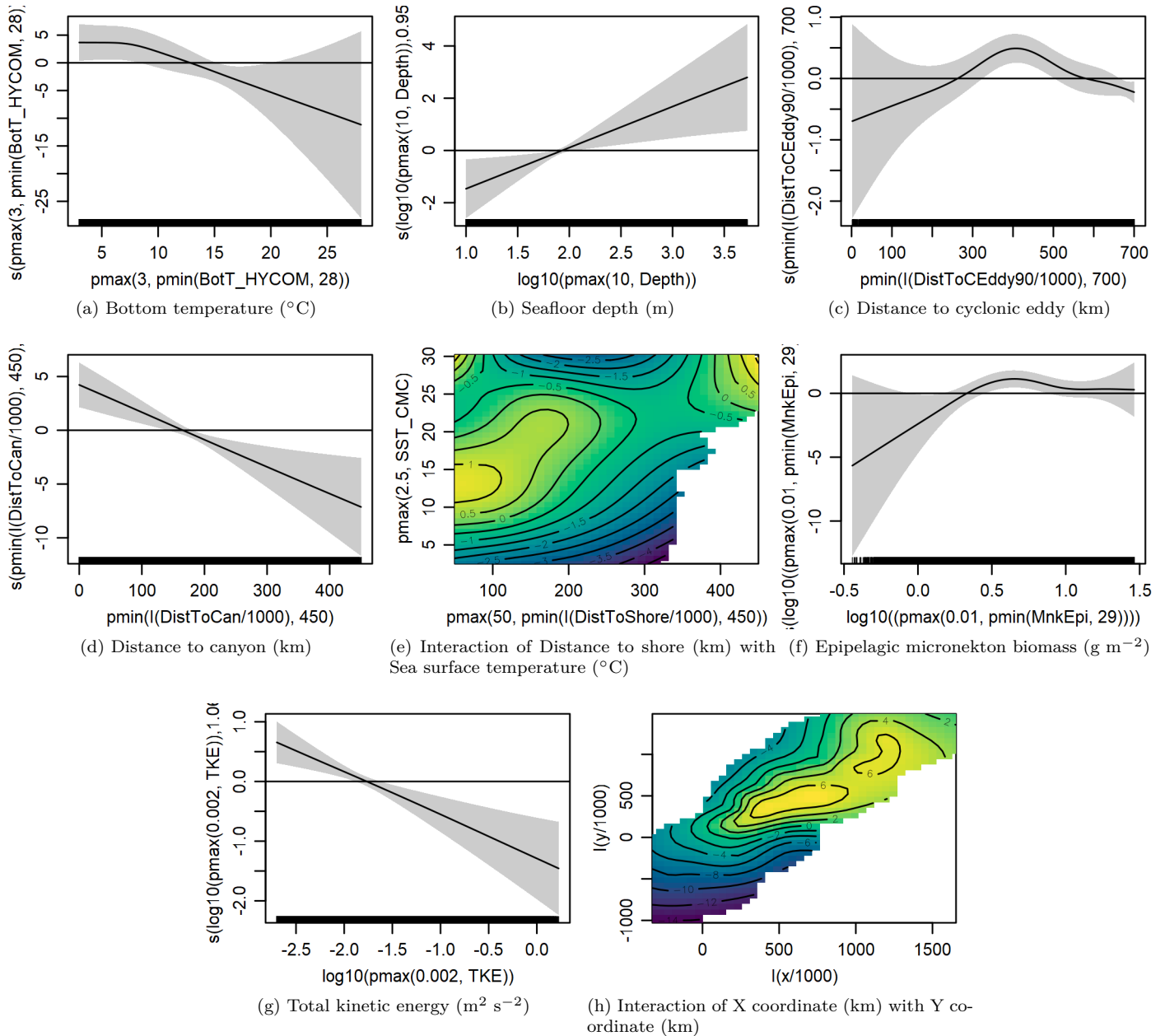


Figure 57: Functional plots for the final model. Transforms and other treatments are indicated in axis labels. \log_{10} indicates the covariate was \log_{10} transformed. $pmax$ and $pmin$ indicate the covariate's minimum and maximum values, respectively, were Winsorized to the values shown. Winsorization was used to prevent runaway extrapolations during prediction when covariates exceeded sampled ranges, or for ecological reasons, depending on the covariate. $/1000$ indicates meters were transformed to kilometers for interpretation convenience.

Table 25: Covariates used in the final model.

Covariate	Description
BotT_HYCOM	Monthly mean bottom temperature ($^{\circ}\text{C}$) from the HYCOM GOFS 3.1 $1/12^{\circ}$ ocean model (Chassignet et al. (2009))
Depth	Depth (m) of the seafloor, from SRTM30_PLUS (Becker et al. (2009))

Table 25: Covariates used in the final model. (continued)

Covariate	Description
DistToCEddy90	Monthly mean distance (km) to the edge of the closest cyclonic mesoscale eddy at least 90 days old, derived with MGET (Roberts et al. (2010)) from the Aviso Mesoscale Eddy Trajectories Atlas (META2.0), produced by SSALTO/DUACS and distributed by AVISO+ (https://aviso.altimetry.fr) with support from CNES, in collaboration with Oregon State University with support from NASA, using the method of Schlax and Chelton (2016), based on Chelton et al. (2011)
DistToCan	Distance (km) to the closest submarine canyon, derived from the Harris et al. (2014) geomorphology
DistToShore	Distance (km) to shore excluding Bermuda and Sable Island, derived from SRTM30_PLUS (Becker et al. (2009))
MnkEpi	Monthly mean micronekton biomass available in the epipelagic zone, expressed as wet weight (g m^{-2}), from SEAPODYM (Lehodey et al. (2008); Lehodey et al. (2015)), provided by E.U. Copernicus Marine Service. doi: 10.48670/moi-00020 . Computed as the sum of the SEAPODYM mnkc_epi, mnkc_mumeso, and mnkc_hmlmeso variables.
SST_CMC	Monthly mean sea surface temperature ($^{\circ}\text{C}$) from GHRSSST Level 4 CMC0.2deg and CMC0.1deg (Brasnett (2008); Canada Meteorological Center (2012); Meissner et al. (2016); Canada Meteorological Center (2016))
TKE	Monthly mean total kinetic energy ($\text{m}^2 \text{s}^{-2}$) derived from Aviso Ssalto/Duacs global gridded L4 reprocessed geostrophic currents, produced and distributed by E.U. Copernicus Marine Service. doi: 10.48670/moi-00148
x	X coordinate (km) in the Albers equal area map projection of the analysis
y	Y coordinate (km) in the Albers equal area map projection of the analysis

4.2 Diagnostic Plots

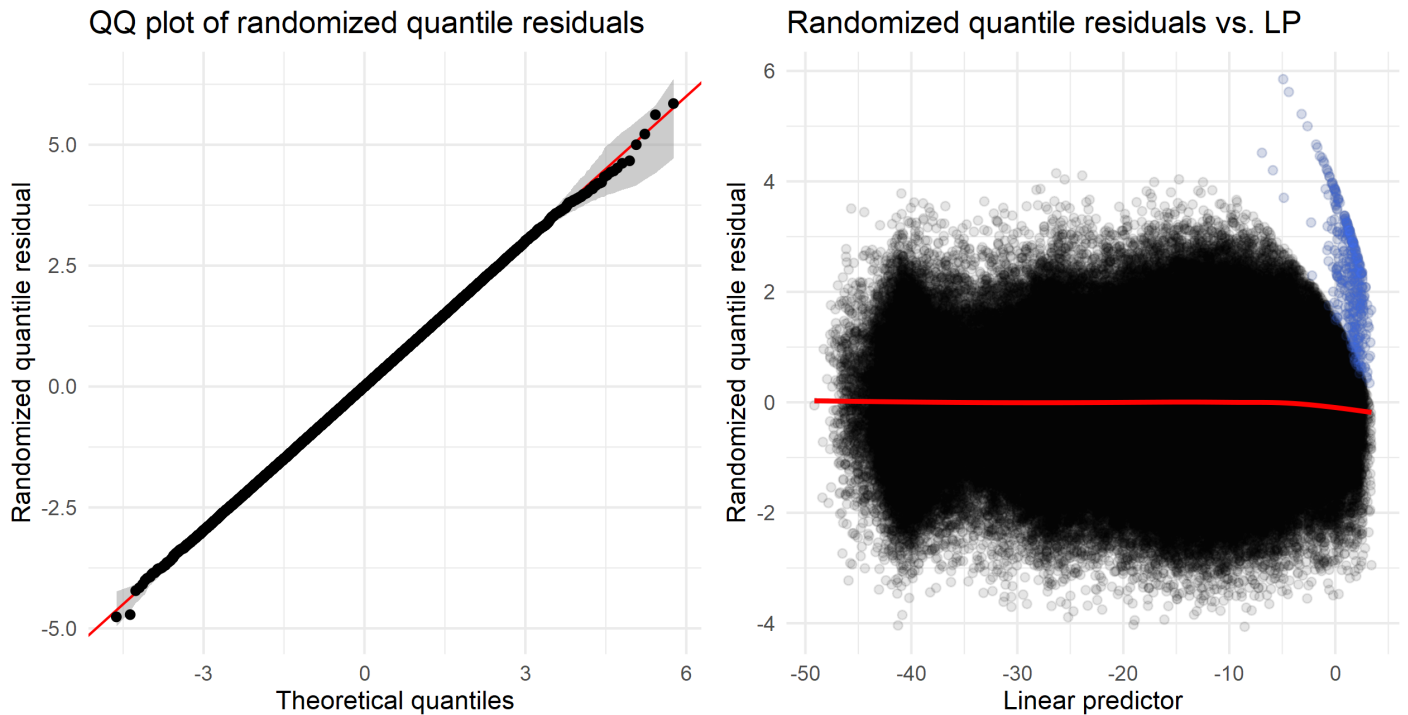


Figure 58: Residual plots for the final model.

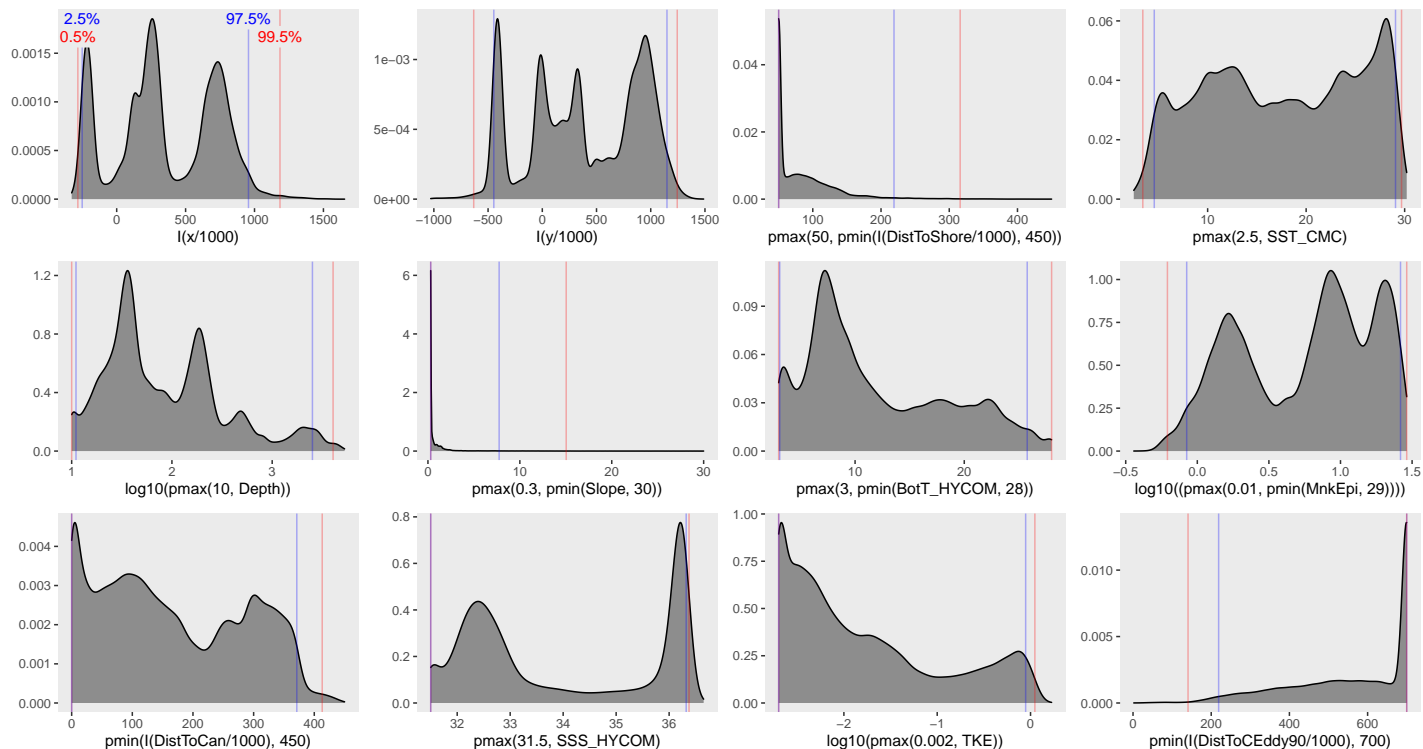


Figure 59: Density histograms showing the distributions of the covariates considered during the final model selection step. The final model may have included only a subset of the covariates shown here (see Figure 57), and additional covariates may have been considered in preceding selection steps. Red and blue lines enclose 99% and 95% of the distributions, respectively. Transforms and other treatments are indicated in axis labels. \log_{10} indicates the covariate was \log_{10} transformed. $pmax$ and $pmin$ indicate the covariate's minimum and maximum values, respectively, were Winsorized to the values shown. Winsorization was used to prevent runaway extrapolations during prediction when covariates exceeded sampled ranges, or for ecological reasons, depending on the covariate. $/1000$ indicates meters were transformed to kilometers for interpretation convenience.

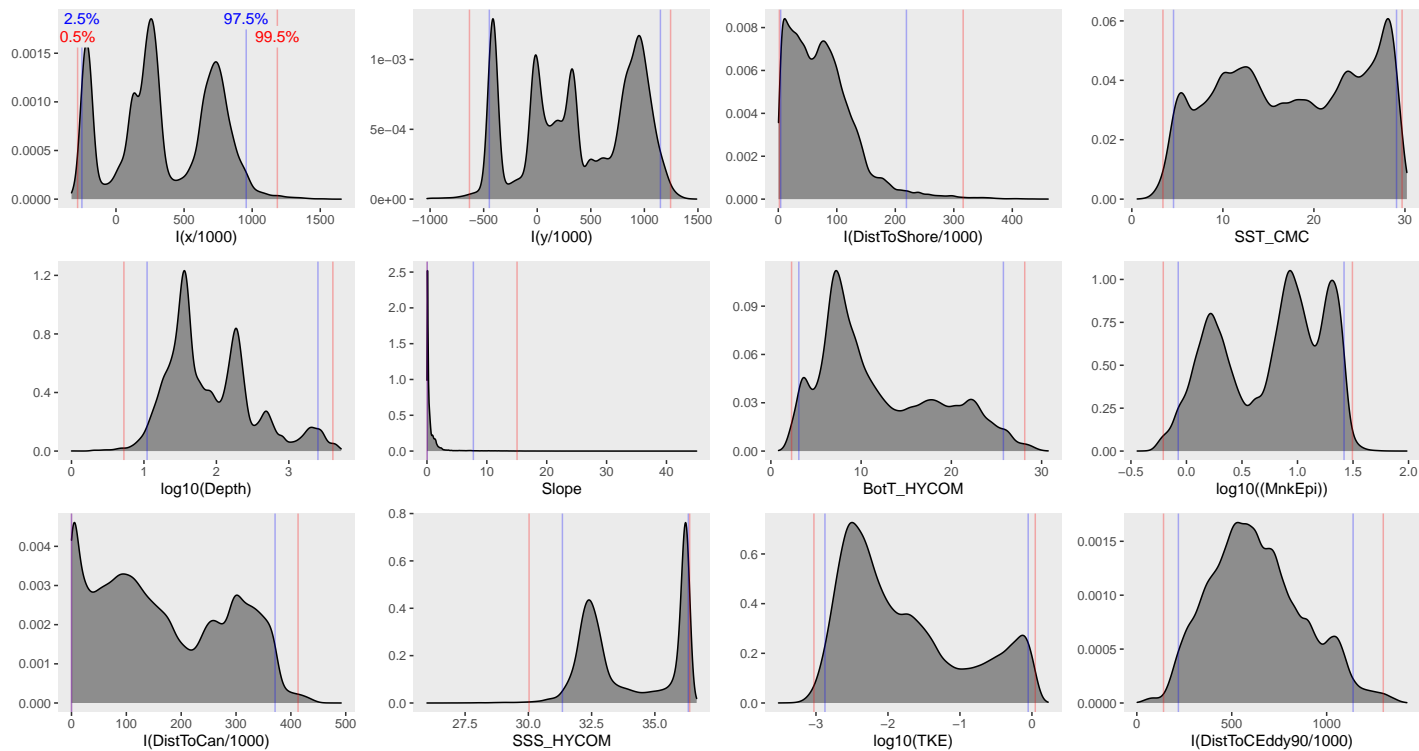


Figure 60: Density histograms shown in Figure 59 replotted without Winsorization, to show the full range of sampling represented by survey segments.

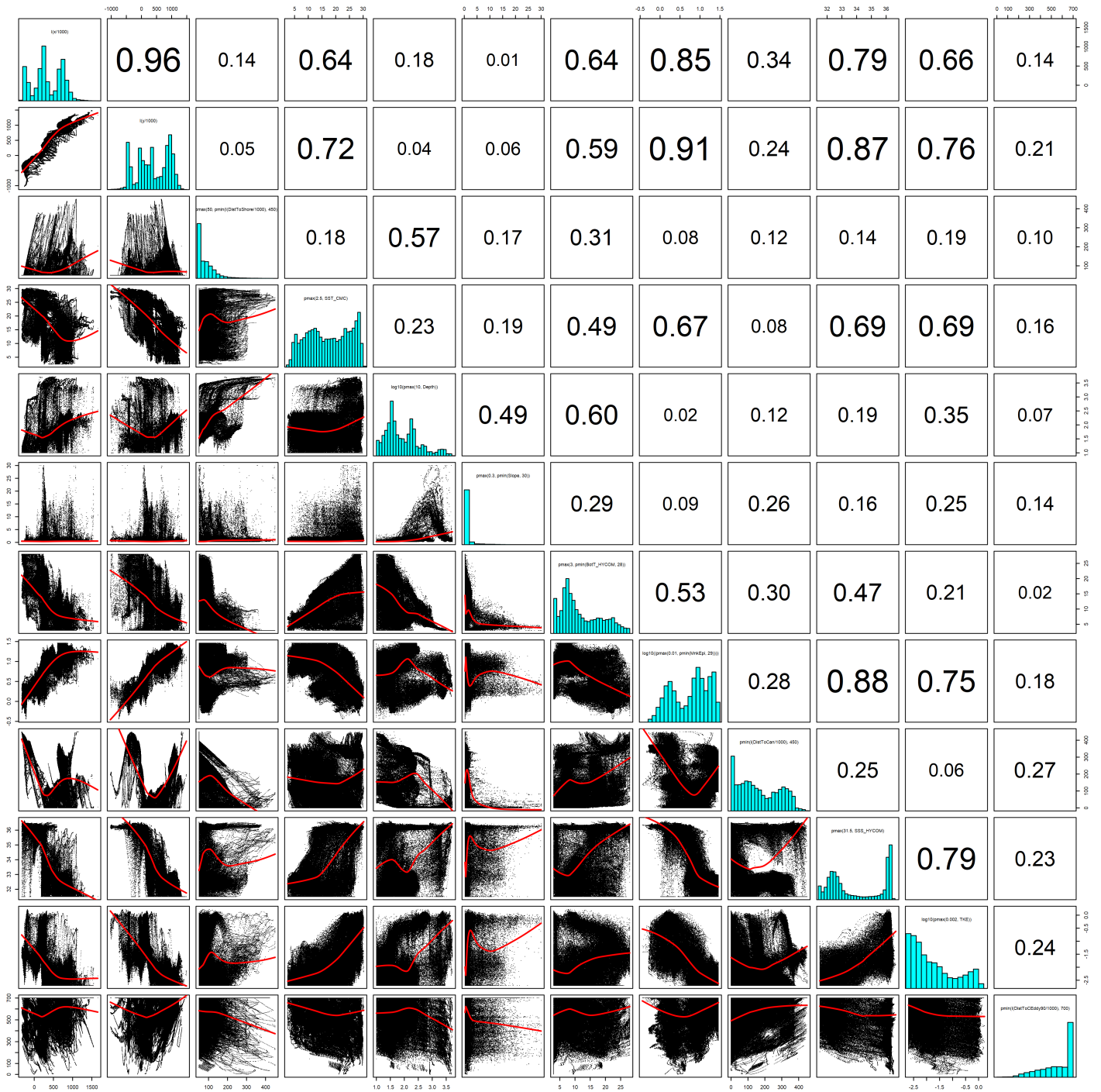


Figure 61: Scatterplot matrix of the covariates considered during the final model selection step. The final model may have included only a subset of the covariates shown here (see Figure 57), and additional covariates may have been considered in preceding selection steps. Covariates are transformed and Winsorized as shown in Figure 59. This plot is used to check simple correlations between covariates (via pairwise Pearson coefficients above the diagonal) and visually inspect for concurvity (via scatterplots and red loess curves below the diagonal).

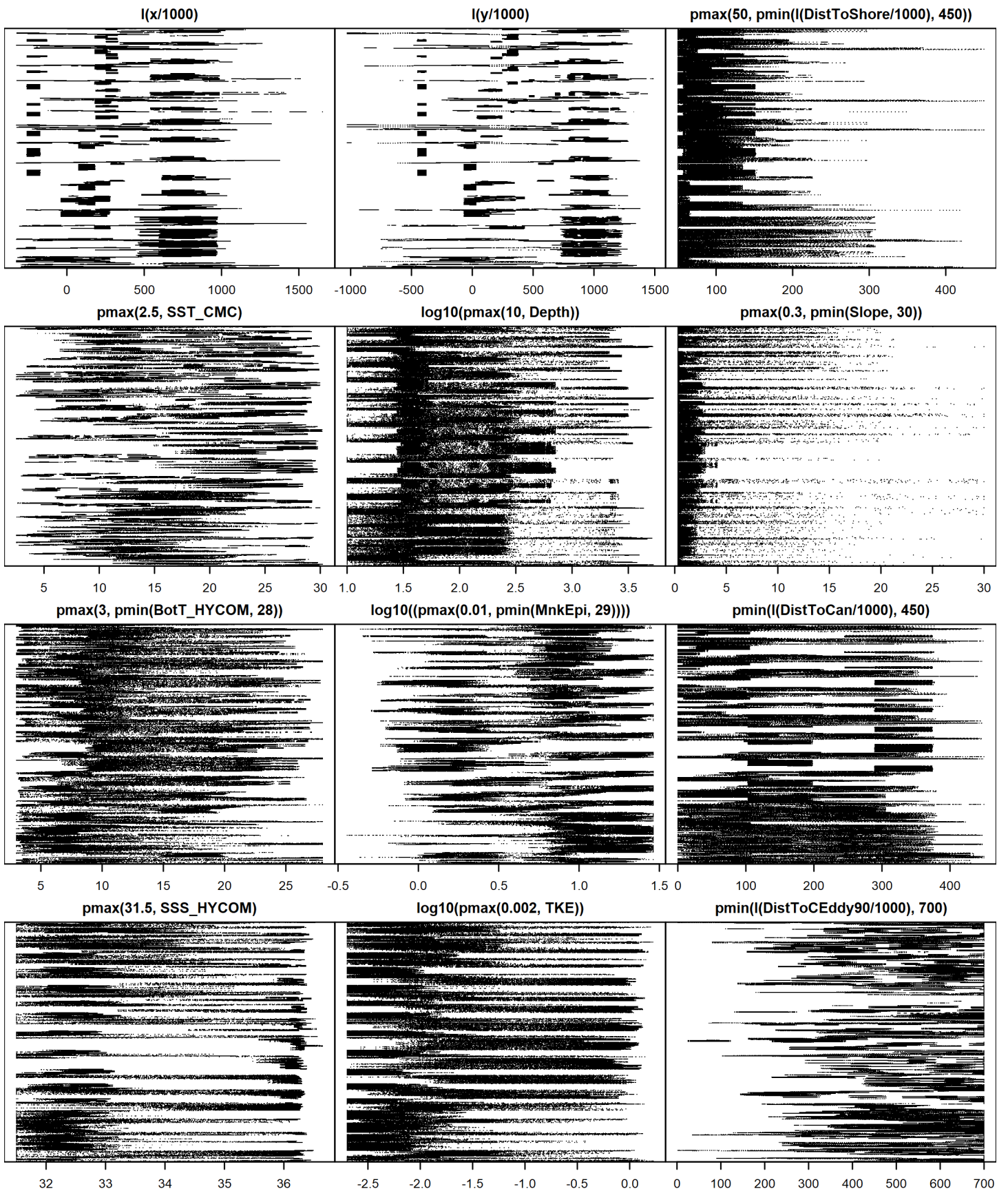


Figure 62: Dotplot of the covariates considered during the final model selection step. The final model may have included only a subset of the covariates shown here (see Figure 57), and additional covariates may have been considered in preceding selection steps. Covariates are transformed and Winsorized as shown in Figure 59. This plot is used to check for suspicious patterns and outliers in the data. Points are ordered vertically by segment ID, sequentially in time.

4.3 Extrapolation Diagnostics

4.3.1 Univariate Extrapolation

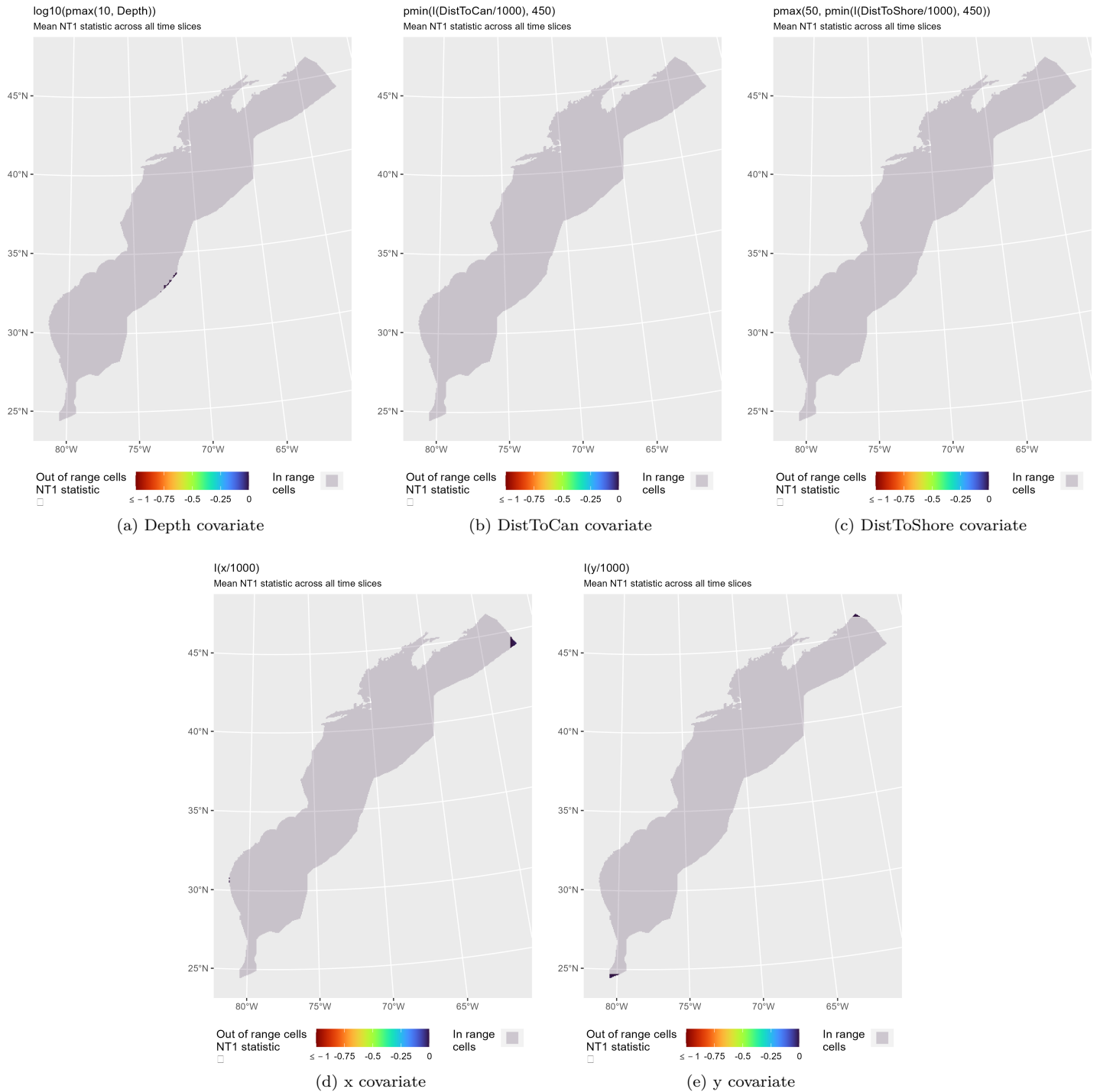


Figure 63: NT1 statistic (Mesgaran et al. (2014)) for static covariates used in the model. Areas outside the sampled range of a covariate appear in color, indicating univariate extrapolation of that covariate occurred there. Areas within the sampled range appear in gray, indicating it did not occur.

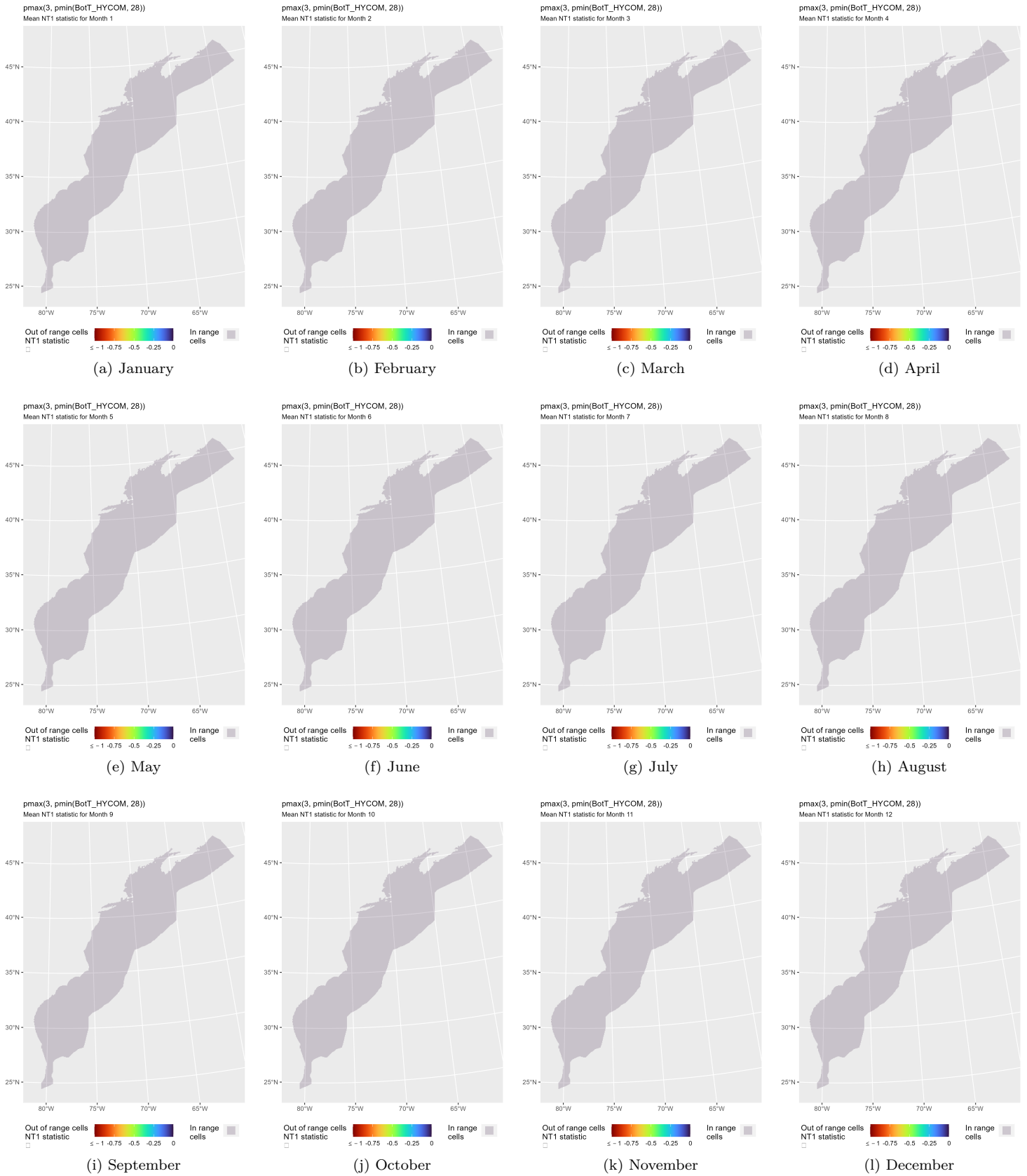


Figure 64: NT1 statistic (Mesgaran et al. (2014)) for the BotT_HYCOM covariate in the model. Areas outside the sampled range of a covariate appear in color, indicating univariate extrapolation of that covariate occurred there during the month. Areas within the sampled range appear in gray, indicating it did not occur.

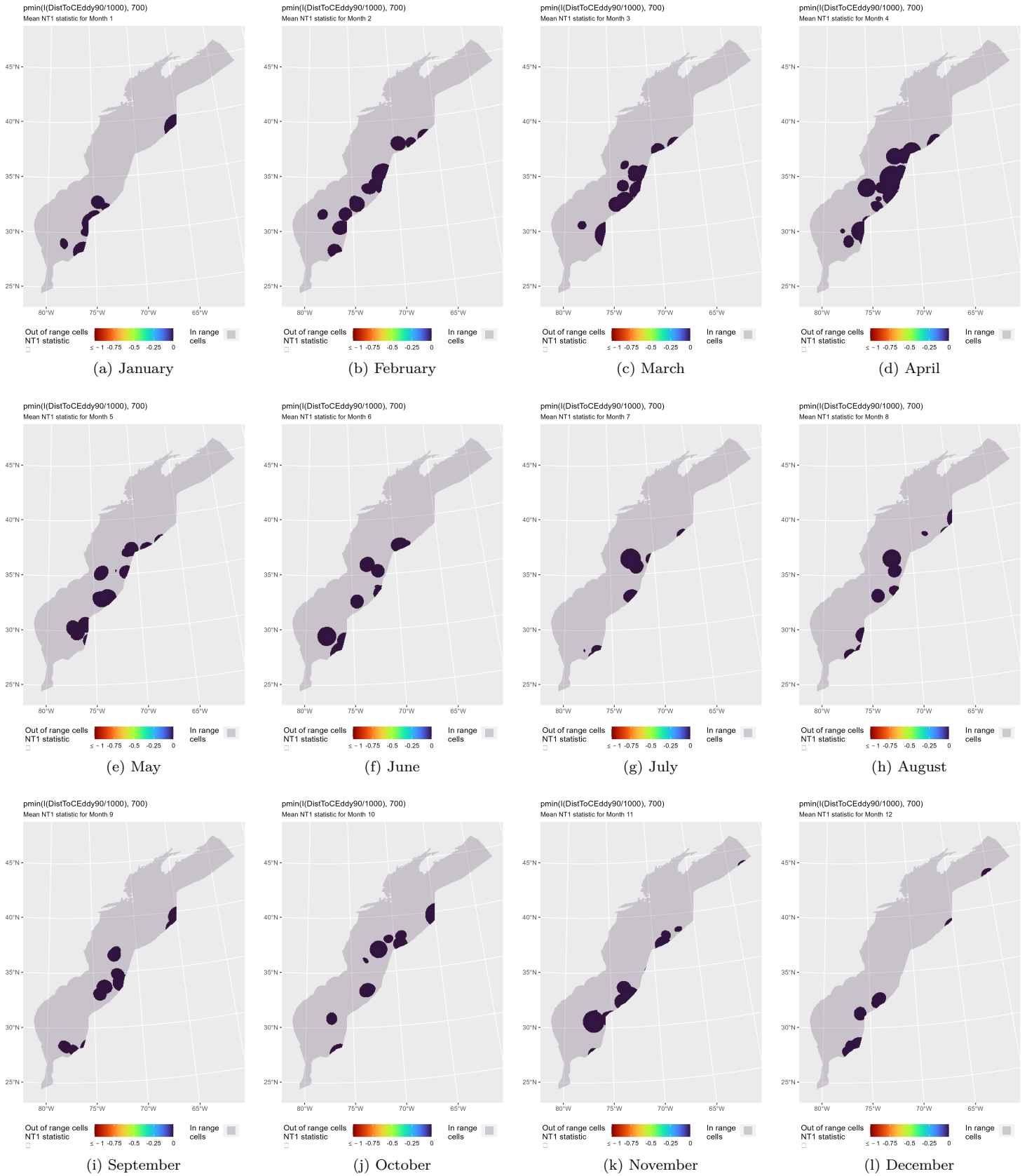


Figure 65: NT1 statistic (Mesgaran et al. (2014)) for the DistToEddy90 covariate in the model. Areas outside the sampled range of a covariate appear in color, indicating univariate extrapolation of that covariate occurred there during the month. Areas within the sampled range appear in gray, indicating it did not occur.

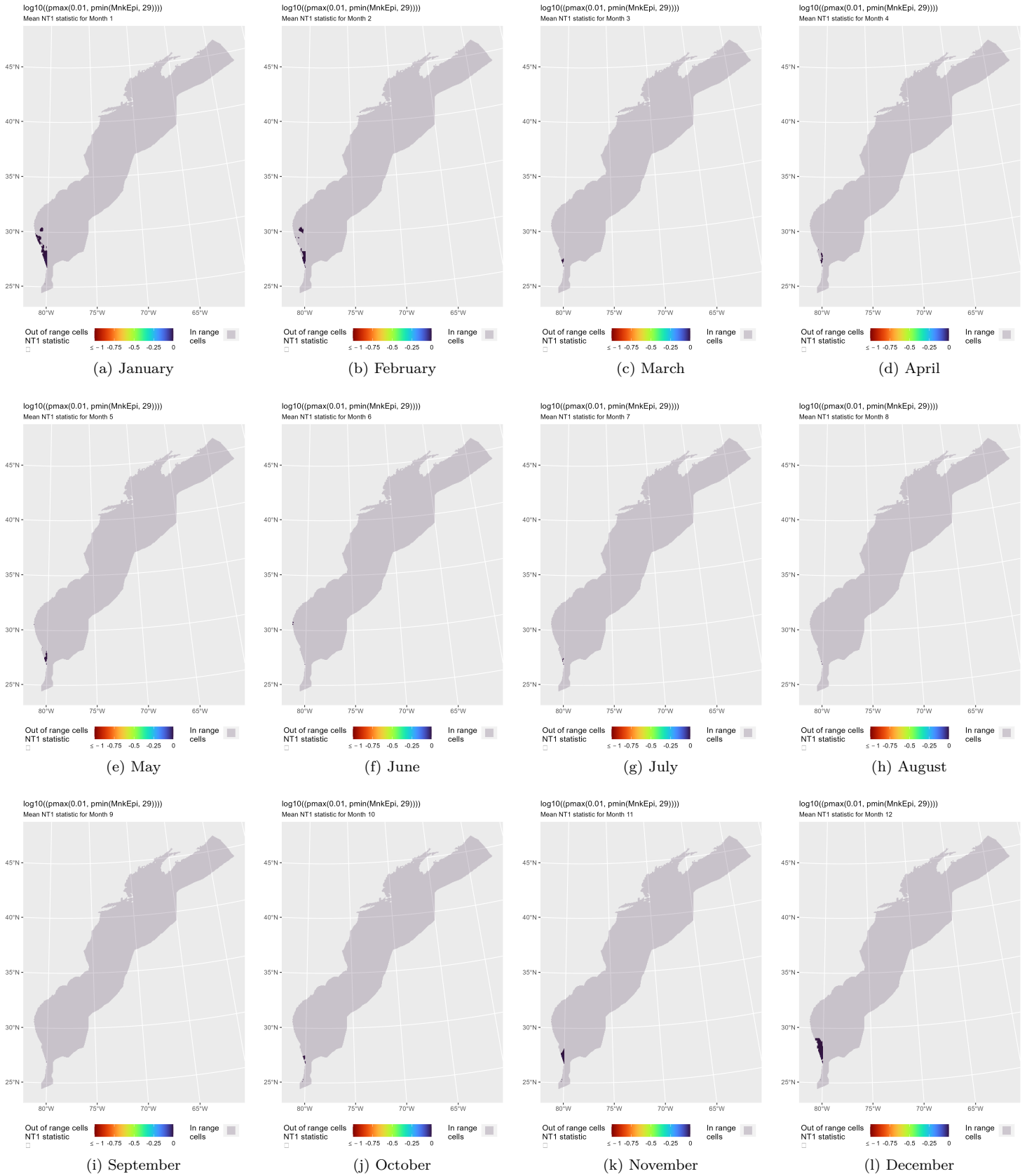


Figure 66: NT1 statistic (Mesgaran et al. (2014)) for the MnkEpi covariate in the model. Areas outside the sampled range of a covariate appear in color, indicating univariate extrapolation of that covariate occurred there during the month. Areas within the sampled range appear in gray, indicating it did not occur.

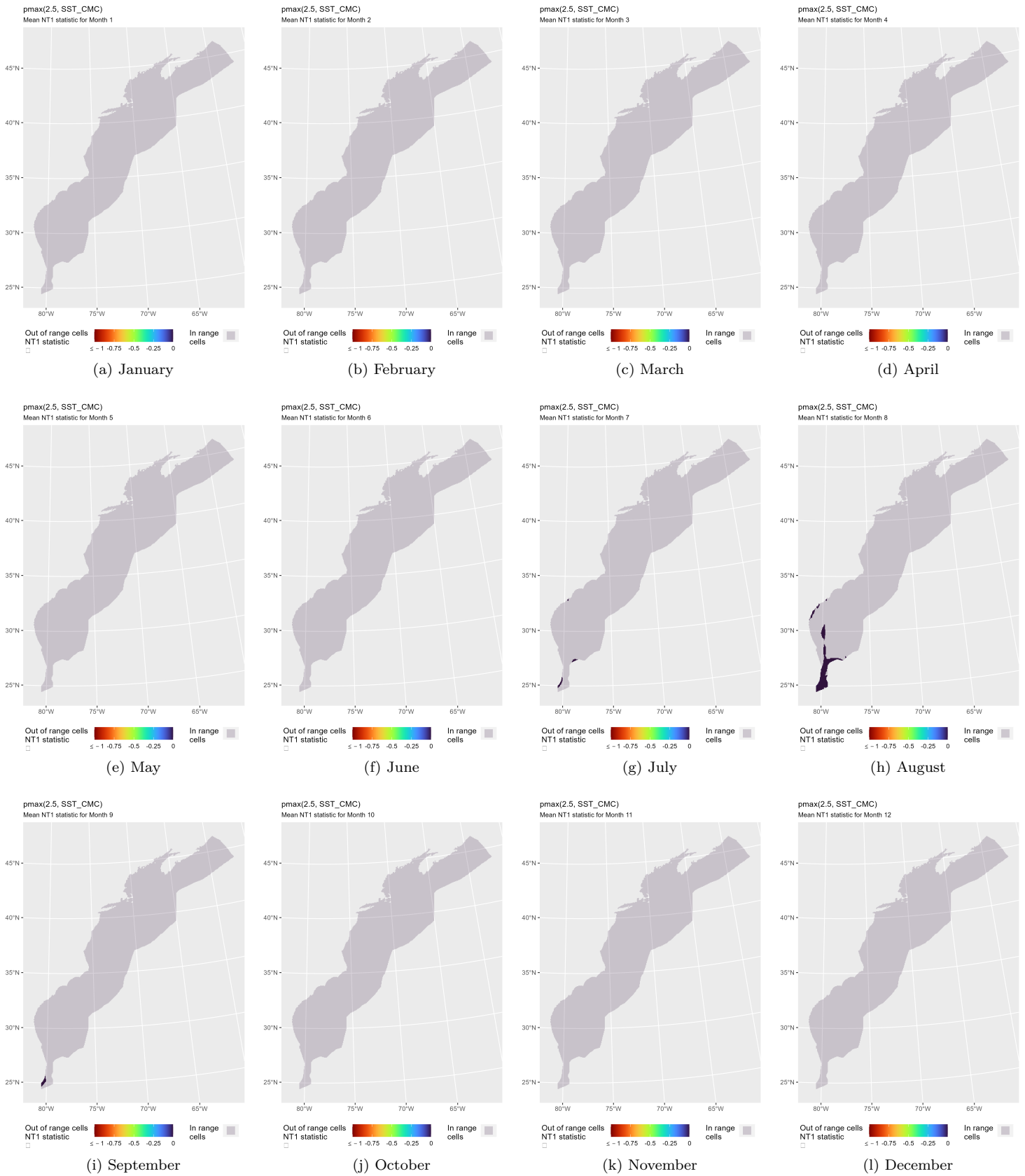


Figure 67: NT1 statistic (Mesgaran et al. (2014)) for the SST_CMC covariate in the model. Areas outside the sampled range of a covariate appear in color, indicating univariate extrapolation of that covariate occurred there during the month. Areas within the sampled range appear in gray, indicating it did not occur.

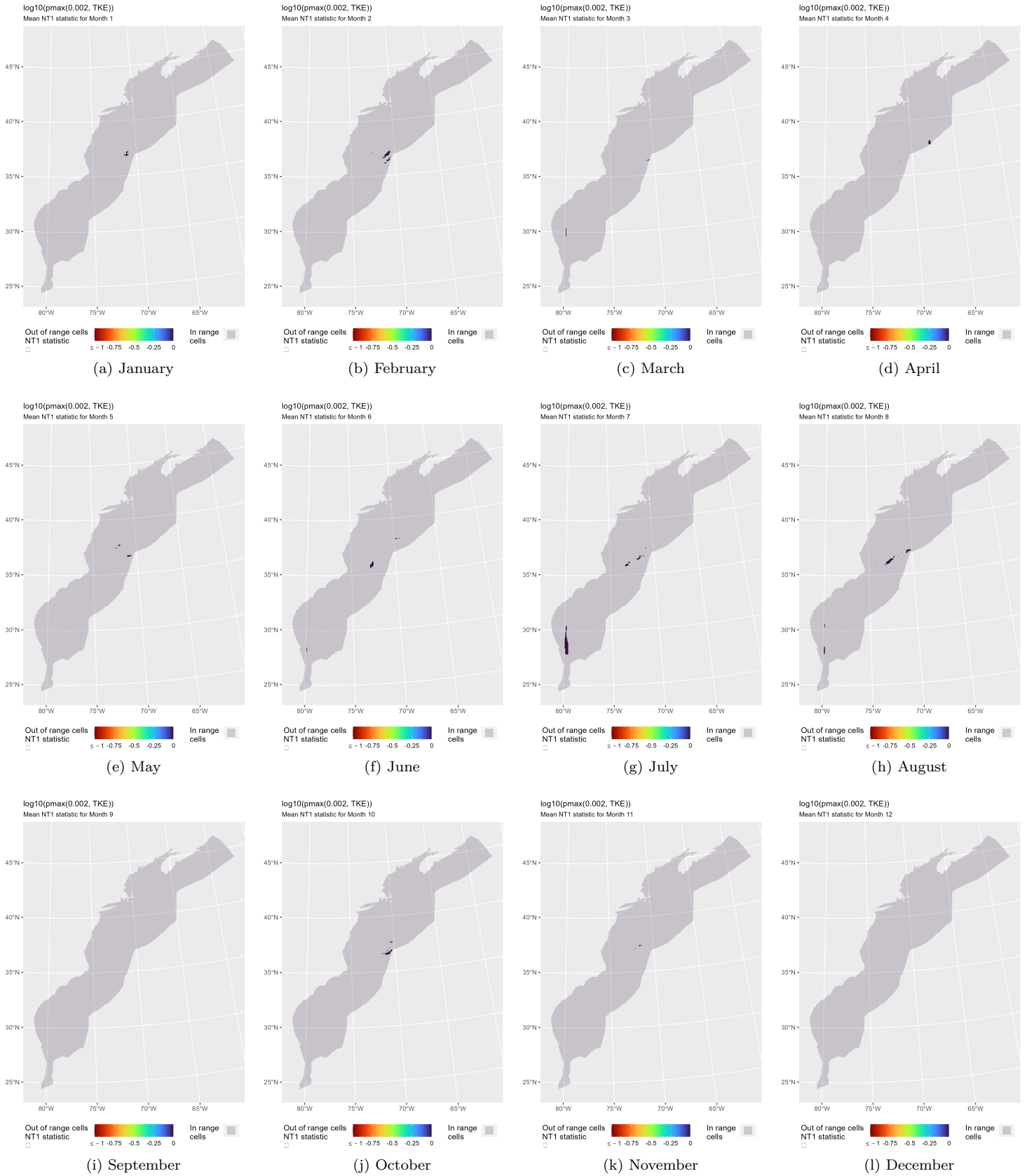


Figure 68: NT1 statistic (Mesgaran et al. (2014)) for the TKE covariate in the model. Areas outside the sampled range of a covariate appear in color, indicating univariate extrapolation of that covariate occurred there during the month. Areas within the sampled range appear in gray, indicating it did not occur.

4.3.2 Multivariate Extrapolation

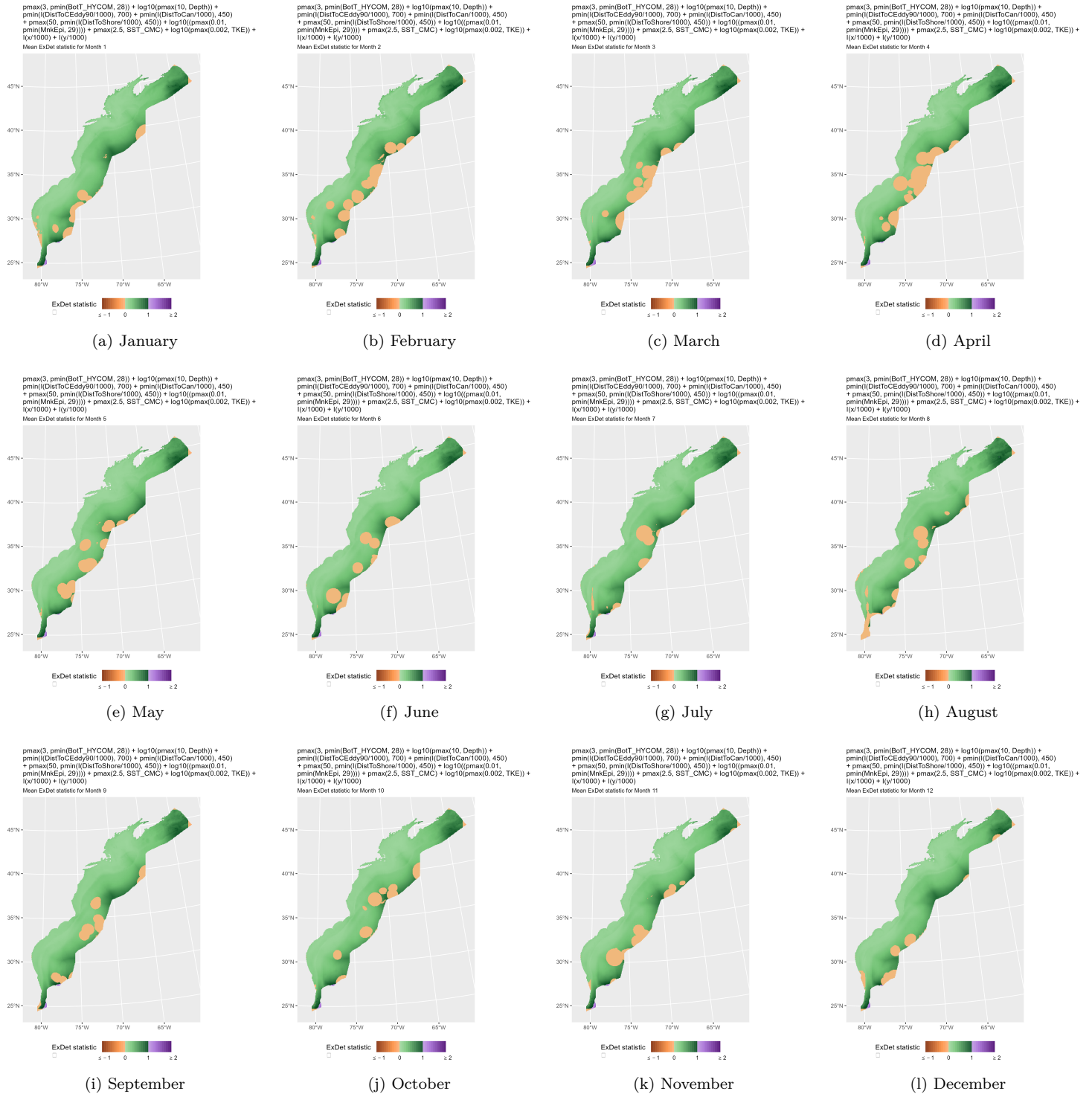


Figure 69: ExDet statistic (Mesgaran et al. (2014)) for all of the covariates used in the model. Areas in orange ($\text{ExDet} < 0$) required univariate extrapolation of one or more covariates (see previous section). Areas in purple ($\text{ExDet} > 1$), did not require univariate extrapolation but did require multivariate extrapolation, by virtue of having novel combinations of covariates not represented in the survey data, according to the NT2 statistic (Mesgaran et al. (2014)). Areas in green ($0 \geq \text{ExDet} \leq 1$) did not require either type of extrapolation.

5 Predictions

Based on our evaluation of this model in the context of what is known of this species (see Section 4), we summarized its predictions into single, year-round climatological density and uncertainty surfaces (Figure 71). To illustrate the seasonal dynamics that result when predictions are summarized monthly instead, we included monthly mean abundances (Figure 70, Table 26), but to avoid confusion we did not include monthly maps in this report. They are available from us on request, but we recommend the year-round map be used for decision-making purposes, as discussed in Section 6.

5.1 Summarized Predictions

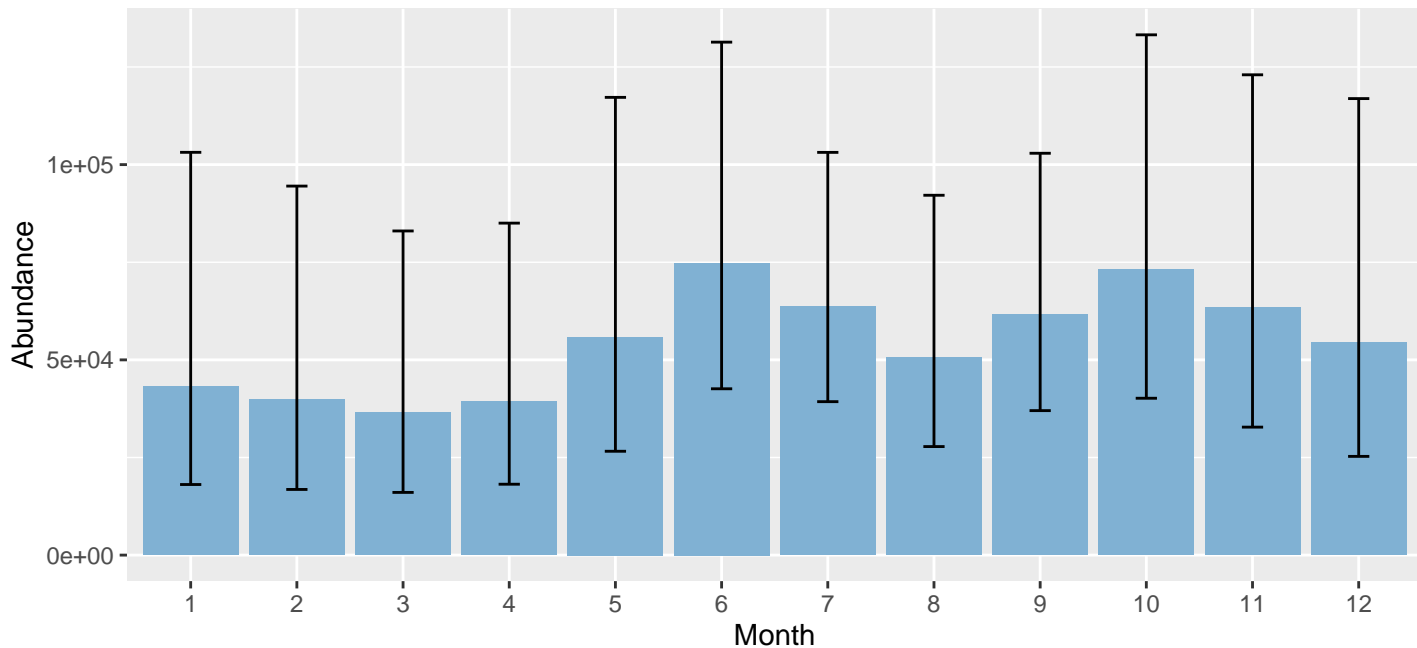


Figure 70: Mean monthly abundance for the prediction area for 1998-2019. Error bars are a 95% interval, made with a log-normal approximation using the prediction’s CV. The CV was estimated with the analytic approach given by Miller et al. (2022), Appendix S1, and accounts both for uncertainty in model parameter estimates and for temporal variability in dynamic covariates.

Table 26: Mean monthly abundance and density for the prediction area for 1998-2019. CV and intervals estimated as described for the previous figure.

Month	Abundance	CV	95% Interval	Area (km ²)	Density (individuals / 100 km ²)
1	43,186	0.467	18,081 - 103,149	1,272,925	3.39
2	39,868	0.463	16,819 - 94,502	1,272,925	3.13
3	36,508	0.438	16,056 - 83,014	1,272,925	2.87
4	39,283	0.410	18,152 - 85,015	1,272,925	3.09
5	55,835	0.392	26,595 - 117,224	1,272,925	4.39
6	74,806	0.293	42,598 - 131,364	1,272,925	5.88
7	63,661	0.250	39,296 - 103,133	1,272,925	5.00
8	50,610	0.313	27,795 - 92,152	1,272,925	3.98
9	61,706	0.265	37,000 - 102,909	1,272,925	4.85
10	73,158	0.313	40,170 - 133,235	1,272,925	5.75
11	63,493	0.347	32,775 - 123,001	1,272,925	4.99
12	54,365	0.406	25,281 - 116,909	1,272,925	4.27

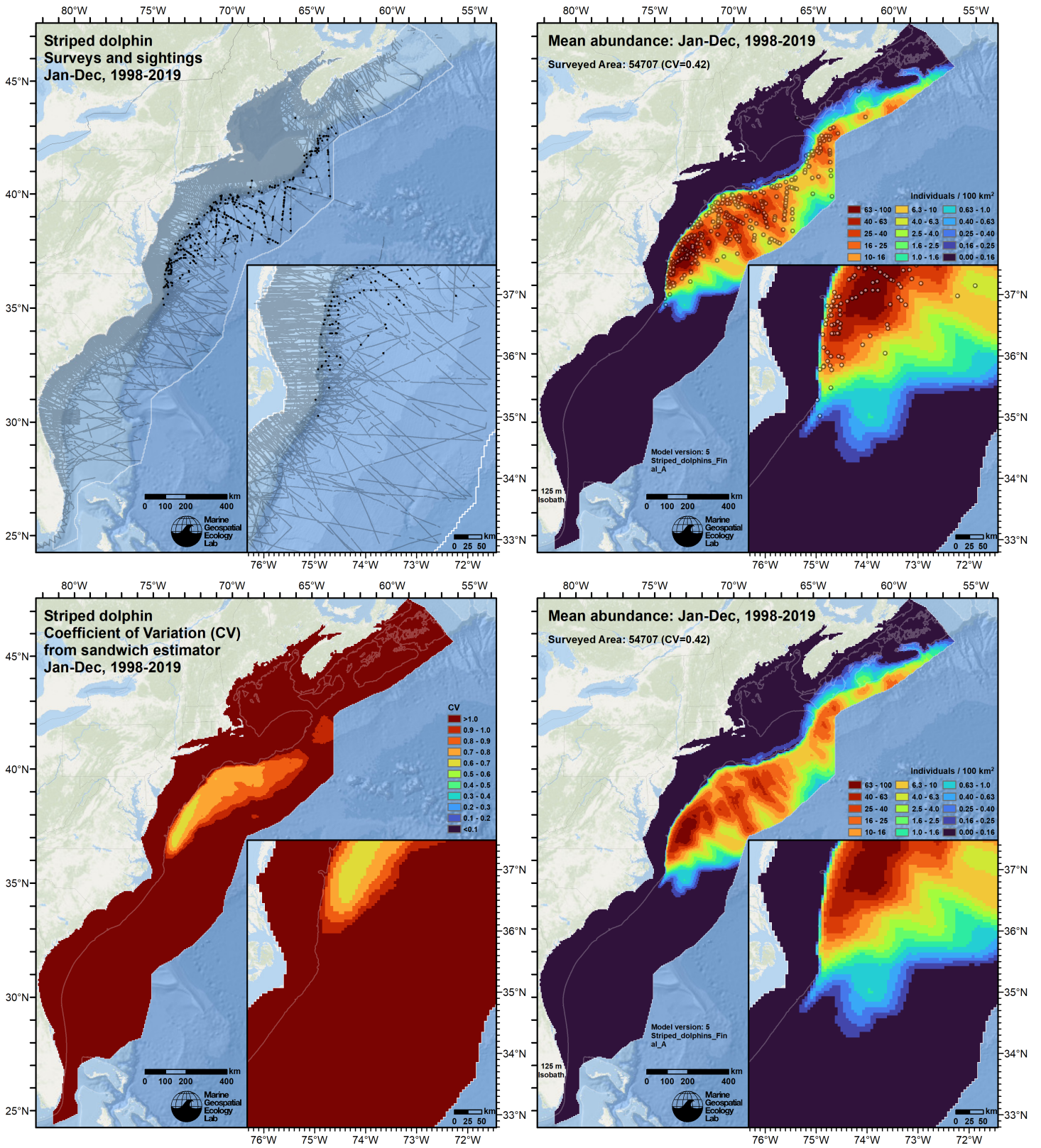


Figure 71: Survey effort and observations (top left), predicted density with observations (top right), predicted density without observations (bottom right), and coefficient of variation of predicted density (bottom left), for the given era. Variance was estimated with the analytic approach given by Miller et al. (2022), Appendix S1, and accounts both for uncertainty in model parameter estimates and for temporal variability in dynamic covariates.

5.2 Abundance Comparisons

5.2.1 NOAA Stock Assessment Report

Table 27: Comparison of regional abundance estimates from the 2021 NOAA Stock Assessment Report (SAR) (Hayes et al. (2022)) to estimates from this density model extracted from roughly comparable zones (Figure 72 below). The SAR estimates were based on a single year of surveying, while the model estimates were taken from the multi-year mean density surfaces we provide to model users (Section 5.1).

2021 Stock Assessment Report			Density Model		
Month/Year	Area	N_{est}	Period	Zone	Abundance
Jun-Sept 2016	Central Virginia to lower Bay of Fundy ^a	42,783	Year-Round 1998-2019	NEFSC	39,411
Jun-Sept 2016	Florida to central Virginia ^b	27,163	Year-Round 1998-2019	SEFSC	11,667
Jun-Sept 2016	Total	67,037	Year-Round 1998-2019	Total	56,618
	Bay of Fundy/Scotian Shelf		Year-Round 1998-2019	Canada ^c	3,942

^a Estimate originally from Palka (2020).

^b Estimate originally from Garrison (2020).

^c Our Canada zone is roughly comparable to the SAR's Bay of Fundy/Scotian Shelf area (excluding the Gulf of St. Lawrence) however no estimates were provided by the SAR for this region.

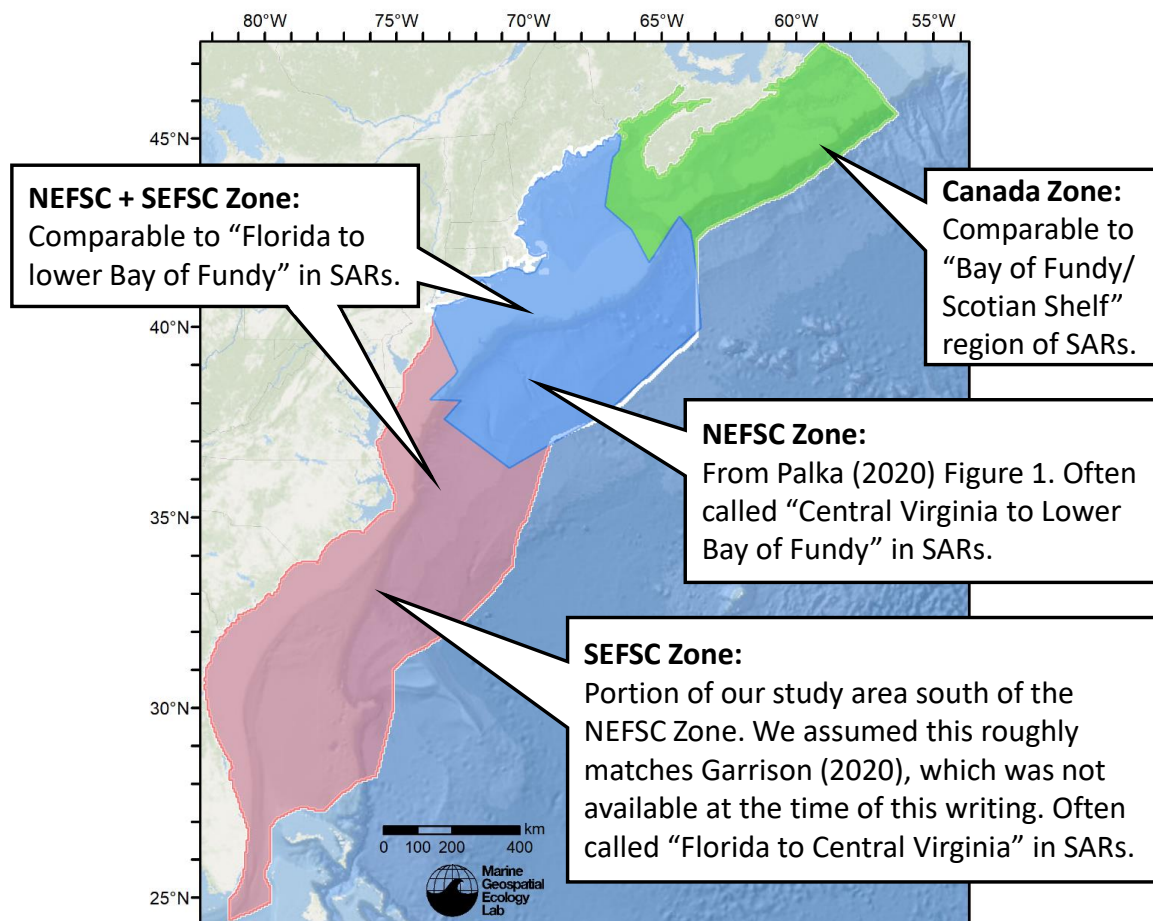


Figure 72: Zones for which we extracted abundance estimates from the density model for comparison to estimates from the NOAA Stock Assessment Report.

5.2.2 Previous Density Model

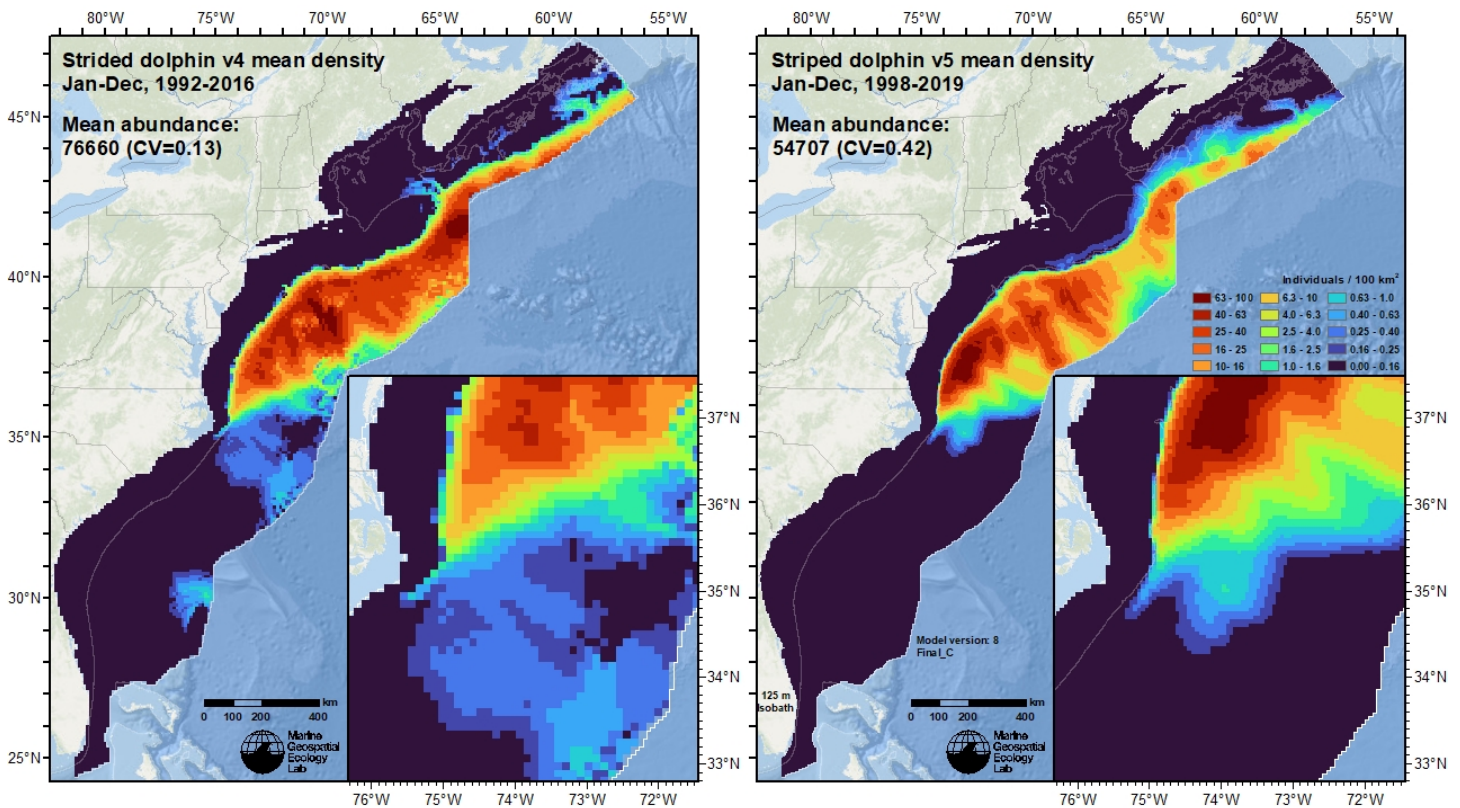


Figure 73: Comparison of the mean density predictions from the previous model (left) released by Roberts et al. (2017) to those from this model (right).

6 Discussion

The model predicted a mean abundance is 54,707 animals with highest abundance predicted at the slope and offshore of the slope and in deep offshore waters, primarily north of Cape Hatteras. Overall, the model appeared to fit the data well.

In the northeast, the model predicted increased abundance along the slope of the Scotian Shelf through summer and fall. In general, monthly predicted abundance (Figure 70) showed some seasonal variation, with the lowest abundance predicted in March (36,508) and the highest abundance predicted in June (74,806) and October (73,158). However, given that there was nothing found in the literature to indicate seasonal movement in this species within the study area, we elected to provide year-round mean density estimates.

The extrapolation statistics show some extrapolation in univariate space. Longitude (x) showed a few cells of extrapolated values at the northeast edge of the study area and latitude (y) showed a few cells of extrapolation at the northern and southern most edges of the study area. The distance to cyclonic eddy covariate showed some univariate extrapolation in all months (Figure 65). In this case distances “inside” the eddy ring are negative values, and the extrapolation cells indicate very large eddies, with large cores that are far from the ring in the negative direction. This is unlikely to be a major issue, as the functional relationship to the cyclonic eddy covariate showed a rising relationship as distance to the eddy gets larger (Figure 57). Additionally, large eddies needed to trigger the extrapolation were infrequent and as such, unlikely to have yielded a big effect in the final model. A few out of range cells of epipelagic micronekton occur in the southeastern study area where no animals were observed or predicted, thereby there were no expected effects in the final model (Figure 66). SST showed a few southern cells that were out of range and given the absence of observations and predictions, again unlikely to have yielded an effect in the final model (Figure 67). Finally, TKE showed a few out of range cells in the mid-Atlantic in most months, and in the southeast in March and July (Figure 68).

In comparison to the SAR (Hayes et al. 2020) the abundance reported for the NEFSC region summer estimate (42,783) was similar to this model, with our year-round mean abundance predicting only about 8% or 3,000 fewer animals (39,411). In the SEFSC region our model predicted substantially (57%) fewer animals (11,667) from the year-round mean than the SAR summer estimate (27,163). This resulted in an overall 15% lower total abundance in the year-round estimate for this species

in comparison to the SAR. Differences may be because the SAR estimates are based on a single year of summer survey data, whereas our estimates, are extracted from the year-round estimate, and are influenced by additional surveys, seasons, and years.

In comparison to the Roberts et al. (2017) model, which predicted a mean abundance of 76,660 animals, mean abundance was almost 29% lower in the new model, however it is important to note that the previous model was climatological whereas this was a contemporaneous model and as such, the lower predictions in winter months in this model resulted in lower mean year-round abundance. Additionally, the Roberts et al. (2017) model predicted some density south of Cape Hatteras and in the southeastern portion of the study area where no observations have occurred, whereas, this model predicted striped dolphin occurrence only north of Cape Hatteras within the known range of occurrence for this species.

References

- Archer FI, Perrin WF (1999) *Stenella coeruleoalba*. Mammalian Species 603:1–9.
- Baird RW, Stacey PJ, Whitehead H (1993) [Status of the striped dolphin, *Stenella coeruleoalba*, in Canada](#). Canadian field-naturalist Ottawa ON 107:455–465.
- Baird RW, Hooker SK, Whitehead H, Etcheberry R (1997) [A review of records of striped dolphins \(*Stenella coeruleoalba*\) from Canadian waters](#).
- Barco SG, Burt L, DePerte A, Digiovanni R Jr. (2015) Marine Mammal and Sea Turtle Sightings in the Vicinity of the Maryland Wind Energy Area July 2013-June 2015, VAQF Scientific Report #2015-06. Virginia Aquarium & Marine Science Center Foundation, Virginia Beach, VA
- Barlow J, Forney KA (2007) [Abundance and population density of cetaceans in the California Current ecosystem](#). Fishery Bulletin 105:509–526.
- Becker JJ, Sandwell DT, Smith WHF, Braud J, Binder B, Depner J, Fabre D, Factor J, Ingalls S, Kim S-H, Ladner R, Marks K, Nelson S, Pharaoh A, Trimmer R, Von Rosenberg J, Wallace G, Weatherall P (2009) Global Bathymetry and Elevation Data at 30 Arc Seconds Resolution: SRTM30_PLUS. Marine Geodesy 32:355–371. doi: [10.1080/01490410903297766](https://doi.org/10.1080/01490410903297766)
- Bloch D, Desportes G, Petersen A, Sigurjónsson J (1996) [Strandings of striped dolphins \(*Stenella coeruleoalba*\) in Iceland and the Faroe Islands and sightings in the northeast Atlantic, north of 500N latitude](#). Marine Mammal Science 12:125–132.
- Brasnett B (2008) The impact of satellite retrievals in a global sea-surface-temperature analysis. Quarterly Journal of the Royal Meteorological Society 134:1745–1760. doi: [10.1002/qj.319](https://doi.org/10.1002/qj.319)
- Buckland ST, Anderson DR, Burnham KP, Laake JL, Borchers DL, Thomas L (2001) Introduction to Distance Sampling: Estimating Abundance of Biological Populations. Oxford University Press, Oxford, UK
- Burt ML, Borchers DL, Jenkins KJ, Marques TA (2014) Using mark-recapture distance sampling methods on line transect surveys. Methods in Ecology and Evolution 5:1180–1191. doi: [10.1111/2041-210X.12294](https://doi.org/10.1111/2041-210X.12294)
- Canada Meteorological Center (2012) GHRSSST Level 4 CMC0.2deg Global Foundation Sea Surface Temperature Analysis Version 2.0. PODAAC, CA, USA. doi: [10.5067/GHCMC-4FM02](https://doi.org/10.5067/GHCMC-4FM02)
- Canada Meteorological Center (2016) GHRSSST Level 4 CMC0.1deg Global Foundation Sea Surface Temperature Analysis Version 3.0. PODAAC, CA, USA. doi: [10.5067/GHCMC-4FM03](https://doi.org/10.5067/GHCMC-4FM03)
- Carretta JV, Lowry MS, Stinchcomb CE, Lynn MS, E. CR (2000) Distribution and abundance of marine mammals at San Clemente Island and surrounding offshore waters: Results from aerial and ground surveys in 1998 and 1999. NOAA Administrative Report LJ-00-02. NOAA National Marine Fisheries Service, Southwest Fisheries Center, La Jolla, CA
- Chassignet E, Hurlburt H, Metzger EJ, Smedstad O, Cummings J, Halliwell G, Bleck R, Baraille R, Wallcraft A, Lozano C, Tolman H, Srinivasan A, Hankin S, Cornillon P, Weisberg R, Barth A, He R, Werner F, Wilkin J (2009) US GODAE: Global Ocean Prediction with the HYbrid Coordinate Ocean Model (HYCOM). Oceanog 22:64–75. doi: [10.5670/oceanog.2009.39](https://doi.org/10.5670/oceanog.2009.39)
- Chelton DB, Schlax MG, Samelson RM (2011) Global observations of nonlinear mesoscale eddies. Progress in Oceanography 91:167–216. doi: [10.1016/j.pocean.2011.01.002](https://doi.org/10.1016/j.pocean.2011.01.002)
- Cole T, Gerrior P, Merrick RL (2007) [Methodologies of the NOAA National Marine Fisheries Service Aerial Survey Program for Right Whales \(*Eubalaena glacialis*\) in the Northeast U.S., 1998-2006](#). U.S. Department of Commerce, Woods Hole, MA
- Cotter MP (2019) Aerial Surveys for Protected Marine Species in the Norfolk Canyon Region: 2018–2019 Final Report. HDR, Inc., Virginia Beach, VA

- Doksæter L, Olsen E, Nøttestad L, Fernö A (2008) Distribution and feeding ecology of dolphins along the Mid-Atlantic Ridge between Iceland and the Azores. *Deep Sea Research Part II: Topical Studies in Oceanography* 55:243–253. doi: [10.1016/j.dsr2.2007.09.009](https://doi.org/10.1016/j.dsr2.2007.09.009)
- Foley HJ, Paxton CGM, McAlarney RJ, Pabst DA, Read AJ (2019) Occurrence, Distribution, and Density of Protected Species in the Jacksonville, Florida, Atlantic Fleet Training and Testing (AFTT) Study Area. Duke University Marine Lab, Beaufort, NC
- Fulling GL, Mullin KD, Hubard CW (2003) [Abundance and distribution of cetaceans in outer continental shelf waters of the US Gulf of Mexico](#). *Fishery Bulletin* 101:923–932.
- Garrison LP (2020) [Abundance of cetaceans along the southeast U.S. East coast from a summer 2016 vessel survey](#). PRD Contribution # PRD-2020-04. NOAA National Marine Fisheries Service, Southeast Fisheries Science Center, Miami, FL
- Garrison LP, Martinez A, Maze-Foley K (2010) [Habitat and abundance of cetaceans in Atlantic Ocean continental slope waters off the eastern USA](#). *Journal of Cetacean Research and Management* 11:267–277.
- Geo-Marine, Inc. (2010) [New Jersey Department of Environmental Protection Baseline Studies Final Report Volume III: Marine Mammal and Sea Turtle Studies](#). Geo-Marine, Inc., Plano, TX
- Gowans S, Whitehead H (1995) Distribution and habitat partitioning by small odontocetes in the Gully, a submarine canyon on the Scotian Shelf. *Can J Zool* 73:1599–1608. doi: [10.1139/z95-190](https://doi.org/10.1139/z95-190)
- Harris PT, Macmillan-Lawler M, Rupp J, Baker EK (2014) Geomorphology of the oceans. *Marine Geology* 352:4–24. doi: [10.1016/j.margeo.2014.01.011](https://doi.org/10.1016/j.margeo.2014.01.011)
- Hayes SA, Josephson E, Maze-Foley K, Rosel PE, Byrd B, Chavez-Rosales S, Cole TV, Garrison LP, Hatch J, Henry A, Horstman SC, Litz J, Lyssikatos MC, Mullin KD, Orphanides C, Pace RM, Palka DL, Powell J, Wenzel FW (2020) [US Atlantic and Gulf of Mexico Marine Mammal Stock Assessments - 2019](#). NOAA National Marine Fisheries Service, Northeast Fisheries Science Center, Woods Hole, MA
- Hayes SA, Josephson E, Maze-Foley K, Rosel PE, Wallace J, Brossard A, Chavez-Rosales S, Cole TVN, Garrison LP, Hatch J, Henry A, Horstman SC, Litz J, Lyssikatos MC, Mullin KD, Murray K, Orphanides C, Ortega-Ortiz J, Pace RM, Palka DL, Powell J, Rappucci G, Soldevilla M, Wenzel FW (2022) [US Atlantic and Gulf of Mexico Marine Mammal Stock Assessments 2021](#). NOAA National Marine Fisheries Service, Northeast Fisheries Science Center, Woods Hole, MA
- Hooker SK, Whitehead H, Gowans S (1999) Marine Protected Area Design and the Spatial and Temporal Distribution of Cetaceans in a Submarine Canyon. *Conservation Biology* 13:592–602. doi: [10.1046/j.1523-1739.1999.98099.x](https://doi.org/10.1046/j.1523-1739.1999.98099.x)
- Laake JL, Calambokidis J, Osmek SD, Rugh DJ (1997) Probability of Detecting Harbor Porpoise From Aerial Surveys: Estimating g(0). *Journal of Wildlife Management* 61:63–75. doi: [10.2307/3802415](https://doi.org/10.2307/3802415)
- Ledwell W, Huntington J, Enserink K (2018) Ncidental entrapments and entanglements of cetaceans and leatherback sea turtles, strandings, ice entrapments reported to the Whale Release and Strandings Group in Newfoundland and Labrador and a summary of the Whale Release and Strandings program during 2017.
- Lehodey P, Senina I, Murtugudde R (2008) A spatial ecosystem and populations dynamics model (SEAPODYM)–Modeling of tuna and tuna-like populations. *Progress in Oceanography* 78:304–318. doi: [10.1016/j.pocean.2008.06.004](https://doi.org/10.1016/j.pocean.2008.06.004)
- Lehodey P, Conchon A, Senina I, Domokos R, Calmettes B, Jouanno J, Hernandez O, Kloser R (2015) Optimization of a micronekton model with acoustic data. *ICES Journal of Marine Science* 72:1399–1412. doi: [10.1093/icesjms/fsu233](https://doi.org/10.1093/icesjms/fsu233)
- Mallette SD, Lockhart GG, McAlarney RJ, Cummings EW, McLellan WA, Pabst DA, Barco SG (2014) Documenting Whale Migration off Virginia’s Coast for Use in Marine Spatial Planning: Aerial and Vessel Surveys in the Proximity of the Virginia Wind Energy Area (VA WEA), VAQF Scientific Report 2014-08. Virginia Aquarium & Marine Science Center Foundation, Virginia Beach, VA
- Mallette SD, Lockhart GG, McAlarney RJ, Cummings EW, McLellan WA, Pabst DA, Barco SG (2015) Documenting Whale Migration off Virginia’s Coast for Use in Marine Spatial Planning: Aerial Surveys in the Proximity of the Virginia Wind Energy Area (VA WEA) Survey/Reporting Period: May 2014 - December 2014, VAQF Scientific Report 2015-02. Virginia Aquarium & Marine Science Center Foundation, Virginia Beach, VA
- Mallette SD, McAlarney RJ, Lockhart GG, Cummings EW, Pabst DA, McLellan WA, Barco SG (2017) [Aerial Survey Baseline Monitoring in the Continental Shelf Region of the VACAPES OPAREA: 2016 Annual Progress Report](#). Virginia Aquarium & Marine Science Center Foundation, Virginia Beach, VA
- Marsh H, Sinclair DF (1989) Correcting for Visibility Bias in Strip Transect Aerial Surveys of Aquatic Fauna. *The Journal of Wildlife Management* 53:1017. doi: [10.2307/3809604](https://doi.org/10.2307/3809604)

- McAlearney R, Cummings E, McLellan W, Pabst A (2018) Aerial Surveys for Protected Marine Species in the Norfolk Canyon Region: 2017 Annual Progress Report. University of North Carolina Wilmington, Wilmington, NC
- McLellan WA, McAlearney RJ, Cummings EW, Read AJ, Paxton CGM, Bell JT, Pabst DA (2018) Distribution and abundance of beaked whales (Family Ziphiidae) Off Cape Hatteras, North Carolina, U.S.A. *Marine Mammal Science*. doi: [10.1111/mms.12500](https://doi.org/10.1111/mms.12500)
- Meissner T, Wentz FJ, Scott J, Vazquez-Cuervo J (2016) Sensitivity of Ocean Surface Salinity Measurements From Spaceborne L-Band Radiometers to Ancillary Sea Surface Temperature. *IEEE Trans Geosci Remote Sensing* 54:7105–7111. doi: [10.1109/TGRS.2016.2596100](https://doi.org/10.1109/TGRS.2016.2596100)
- Mesgaran MB, Cousens RD, Webber BL (2014) Here be dragons: A tool for quantifying novelty due to covariate range and correlation change when projecting species distribution models. *Diversity Distrib* 20:1147–1159. doi: [10.1111/ddi.12209](https://doi.org/10.1111/ddi.12209)
- Miller DL, Becker EA, Forney KA, Roberts JJ, Cañadas A, Schick RS (2022) Estimating uncertainty in density surface models. *PeerJ* 10:e13950. doi: [10.7717/peerj.13950](https://doi.org/10.7717/peerj.13950)
- Mullin KD, Fulling GL (2003) [Abundance of cetaceans in the southern U.S. North Atlantic Ocean during summer 1998](#). *Fishery Bulletin* 101:603–613.
- Palka D (2020) [Cetacean Abundance in the US Northwestern Atlantic Ocean Summer 2016](#). *Northeast Fish Sci Cent Ref Doc. 20-05*. NOAA National Marine Fisheries Service, Northeast Fisheries Science Center, Woods Hole, MA
- Palka D, Read A, Potter C (1997) Summary of knowledge of white-sided dolphins (*Lagenorhynchus acutus*) from US and Canadian Atlantic Waters. *Rep Int Whal Commn* 47:729–734.
- Palka D, Aichinger Dias L, Broughton E, Chavez-Rosales S, Cholewiak D, Davis G, DeAngelis A, Garrison L, Haas H, Hatch J, Hyde K, Jech M, Josephson E, Mueller-Brennan L, Orphanides C, Pegg N, Sasso C, Sigourney D, Soldevilla M, Walsh H (2021) [Atlantic Marine Assessment Program for Protected Species: FY15 – FY19 \(OCS Study BOEM 2021-051\)](#). U.S. Department of the Interior, Bureau of Ocean Energy Management, Washington, DC
- Palka DL (2006) [Summer abundance estimates of cetaceans in US North Atlantic navy operating areas \(NEFSC Reference Document 06-03\)](#). U.S. Department of Commerce, Northeast Fisheries Science Center, Woods Hole, MA
- Palka DL, Chavez-Rosales S, Josephson E, Cholewiak D, Haas HL, Garrison L, Jones M, Sigourney D, Waring G, Jech M, Broughton E, Soldevilla M, Davis G, DeAngelis A, Sasso CR, Winton MV, Smolowitz RJ, Fay G, LaBrecque E, Leiness JB, Dettloff K, Warden M, Murray K, Orphanides C (2017) [Atlantic Marine Assessment Program for Protected Species: 2010-2014 \(OCS Study BOEM 2017-071\)](#). U.S. Department of the Interior, Bureau of Ocean Energy Management, Washington, DC
- Read AJ, Barco S, Bell J, Borchers DL, Burt ML, Cummings EW, Dunn J, Fougères EM, Hazen L, Hodge LEW, Laura A-M, McAlearney RJ, Peter N, Pabst DA, Paxton CGM, Schneider SZ, Urian KW, Waples DM, McLellan WA (2014) [Occurrence, distribution and abundance of cetaceans in Onslow Bay, North Carolina, USA](#). *Journal of Cetacean Research and Management* 14:23–35.
- Ringelstein J, Pusineri C, Hassani S, Meynier L, Nicolas R, Ridoux V (2006) Food and feeding ecology of the striped dolphin, *Stenella Coeruleoalba*, in the oceanic waters of the north-east Atlantic. *J Mar Biol Ass* 86:909–918. doi: [10.1017/S0025315406013865](https://doi.org/10.1017/S0025315406013865)
- Roberts JJ, Best BD, Dunn DC, Trembl EA, Halpin PN (2010) Marine Geospatial Ecology Tools: An integrated framework for ecological geoprocessing with ArcGIS, Python, R, MATLAB, and C++. *Environmental Modelling & Software* 25:1197–1207. doi: [10.1016/j.envsoft.2010.03.029](https://doi.org/10.1016/j.envsoft.2010.03.029)
- Roberts JJ, Best BD, Mannocci L, Fujioka E, Halpin PN, Palka DL, Garrison LP, Mullin KD, Cole TVN, Khan CB, McLellan WA, Pabst DA, Lockhart GG (2016) Habitat-based cetacean density models for the U.S. Atlantic and Gulf of Mexico. *Scientific Reports* 6:22615. doi: [10.1038/srep22615](https://doi.org/10.1038/srep22615)
- Roberts JJ, Mannocci L, Halpin PN (2017) Final Project Report: Marine Species Density Data Gap Assessments and Update for the AFTT Study Area, 2016-2017 (Opt. Year 1), Document Version 1.4. Duke University Marine Geospatial Ecology Lab, Durham, NC
- Roberts JJ, Yack TM, Halpin PN (2023) Marine mammal density models for the U.S. Navy Atlantic Fleet Training and Testing (AFTT) study area for the Phase IV Navy Marine Species Density Database (NMSDD), Document Version 1.3. Duke University Marine Geospatial Ecology Lab, Durham, NC
- Robertson FC, Koski WR, Brandon JR, Thomas TA, Trites AW (2015) [Correction factors account for the availability of bowhead whales exposed to seismic operations in the Beaufort Sea](#). *Journal of Cetacean Research and Management* 15:35–44.

- Ryan C, Boisseau O, Cucknell A, Romagosa M, Moscrop A, McLanaghan R (2013) [Final report for trans-Atlantic research passages between the UK and USA via the Azores and Iceland, conducted from R/V Song of the Whale 26 March to 28 September 2012](#). Marine Conservation Research International, Essex, UK
- Schlx MG, Chelton DB (2016) [The "Growing Method" of Eddy Identification and Tracking in Two and Three Dimensions](#). College of Earth, Ocean and Atmospheric Sciences, Oregon State University, Corvallis, OR
- Torres LG, Mclellan WA, Meagher E, Pabst DA (2005) [Seasonal distribution and relative abundance of bottlenose dolphins, *Tursiops truncatus*, along the US mid-Atlantic coast](#). Journal of Cetacean Research and Management 7:153.
- Waring GT, Josephson E, Maze-Foley K, Rosel PE, Cole TVN, Engleby L, Garrison LP, Henry A, Mullin KD, Orphanides C, Pace RM, Palka DL, Lyssikatos M, Wenzel FW (2014) [US Atlantic and Gulf of Mexico Marine Mammal Stock Assessments - 2013](#). National Marine Fisheries Service, Woods Hole, MA
- Whitt AD, Powell JA, Richardson AG, Bosyk JR (2015) [Abundance and distribution of marine mammals in nearshore waters off New Jersey, USA](#). Journal of Cetacean Research and Management 15:45–59.
- Winn HE (1982) CeTAP: A Characterization of Marine Mammals and Turtles in the Mid- and North Atlantic Areas of the U.S. Outer Continental Shelf: Final Report. University of Rhode Island Graduate School of Oceanography, Kingston, RI
- Wood SN (2011) Fast stable restricted maximum likelihood and marginal likelihood estimation of semiparametric generalized linear models. Journal of the Royal Statistical Society: Series B (Statistical Methodology) 73:3–36. doi: [10.1111/j.1467-9868.2010.00749.x](https://doi.org/10.1111/j.1467-9868.2010.00749.x)